A Structural Concept for Free-Form Timber Structures

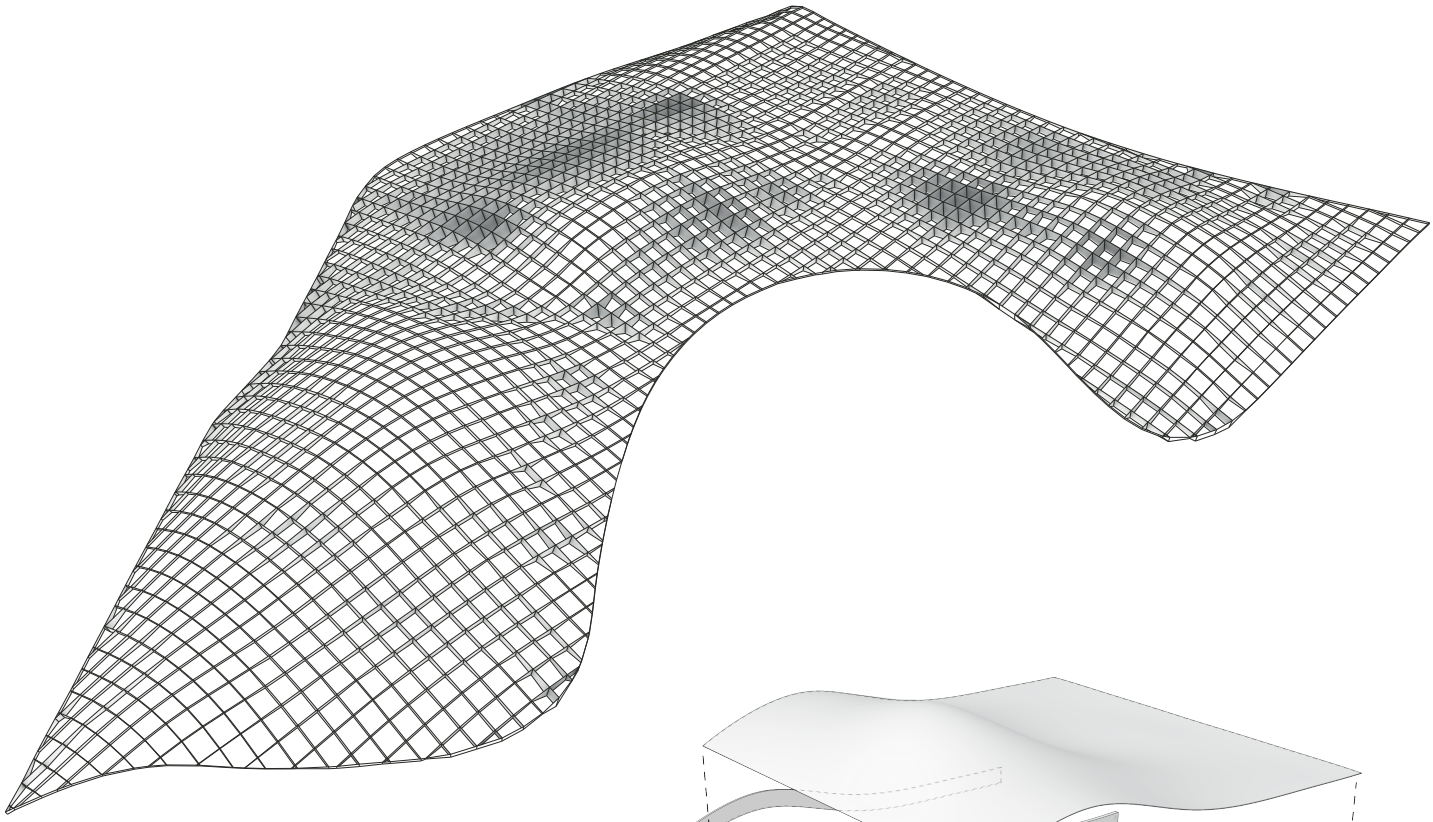

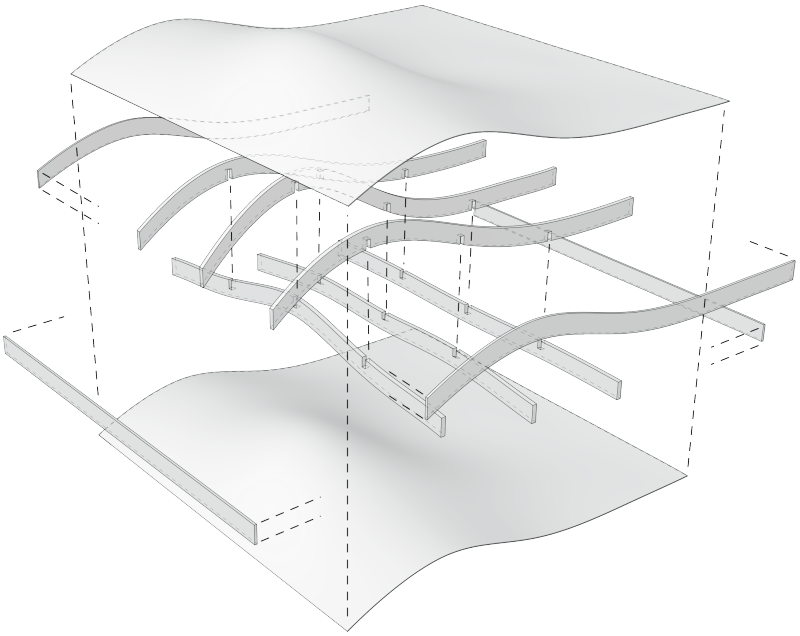

TU Delft

Knippers Helbig
Advanced Engineering

MSc. Thesis
Tessa Ruseler

A Structural Concept for Free-Form Timber Structures

by

T.T. Ruseler

to obtain the degree of Master of Science
at Delft University of Technology

Thesis committee:	Prof. ir. R. Nijsse,	Delft University of Technology
	Dr. ir. G. J. P. Ravenshorst,	Delft University of Technology
	Prof. dr. ir. J. W. G. van de Kuilen,	Delft University of Technology
	Dr. ir. L. Giampellegrini,	Knippers Helbig GmbH

Faculty of Civil Engineering in cooperation with Knippers Helbig

TU Delft

Acknowledgements

This thesis has been written as part of the Civil Engineering master curriculum at the Delft University of Technology, for the master track Building Engineering with specialisation Structural Design. The research has been carried out in cooperation with Knippers Helbig Advanced Engineering, which is an engineering firm based in Stuttgart, Berlin and New York. This report forms the final step in completing this study and thereby also ends my time as a student. I would like to acknowledge all the people who made a contribution to this master thesis and during my studies.

First of all, I would like to thank the committee members for their supervision and guidance during my thesis. I am thankful for the willingness of Rob Nijsse to chair the thesis committee. In particular for his enthusiasm, which encouraged me from the start of my master and for his support to do my thesis abroad. I am very grateful for the input, effort and support of Laurent Giampellegrini. Next to all his work at Knippers Helbig, he was willing to review and discuss my work and share his knowledge and experience with me. I would like to thank Geert Ravenshorst for his comments and knowledge about timber, which brought the work to a higher level. Jan-Willem van de Kuilen, thank you for being part of my committee.

Furthermore I would like to thank my colleagues at Knippers Helbig. I would like to thank them for supporting my research and for sharing their knowledge and skills from which I could draw. In particular I would like to thank Jacqueline and Andreas for their kindness.

Secondly, I would like to thank all the people that helped me enjoy my time as student in Delft. In particular I would like to thank my friends Crispijn, Harm and Loes for always encouraging me during my studies. I am thankful that Sara and Crispijn have read through part of my final thesis and providing it with valuable comments, resulting in the current work.

Finally, an enormous amount of credits go to my boyfriend Oscar, who was supportive and motivating to complete my studies. It would have been almost impossible without his help. In particular I would like to thank my parents, Thea and Coen, for their tremendous support and love, not only this last year but during my entire studies. And last but not least, I would like to thank my crazy little brother Rowan.

Hope you will enjoy reading it!

Tessa Ruseler
Stuttgart, October 2017

Summary

Timber construction has a promising future in the face of global sustainable development challenges. Using timber as the main structural material, the carbon footprint of a building is strongly reduced since the carbon will be stored for as long as the building stands or the timber is used. Wood is not only widely available, trees in our forests and plantations will continue to be grown; timber will continue to be available.

Over the last couple of years advances in analysis and fabrication techniques have enabled the construction of complex timber structures. The choice of material has large effects on the digital design process of free-form structures from an early stage. This in particular is the case for timber structures, since constraints due to connection techniques and fabrication may significantly affect the design. Despite the advances in computational manufacturing, limits in fabrication may impose severe constraints on what can be achieved in practice and within budget. Therefore, a close collaboration between the architect and the structural engineer needs to take place early in the design phase.

With the advent of increasingly powerful yet easy to use parametric modelling tools, the geometry is often set by the architect based on aesthetic and functional criteria but without much consideration for structural performance. The resulting free-form geometries therefore often combine areas with strong curvature where shell behaviour will be activated, with flat or shallow regions where the forces need to be transferred in bending. Implementing such digital processes often results in projects that neglect actual material characteristics, thereby not considering the strength and weaknesses of timber.

The aim of this master thesis is to explore and develop a structural concept in timber that takes into account both shell and bending behaviour. An integrated structural concept can be adapted to a free-form structure to satisfy the local structural demands of timber in an efficient manner. Resulting from this the following main research question was raised:

"How can timber be used to design an integrated structural concept for free-form structures that exhibits both shell and bending behaviour in a smooth, continuous and seamless fashion?"

An integrated structural concept was designed for free-form timber structures, which consists of ribbed elements that are covered with plates on the top and the bottom. The structural concept has been applied to the design of the timber roof project to assess the feasibility. After multiple iterations, a smooth height variation was applied for developing this structural concept with the use of timber. The structure has been optimised so that material is present where it is needed and in the right quantity. It is efficient since it is thin, strong and lightweight. For an efficient design, the depth of the structure can be shallow where pure shell behaviour occurs due to the curved shape. The most critical areas of the structure are flat, where larger depths are required. In order to accommodate this efficient design, the principle of smooth height variation has been applied for developing this structural concept with the use of timber.

The ease of fabrication is achieved by designing simple connections. A simple connection has been made for intersecting the different ribbed elements. In the ribbed elements an incision is made of half the length and the width. The plates are bent to the desired curvature and attached to the ribbed elements by screws. The bottom parts of the ribbed elements will

be tapered as a result of the depth optimisation of the structure. Taking this into consideration, the ribbed elements will be sawn at an angle to the grain direction and in these elements an incision will be made. A drawback is that the allowable stresses need to be highly reduced by a factor of two. Overall it was still achievable to meet the bending and shear stresses.

This research shows that an integrated structural concept can successfully be used for a free-form timber structure. As shown with the timber roof project, the designed structural concept is applicable for both shell and bending behaviour. Therefore it has been possible to meet the desired shape from the architectural design's point-of-view. In order to achieve an integrated structural concept, the inhomogeneous material properties of timber were incorporated in the structural concept. Precaution has been taken in the computational modelling by also taking into account the different directions for the anisotropic material properties.

Contents

1 Introduction

1.1. Introduction

For centuries timber has been used as structural material in a great variety of building and civil engineering applications. Timber construction has a promising future in the face of global sustainable development challenges. Using timber as the main structural material the carbon footprint of a building is strongly reduced as the carbon will be stored for as long as the building stands or the timber is used. Wood is not only widely available, trees in our forests and plantations will continue to be grown; timber will continue to be available.

The choice of material has large affects on the digital design process of free-form structures from an early stage. Each material has different properties that determine in large part the freedom of design. This in particular is the case of timber structures, since constraints due to connection techniques and fabrication may significantly affect the design. Despite the advances in computational manufacturing, limits in fabrication may impose severe constraints on what can be achieved in practice and within budget. If not taken into account early in the process it may result in the need to adjust the geometries or to re-assess the structural concept with the structural engineers, contractor and architect. Therefore a close collaboration between the architect and the structural engineer needs to take place early in the design phase. The consequences and possibilities of the chosen structural concept with regard to manufacturing, detailing, and assembly need to be assessed in the conceptual design phase.

1.2. Problem Definition

With the advent of increasingly powerful yet easy to use parametric modelling tools, the geometry is often set by the architect based on aesthetic and functional criteria but without much consideration for structural performance. The resulting free-form geometries therefore often combine areas with strong curvature where shell behaviour will be activated, with flat or shallow regions where the forces need to be transferred in bending. The usage of the digital processes often results in projects that neglect actual material characteristics [35] without considering the strength and weaknesses of timber. The challenge for the engineer is to devise an integrated structural concept that can be adapted to a free-form structure to satisfy the local structural demands of timber in an efficient manner.

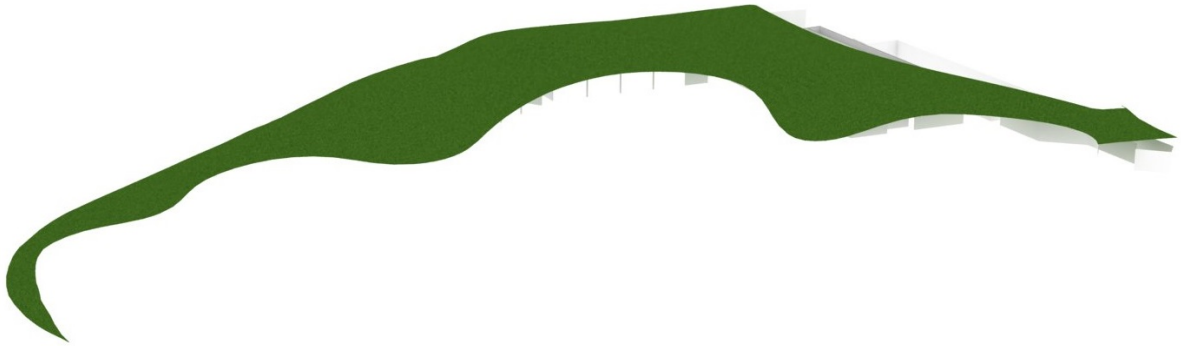

Figure 1.1: Perspective of the timber roof project

1.3. Research Topic

Over the last couple of years advances in analysis and fabrication techniques have enabled the construction of complex timber structures [3]. The aim of this master thesis is to explore and develop a structural concept in timber that takes into account both shell and bending behaviour. The design will be elaborated from global design down to details. Resulting from this, the following main research question arises:

"How can timber be used to design an integrated structural concept for free-form structures that exhibits both shell and bending behaviour in a smooth, continuous and seamless fashion?"

1.4. Methodology

The primary scope of this research is to elaborate a structural concept in timber to cover a free-form surface. First a literature study about the developments in the timber industry is carried out. Secondly, a design study is conducted whereby the concept is developed based on a case study of a free-form timber roof project that is relevant for the company Knippers Helbig. The chapters of this thesis follow the steps taken during this research project. Below a description is given per chapter.

Chapter 2 Timber Structures

This chapter describes the developments in the timber industry. The advent and impact of increasingly powerful parametric modelling tools will be discussed and how the choice of the material affects the digital design process of free-form structures. The chapter will be concluded with the latest developments in timber production techniques and the increasing possibilities that constructing with timber brings. The following sub-questions will be answered:

- What is the definition of a free-form structure?
- What issues arises from architectural design using digital modelling tools?
- What kind of structural timber materials are developed and which are suitable for free-form structures?
- What innovative timber manufacturing techniques are available and how will timber be further developed?

Chapter 3 State-of-the-Art for Free-form Timber Structures

The third chapter gives an overview of current state-of-the-art for free-form timber structures, grouping various structures based on its structural system. An overview will be given based on structural efficiency, material choice, connection techniques and manufacturing. In this chapter the following sub-questions will be answered:

- Which free-form timber structures exist today and what are their characteristics?
- What kind of structural systems have been developed for these structures?
- What are the advantages and disadvantages of these complex timber buildings?
- In which area does the expertise need to improve?

Chapter 4 Design Criteria

The design criteria and the boundary conditions of the case study are provided in the fourth chapter. This free-form timber structure will have shell behaviour, bending behaviour and a combination of both. The design tools and programs for computational modelling will be discussed. The following sub-questions will be answered:

- Which design principles will be applied?
- What load assumptions will be used?
- What are the boundary conditions for the case study of the timber roof project?
- Which structural system is used for the structure of the roof?

Chapter 5 Design Approach

In this chapter the structural concepts will be investigated and assessed on their suitability for the case study. A principle of smooth height variation will be developed to get the optimal height. The different steps to achieve this will be shown on a simplified example as proof of concept. In this chapter the following sub-questions will be answered:

- Which structural concept will be selected for further development?
- How can the height of the elements of the structure be determined?
- what kind of checking strategy is applicable for a complex structure?

Chapter 6 Structural Design

Chapter 6 explains the structural design and analysis of the chosen structural concept. This concept will be applied to the design of the roof project to assess the feasibility. A general analysis of the structural model will be discussed, in which the design of connections will also be included. The following sub-questions will be answered:

- How could this structural concept be manufactured and assembled?
- What is the structural behaviour of the concept on the roof project and what are the results?

Chapter 7 Conclusions and Recommendations

In the final chapter an answer will be given to the main research question. The results obtained from the different parts of the research will be analysed. Conclusions are given and the thesis finishes with recommendations for future research.

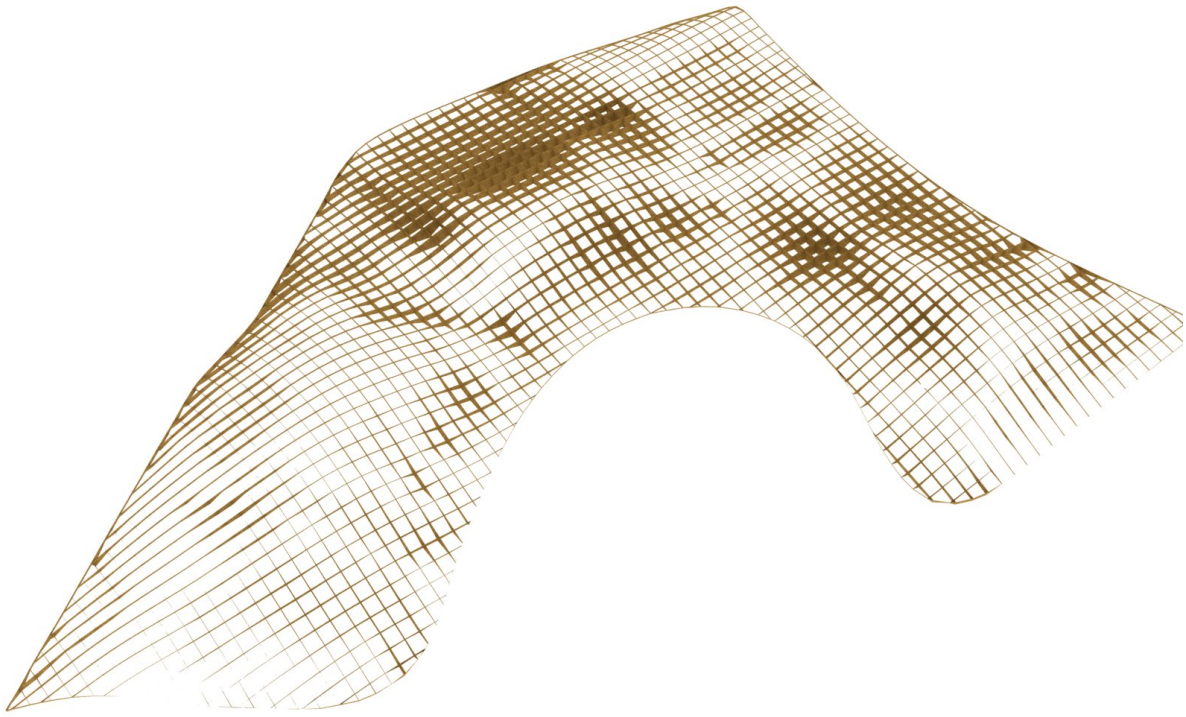

Figure 1.2: The smooth height variation of the free-form timber structures without plates

1.5. Scope and Limitations

The main focus of this research will lay on the case study. In the optimized design process, the shape of a free-form structure will be further developed after the first structural analysis has been performed to find the optimal balance between structural integrity and design. For the case study the shape and the physical boundary conditions of the timber roof have been fixed. The design criteria presented in the fourth chapter of this thesis set the boundary of the design freedom. However, there are no limitations regarding the depth of the roof structure.

This study used manual calculations and computational modelling for the design of the structural concept. Physical tests are beyond the scope of this research. Design and calculations are based on the European Standards, EN 1991-1-1 and EN 1995-1-1. The project is located in Sindelfingen, Germany, therefore the national annex of Germany will be consulted.

2

Timber Structures

A literature study about the developments in the timber industry will be carried out. The advantages and disadvantages of using timber for free-form structures will be explained. The chapter will be concluded with the developments of the timber production process discussing the corresponding techniques.

2.1. Possibilities of Timber Constructions

Timber is used as a structural material in a great variety of building and civil engineering applications. Timber construction has a promising future in the face of global sustainable development challenges. Wood is continually being grown in our forests and plantations; it will continue to be available. Using timber in buildings stores the carbon for as long as the buildings stand or the timber is used. Therefore using timber in constructions is one of the possible approaches that helps to meet the urgent need for sustainability and CO_2 emission reduction in the building industry.

In the recent years considerable progress has been made with the interacting construction components for timber materials and their joints. The common types of timber joints are load bearing connections like dowel type fasteners and bonded rods. Especially for free-form structures it all comes down to the design of the connections. Timber is very suitable for free-form structures as it has a very high strength to weight ratio. Prefabrication is desired as much as possible as it allows for better quality control since changeable weather and site conditions are avoided. This allows control of the moisture content with the required temperature and relative humidity conditions.

2.2. Free-Form Structures

The definition of free-form structure is not clearly defined since there are multiple interpretations. A free-form design could be based on form follow force. One can say that a structure will be free-form when it has no mathematical expression but defining it using a computer will create a mathematical expression of the form. The term free-form from a dictionary gives the following definition: ”Free-form is not conforming to a regular or formal structure or shape”. In the context of this research a free-form structure is defined as double curved shapes of which the shape is not structurally optimised.

A double curved, complex surface has double curvature in different directions. The curvature can be measured by determining the curvature in every point on the surface. Each curve could be specified using the radius as the curvature equals the inverse of radius: $k = \frac{1}{R}$.

Points with minimum or a maximum curvature can be used to characterise the principal curvatures of a surface. The theory behind the specification of the surfaces has been published by Carl Friedrich Gauss. The Gaussian curvature is defined as the product of the two principal curvatures of a surface:

$$K = k_1 \cdot k_2 = \frac{1}{R_1} \cdot \frac{1}{R_2} \tag{2.1}$$

This outcome of the Gaussian curvature can give different kind of surfaces. If the Gaussian curvature is positive than both curvatures are pointing in the same direction. When the Gaussian curvature is negative than both curvatures are pointing in another direction. The Gaussian curvature could also be zero, which implies that either both curvatures are zero or one of the two curvatures is zero [6].

- K > 0, a positive Gaussian curvature: synclastic surface
- K < 0, a negative Gaussian curvature: anticlastic surface
- K = 0, a zero Gaussian curvature: monoclastic surface when one curvature is zero and zeroclastic surface when both curvatures are zero

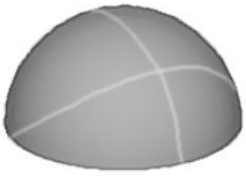

Figure 2.1: K > 0 : synclastic surface [6]

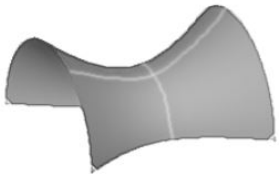

Figure 2.2: K < 0 : anticlastic surface [6]

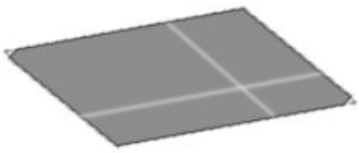

Figure 2.3: K = 0 : zeroclastic surface [6]

In structural terms one speaks of a synclastic surface when the Gaussian curvature is positive at all points, and the surface is completely in compression or in tension. When the Gaussian curvature is negative at all points one speaks of an anticlastic surface. In that case the surface is subjected to a combination of compression and tension. A complex surface consists of a combination of these defined surfaces [6].

2.3. Issue of Architectural Design

Since several years these free-form structures have emerged in architectural practice. With the advent of increasingly powerful yet easy to use parametric modelling tools, the geometry is often set by the architect based on aesthetic and functional criteria but without much consideration for structural performance. The resulting free-form geometries therefore often combine areas with strong curvature where shell behaviour can be activated, with flat or shallow regions where the forces need to be transferred in bending. The architectural functionality of those geometries is vaguely understood by the developers.

A digital revolution has taken place in the architecture and construction industry, especially from 2D programs into 3D modelling. This has contributed to an increase of free-form structures around the world. The modelling technology has made it possible to make complex geometries from minimal design input [14]. Architects started designing beyond the conventional limits, which has made it possible to create and develop complex buildings. However, the side effect of being able to create any kind of form in the computer is that it can result in extreme shapes that require extreme structures and years of development, if possible at all. Therefore it should be questioned what is still reasonable to be constructed. The lack of taking this into account is an issue when generating complex structures. Moreover the usage of the digital processes often results in projects that neglect actual material characteristics [35].

These structures emphasize the structural engineer's problem of dealing with complex geometry. The challenge for the engineer is to devise an integrated structural concept that can be adapted in a free-form structure to satisfy the local structural demands of the material in an efficient manner. Over the last couple of years advances in analysis and fabrication techniques have enabled the construction of complex timber structures [3]. The architect is the one who has the creative ideas and the structural engineer makes it possible to realize these buildings. A combination of both fields makes it possible to reach to a next level in the construction industry. Therefore the applications for architectural design should be better compatible with the applications for structural design [13]. This will make it easier for the architect and the structural engineer to have a close collaboration and deal with the architectural design issues better to find an optimal solution.

2.4. Development in Timber Production Techniques

There is a long production process required before the wood from the tree becomes a structural element. This process involves the making of a particular products form the tree and assembling them into the desired products. Timber products have to meet structural requirements and different types of constrains related to fabrication [29]. Therefore it is important to take the production technology of timber into account during the design process. The term timber is used when wood has been processed or converted into structural elements. Wood as a natural material is anisotropic as it has different properties in different directions. To improve the properties for specific structural uses the wood is made into parts which are combined in different ways to create timber with specific characteristics. Different wood-based products have occurred on the market in the last couple of years.

2.4.1. Structural Timber

Timber is an anisotropic material and strength grading is important in the process of converting wood. Visual and machine strength grading are needed to make timber a reliable structure material. Wood is originally a natural raw material and the properties not only vary from species to species but even within a particular species. The standard wood-based product is solid timber, which has one strong axes parallel to the grain. The product $C24$ is a solid softwood product, which has a bending strength (f_{mk}) of 24 N/mm^2, a mean elastic modulus ($E_{0,mean}$) of 11000 N/mm^2 and characteristic density (ρ_k) of 350 kg/m^3.

The goal of structural timber is to generate more homogeneous wood-based products. The production process differs from making planks and veneer products before combining them into a structural element. The production processes and realised properties of developed timber materials will be described. These different materials have widened the range of possibilities for timber constructions. Timber construction is mostly limited to the use of softwood. Hardwood has a higher strength and stiffness but converting this product is costly and are more susceptible for insects. The development of materials with similar structural properties in all directions has resulted in advantages compared to solid timber.

Glue Laminated Timber

Glue Laminated Timber, also called glulam, is an engineered building material which extends the use of traditional use of timber. The product is made of planks with a maximum thickness of approximately $50mm$, which are joined lengthwise by means of finger joints. This continuous section is cut into laminations of the required length. In figure 2.4 the build-up of the cross section will be shown. Then glue is applied to the laminations, which are placed besides each other and they are pressed together. It is not uncommon to see beams with a depth up to 2 m and lengths of 30 to 40 m. Transport of beams exceeding $2,5$ m in width,

Table 2.1: Strength classes for glued laminated timber to EN 14080

Strength classes for glulam				
Strength and stiffness properties in N/mm^2		GL 24 h	GL 28 h	GL 32 h
Bending edgewise	f_{mk}	24	28	32
Tension parallel to the grain	$f_{t,0,k}$	19,2	22,3	25,6
Tension perpendicular to the grain	$f_{t,90,k}$	0,5	0,5	0,5
Compression parallel to the grain	$f_{c,0,k}$	24	28	32
Compression perpendicular to the grain	$f_{c,90,k}$	2,5	2,5	2,5
Shear edgewise	$f_{v,k}$	3,5	3,5	3,5
Mean modulus of elasticity	$E_{0,mean}$	11500	12600	14200
5 % modulus of elasticity	$E_{0,05}$	9600	10500	11800
Density in kg/m^3				
Characteristic density	ρ_k	385	425	440

$3,5\,m$ in height or $16\,m$ in length require specialized transport. The seven strength classes of glulam are $GL\,20$, $GL\,22$, $GL\,24$, $GL\,26$, $GL\,28$, $GL\,30$ and $GL\,32$ could be found in EN 14080 Table 4. Each strength class is followed by the suffix h, where the glulam is homgeneous, or c, it is is combined. In table 2.1 the material properties for $GL24h$, $GL28h$ and $GL32h$ are given.

Glulam is not a new structural timber material but it has been further developed for the application of curved beams. For a single curved beam, the minimum radius of glulam is between 8 and $9\,m$. The recent production with CNC machining or a 3D glulam press made it possible to develop double curved glulam [19]. The production techniques will be explained further at the end of this chapter in section 2.4.2. Double curved beams are bent in one direction and twisted or bent as well in the other direction. The bent in the second direction is restricted by more limitations then the bent in the first direction. Therefore one curvature direction is dominant.

Figure 2.4: Glue laminated timber build-up cross section [22]

Figure 2.5: Cross laminated timber build-up cross section [8]

Table 2.2: Characteristic values for solid timber (EN 338) and cross laminated timber (EN 16351:2015)

Characteristic values for C24 and CLT			
Strength and stiffness properties in N/mm^2		C 24	CLT
Bending edgewise	f_{mk}	24	24
Tension parallel to the grain	$f_{t,0,k}$	14,5	9,8
Tension perpendicular to the grain	$f_{t,90,k}$	0,4	0,12
Compression parallel to the grain	$f_{c,0,k}$	21	21
Compression perpendicular to the grain	$f_{c,90,k}$	2,5	2,5
Shear edgewise	$f_{v,k}$	4,0	2,5
Mean modulus of elasticity	$E_{0,mean}$	11000	11600
5 % modulus of elasticity	$E_{0,05}$	740	650
Density in kg/m^3			
Characteristic density	ρ_k	350	480

Cross Laminated Timber

With regard to materials, it is undeniable that cross-laminated timber (Crosslam or CLT) has widened the range of possibilities of timber constructions the most as it opened up the development of high rise timber buildings. CLT consists out of an uneven number of layers, which are ordered crosswise to each other under an angle of 90 degrees [7]. The different layers are connected by adhesive bonding. The advantage of this product is that it has the ability to transfer the load in two directions. The maximum sizes of CLT are $3,1\ m$ in width, $16,5\ m$ in length and with a thickness of $400\ mm$. For structural calculations the mechanical properties of $C\,24$ should be used [7]. Only lamellas which are arranged in the direction of the mechanical stress may be taken into consideration for the calculation of the characteristic cross-section values. The material properties for $C\,24$ and CLT are given in the table 2.2. The main difference with solid wood $C\,24$ is that the density of CLT is $480\,kg/m^3$. The dimensional stability differs for parallel panel plane $0,01$ % per % and for perpendicular $0,20$ % per % change in moisture content [8].

Laminated Veneer Lumber

Laminated veneer lumber (LVL) is produced from rotary-peeled 3 mm graded softwood veneers [1]. The multiple layers of veneers are glued together to form a continuous wide product. The fabrication of LVL has the benefit of the redistribution of large defects into small ones. During the fabrication logs are peeled to veneers with thickness of 3 mm. In figure 2.6 the build-up of the cross section are shown. The two main products are LVL without crossband veneers and LVL with crossband veneers. In table 2.3 the material properties are given for both products, where suffix S stands for structural. The standard LVL is wood based composite consisting veneers, glued together predominantly parallel to the direction of the grain. LVL $50\,S$ has an high axial strength compared to typical glulam. The panels could be manufactured up to $25\ m$ long. LVL $50\,S$ having a bending strength of $44\ N/mm^2$ compared to $24\ N/mm^2$ for standard glulam, although they are made from the same species of timber. LVL $36\,S$ cross is a similar product with crossband veneer. Crossband veneer, whose fibres are oriented perpendicular to the fibres of the face veneers. This means that every fifth veneer is glued in the perpendicular direction. This way of build-up increases the lateral bending strength and stiffness of the panel, which increases the shear strength of the material. Cross-bonded veneers give a reduction in moisture-dependent variation across

Table 2.3: Characteristic values of LVL according to EN 14374:2016-07

Characteristic values of LVL			
Strength and stiffness properties in N/mm^2		LVL 50 S	LVL 36 S cross
Bending edgewise	f_{mk}	44	32
Tension parallel to the grain	$f_{t,0,k}$	35	24
Tension perpendicular to the grain	$f_{t,90,k}$	0,8	5
Compression parallel to the grain	$f_{c,0,k}$	35	26
Compression perpendicular to the grain	$f_{c,90,k}$	6	9
Shear edgewise	$f_{v,k}$	4,1	4,5
Mean modulus of elasticity	$E_{0,mean}$	13800	10500
5 % modulus of elasticity	$E_{0,05}$	11600	8800
Mean modulus of elasticity, perpendicular	$E_{90,mean}$	-	2400
Mean shear modulus	$G_{0,mean}$	500	550
Density in kg/m^3			
Characteristic density	ρ_k	480	480

the width of the panel. It provides a good two dimensional stability and a high compression strength but it has a lower mean elastic modulus of 10500 N/mm^2.

Baubuche

The recent production of LVL made of high strength hardwood such as beech, oak, chestnut and several tropical hardwoods, further broadens architectural horizons and meets the demands of forestry towards sustainable and soil/climate apt tree cultivation. BauBuche is a laminated veneer lumber made from locally sourced beech wood, see figure 2.7. The costs are kept at the same price level as conventional softwood due to a new process technology [30]. The production line is set up that hardly any loss in value of material will be there. The material properties for Baubuche-S and BauBuche GL70 are given in table 2.4. In table 2.5 the material consumption of Baubuche $GL70$ has been compared with the other material properties of C 24 and GL 28. The calculation of this assumption is based on service class 1, load-duration class: medium-term and an uniform cross-sectional height of 300 mm.

Keel-web Element

A lot of different new timber products have been developed. These products help to create different type of elements, which contributes to more possibilities for the timber construction. However timber is increasingly being used due to its ecological benefits. Therefore new developments seek to create lightweight structures, using less material while creating elements with the same strength. Keel-web element is a double-skinned wooden composite element with thick skins of finger joined softwood. The web consist of S-shaped bent thin wooden based panels, being made of plywood or OSB material [2]. The elements have a high load capacity and stiffness and it provides light weight structures. The build-up of this element is made with a fully automated process and it could have length up to 35 m with an elasticity modulus of 11000 N/mm^2. Currently the relaxation behaviour of the high bending stresses, induced by the S-shaped webs still should be improved [2].

Table 2.4: Characteristic values of BauBuche according to DIBt (EN 14374) [30]

Characteristic values of BauBuche			
Strength and stiffness properties in N/mm^2		BauBuche-S Beam $Z-9.1-838$	BauBuche GL70 $Z-9.1-837$
Bending edgewise	f_{mk}	75	70
Tension parallel to the grain	$f_{t,0,k}$	60	55
Tension perpendicular to the grain	$f_{t,90,k}$	1,5	1,2
Compression parallel to the grain	$f_{c,0,k}$	57,5	49,5
Compression perpendicular to the grain	$f_{c,90,k}$	14	8,3
Shear edgewise	$f_{v,k}$	8	4,0
Mean modulus of elasticity	$E_{0,mean}$	16800	16700
5 % modulus of elasticity	$E_{0,05}$	14900	15300
Mean modulus of elasticity, perpendicular	$E_{90,mean}$	470	470
Mean shear modulus	$G_{0,mean}$	850	850
Density in kg/m^3			
Characteristic density	ρ_k	730	680

Table 2.5: Comparing material consumption [30]

Material consumption %			
	C 24	GL 28	BauBuche GL70
f_{mk}	200 / 100%	92 / 46%	57 / 29%
$f_{t,0,k}$	200 / 100%	129 / 64%	44 / 22%
$f_{c,0,k}$	200 / 100%	152 / 76%	56 / 28%
$f_{v,k}$	200 / 100%	240 / 120%	104 / 52%
$E_{0,mean}$	200 / 100%	175 / 87%	132 / 66%

Figure 2.6: Laminated veneer lumber build-up cross section [32]

Figure 2.7: BauBuche GL70 build-up cross section [30]

2.4.2. Manufacturing Development

In other industries robotic systems are widely used to perform automated manufacturing tasks. The development in the construction industry took a little bit longer due to the already existing complex combination of prefabrication and building on site. The way how a timber structure is modelled with the use of software is essential. Timber is an anisotropic material, which has one strong axes parallel to the grain. This needs to be taken into account for the software of automated manufacturing. The development of materials with more similar structural properties in all directions has resulted in using robotic systems.

A structural simulation of the structures is carried out by structural engineers with the use of Finite Element Method programs to assess the structural integrity. The use of these programs requires theoretical and practical knowledge of the materials used. Estimation will be made for how the structure will behave when it is build. When modelling with timber material it is even more crucial how the structural behaviour is modelled. The possible differences in quality of material and the estimations made during modelling need to be taken into account when the process from design till production will be made digital.

The complexity rises when complex digital designs are used as input for automated manufacturing processes of the building material. This requires advanced computational design tools that can help overcome the architectural challenges and the limitation imposed by the manufacturing techniques. With the proper tools available automated manufacturing could be useful as it makes a direct transfer possible.

For the last couple of years computer numerically controlled (CNC) machines have been used. CNC machining uses computer models to quickly and accurately produce specific pieces out of timber. CNC machine design is developed with capabilities such as multi-axis control, error compensation and multi-process manufacture. However the existing systems are still be limited for the communication with computational design tools. The CNC machine tools have issues of interoperability and adaptability [37]. It is required that all knowledge of each stage should be transferred without information loss. STEP-NC provides a possibility for a complete structure data model, which contains geometrical and technological information. It could be adapted to any CNC machine tool that has the ability to execute the machining tasks [37].

Robotic Timber Construction (RTC) combines robotic assembly procedures and advanced digital design of non-standard timber structures [36]. Robotic fabrication is suitable for iden-

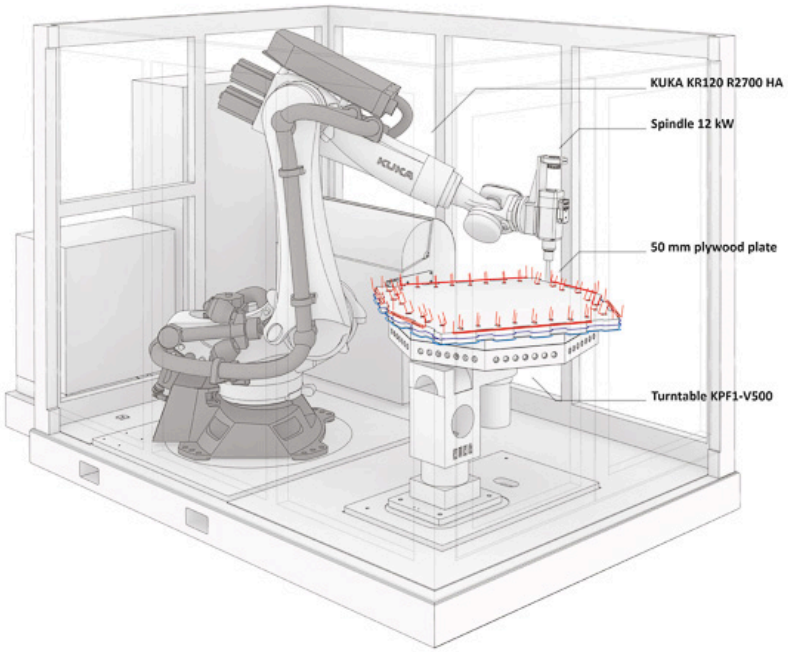

Figure 2.8: Robotic fabrication is suitable for identical or completely different products [34]

tical products or completely different ones. Robotic systems have the ability to transfer digital design data directly to assembly operations. For the design process RTC should be informed over material, construction and fabrication criteria and adapt to multiple functional requirements. It consists the ability to evaluate the structural integrity of the final form and the tolerances of the build-up process. The integration of digital design and automated fabrication makes it possible to prefabricate complex timber structures. RTC is still in its infancy but it will change the traditional view of timber construction [36].

2.5. Conclusion

In this chapter it has become apparent that the design process is much more subtle for free-form structures as it goes beyond the basics of what is known. Free-form is not conforming to a regular or formal structure. This is what makes it interesting to create special and sophisticated buildings. The issues with complex architectural design arise from the increasingly powerful parametric modelling tools without a realistic approach from the use of material. Normally after structural analysis the shape of a free-form structure will be further developed to find the balance between structural integrity and design. It is meaningful to search for a solution for the issues with complex architectural design and making use of the creativity of an architect.

In case of complex structures the choice of material has a lot of influence. Timber products have to meet structural requirements and different types of constrains related to fabrication, transportation and assembly. Therefore it is important to take the production technology of timber into account during the design process. It is also difficult to later on implement the design of connections since this has a large influence for timber structures. However this is normally one of the latest steps in the design process. The research into new possibilities regarding timber materials is beyond the scope of this research. Therefore the different products, which have occurred on the market in the last couple of years have been investigated.

From these products the most suitable timber materials are glued laminated timber (Glulam) and laminated veneer lumber (LVL) for the free-form timber structure since these are

more homogeneous wood-based products. The advantage of using these reconstituted wood products is that larger dimensions are available and higher characteristic strength values can be achieved. Glulam has a higher strength than raw timber material with similar properties. The fabrication of LVL has still more benefit of the redistribution of large defects into small ones.

The development in the timber industry has a promising future in the face of global sustainability challenges. For this project it is interesting to look into designing a structure to realise a shape that is predefined and given by the architect. The benefit of easy to use computational tools brings the construction industry in case of manufacturing and assembly to a higher level. Therefore computational modelling will play an important role during this research. The challenge will be to adapt the architectural design into a free-form structure, which satisfies the local structural demands of timber in an efficient manner.

3

State-of-the-Art for Free-form Timber Structures

In the previous chapter the main development in the timber industry has been outlined. In the past a couple of those developments have already been adapted in complex timber buildings. The purpose of this chapter is to give an overview of the current state-of-the-art for free-form timber structures. This chapter will start with discussing actively bent grid shell structures, followed by the grid shell structures composed of segmented members and it ends with discussing plate structures. The focus will be on the structural systems that are used for the various structures.

3.1. Actively Bent Grid Shells

Grid shell structures are related to shell structures in terms of geometry but there is a difference. The definition of grid shell structures is a ”structure with the shape and strength of a double curvature shell, but made of a grid instead of a solid surface” [12]. Both structures can transmit applied loads into membrane forces, stresses that act in their plane. Both structures have a typical appearance; a grid shell structure consists of steel members and a shell structure consists of concrete surfaces.

A true shell structure made of timber is difficult because wood is anisotropic material. Therefore a grid shell structure suits better for complex timber shapes. There is a way of making these shapes from standard elements with a grid shell technique. The grid shell technique is to lay out a framework as a flat sheet of components and then push it into the desired shape. This is possible due to the low torsional stiffness of timber and in order to have shell action diagonal bracing is added after providing in-plan shear strength and stiffness [17].

This grid shell technique is used for form finding a timber grid shell. Thin sections are possible since these grid shells are structurally efficient by its geometry. A benefit is that the costs are lower for double curved shell roofs made of timber instead of using techniques with other materials.

Timber grid shell structures, such as the Multihalle for the federal garden festival in Mannheim or the Savill Garden Building in Berkshire, have been the result of a creative-generative process. Both grid shells use the elasticity of their elements to create a curved lattice structure from straight wooden laths. Both will be discussed here with explaining their structural system more in detail.

Figure 3.1: Multihalle Mannheim [4]

3.1.1. Multihalle Mannheim, Germany

One of the first free-form timber structure was the Mannheim Bundesgartenschau Multihalle. This structure was built as a temporary building in 1976 but nowadays it is still standing in Mannheim, Germany. The light weight building spans up to 80 metres. The German Architect Frei Otto used physical models for the structure as the primary method of form-finding. The double layer grid mesh contains four layers with 50 mm by 50 mm Hemlock laths [15]. Hemlock is softwood that toughens up over time [15].

During the time of construction, computer analysis had very limited capabilities and working with this was a specialist technique. Therefore, the physical models were important during the design process and to form-find the geometry for the Mannheim shell. The form finding process involved a hanging chain model and an idealization model, which was made with the computer. The interactive nature of form-finding process is important to achieve the full capability of the grid shell technique. The technique of geodesic measurement with stereoscopic cameras was used on the physical model to determine the node locations. The results for the structural analysis were gained by tests on 1 : 60 Perspex model of the Multihalle [15].

The timber material Canadian Hemlock has a mean modulus of elasticity of 10.400 N/mm^2 and a maximum dry bending strength of 38 N/mm^2. The self-weight loads could be supported by the Hemlock laths under long term axial compression. The six-metre-long laths were joined by means of finger joints into $30-40\,m$ long lengths. These were laid out on site at 500 mm spacing with two layers in each direction. The straight grain of the Hemlock allowed for good longitudinal stiffness and made it capable to resist other applied loads, like wind and snow. There are stress limitations on the tightness of curvature to which laths can be bent during construction. A tight radius of curvature of $6-12\,m$ was needed during construction for its final shape. The laths with a moisture content of 12 per cent were delivered on site and impregnated with a fire retardant [11].

The design of the node detail was important because the grid shell structure was made out of a very large numbers of nodes. The Mannheim Multihalle has 33.000 joints to assembly the lattice and to keep the structure in position. The four layers of timber were connected by bolts. The inner two layers had round holes and the outer two layers slotted holes. The function of the slotted holes enables the relative movement between the layers during formation, while the single bolt with round hole enables rotation at the node [15].

Figure 3.2: Savill Garden Gridshell [27]

Although the out of plane shear stiffness was provided by bolting and shear blocks, steel tension cables were needed to provide the diagonal stiffness to the shell. The crossed cables with a thickness of 6 mm provide the bracing for shell action. Bracing triangulates the structure and provides in-plane shear strength [11]. The twin cables were connected at every $6th$ node. The forces on the bracing structure are derived by using a second order analysis, whereby the equilibrium of moments and forces are analysed by considering the deformed shape of the structure. The forces flow down from the shell to the perimeter, which is composed of different boundary types but mostly concrete. The timber laths were connected to a wooden board with bolts, each with a correct angle. The boards were then connected to concrete blocks using steel brackets to flow the forces into the foundation [31]. Using a clamp is a commonly used method for forming the edge of a gridshell. The construction of this building opened the doors for the development of more free-form timber structures.

3.1.2. Savill Garden Gridshell, United Kingdom

The Savill Garden Building was built in 2006 in Windsor Great Park, Berkshire, United Kingdom. This building is also a timber gridshell, which spans up to 90 m with a width of 25 m [16]. The form of the roof of the Savill Building was derived from a basic geometric shape. The perimeter of the shape is set out using arcs of two intersecting circles. The centre line of the roof, which is the mid-line between the circles, is generated by a sine curve. The amplitude of this curve is varying from the top of the domes into the bottom of the valleys. In the other direction, the cross section is set out as parabolic curves of varying shape [15]. From this a surface is generated into the three-domed double curved structure. The surface is divided into a grid of equal lengths elements.

During construction, the timber lattice must allow rotation at the nodes and bending and twisting of its laths. The laths are made from the material Kerto-S (Laminated Veneer Lumber). The timber lattice is supported by a perimeter ring and quadruped legs made of steel tubes. Kerto LVL fingers are bolted to the steel perimeter ring. To save cost and create an elegant structure the cables for bracing are omitted and plywood covering is used. The gridshell is made of a regular grid of 80 mm by 50 mm sections of larch timber [15]. The final layer consists out of cladding in the material oak.

The self-weight load of the structure is not critical since timber is a light weight material. More critical are the variables forces induced by wind and snow load. The structural plywood is used to transfer the forces through the domes or valleys of the roof, to the steelwork and

into the foundations. In case snow is gathered on the roof, which will act as a temporary dead load, then the plywood in the valleys acts in tension and induce compression in the larch laths of the domes. In case that a strong wind blows trough, an uplift force is created under the roof. In this situation, variable load will act in the opposite direction; the valleys go into compression and the domes into tension. In both situations, the timber shell works with the steel perimeter ring to carry the load to the supporting legs.

As mentioned before with the design and construction of the Mannheim Multihalle, most important in a grid shell structure is the design of the nodal connections. With the Savill Garden, there are stress limitations on the tightness of curvature to which the lath can be bent as well. The limited depth of a lath in a single layer grid shell results in an out of plane bending stiffness. The depth of a lath that is needed to resist asymmetric loadings would be too stiff and deep to permit bending of the flat lath into its finale shape. Therefore, a double layer grid shell is utilised. The laths of the lattice have a small section to permit bending into the desired geometry. It is composed of four layers, which consists of two single layers sitting one upon the other. In between the layers timber shear blocks were positioned and fixed with screws [15]. For the Mannheim grid shell all four laths were bent together. For this structure, the bottom two laths were bent into shape and then the shear blocks were put into positions. Upon the shear blocks the upper two laths were screwed into place. This technique enabled greater spacing of the layers, which leads into greater out-of-plane strength and stiffness.

In Summary

The Mannheim Multihalle and the Savill Garden structures have thin sections since these grid shells profit because of their geometry. The depth of the lath is limited to make it possible to bend the structure into the desired shape. Both actively bent grid shells transfer the membrane forces via the roof into the foundation. All the members of these structures are continuous, which is an advantage of this structural system since the flow of forces will not be disturbed. The difference between the two structures is that diagonal stiffness is provided by steel tension cables for the Mannheim Multihalle and by covering the lath with plywood layer for the Savill Garden.

3.2. Grid Shell Structures Composed of Segmented Members

The development of sophisticated computer form-finding and analysis technology provides new opportunities for the modern use of timber structures. Especially when it comes to assembly of the structure out of the computational design. A focus lies on the segmentation strategy that depends on structural requirements and constraints, that are related to fabrication, transportation and assembly. The following free-form timber structures are realised from conception to fabrication by using their complex digital work flow [29]. The flexibility of modern digital fabrication techniques makes it possible to construct and fabricate other types of structure without the grid shell technique. The grid shell timber structures, such as the Haesley Nine Bridges in South Korea or the Centre Pompidou-Metz in France, have been the result of using computational design. Both will be discussed here with explaining their structural system more in detail.

3.2.1. Haesley Nine Bridges, South Korea

The clubhouse, Haesley Nine Bridges, has been built in 2010 with a lattice of beams in single and double curvature. The roof structure has been made out of glued laminated timber (spruce) and it is $72\,m$ and $36\,m$ wide, with a height of $13.6\,m$. The roof has been be supported by 21 columns and with cantilevers of $4.5\,m$ in all directions. The roof surface was divided into a grid of $9\,m$ x $9\,m$ [21]. The structure is unusual since the roof surface turns smoothly into the columns. This makes it an entirely different timber structure compared to the ones

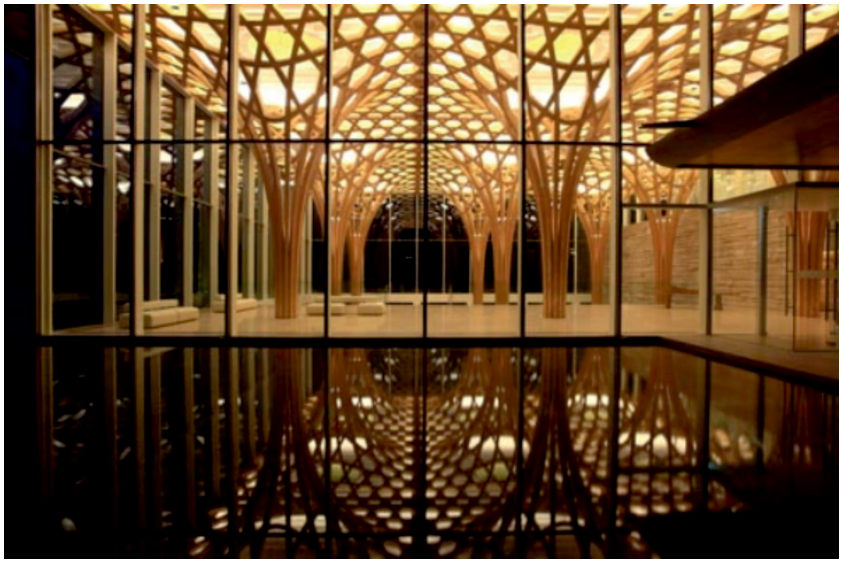

Figure 3.3: Haesley Nine Bridges Golf club [9]

discussed in section 3.1. The hollow circular columns gradually widen from a wide of 0.6 m at the base to 1.5 m at a height of 9.6 m. Each column consists of twelve members of 136 mm x 200 mm, arranged in a circle [21].

The geometry of the roof was developed with computer software as a parametric model. A regular grid was projected onto the curved roof geometry, which enabled the axes of the beams to be determined. The roof was assembled from five types of elements as a result of the regularity of the geometry. The different axes intersect with each other to produce a network of hexagons and triangles. Every beam segment had to be designed individually to fit into the double-curvature roof surface. New software has been developed to make it possible to process this complex structure. It was possible due to the parameterization and due tothe automation of the design steps to plan, design, fabricate, transport and erect the roof structure in eight months.

For the first time, traditional wood joints were used in an engineered timber construction [21]. Therefore a further development in nodes detailing was made for traditional scarf and halving joints. A scarf joint is a method of joining two members, each end of the member has been cut at an angle. The longitudinal connections between the beams are made with this form of joints. The connection at the intersection of the different beams makes use of halving joints. A halving joint is a woodworking joint in which the members are joined by removing material. At the point of intersection a piece of material will be removed from both members to overlap. The advantage of this type of structure is that the bending stiffness of the structure increases and it simplifies the erection.

Despite the fact that the structure could be divided into five type of elements, fabrication was a challenge. Especially the production of the individual glued laminated timber elements proved to be difficult. The thickness of the laminations for these elements depends on the radius of curvature. The beams had to be assembled by hand for those with a radius of curvature smaller than 1 m. The ratio of the component sides changes continuously and therefore the double-curvature beams are twisted. The elements could be no longer than 11 m because they had to be transported to South Korea in containers. The beam segments were assembled on site in a tent, in which the temperature and humidity were maintained at a constant level suitable for gluing. The glued laminated timber members were assembled layer by layer and were joined together by screw-pressure gluing [21]. After this only 32 elements had to be joined together for the erection of this distinctive roof structure.

Figure 3.4: Centre Pompidou-Metz during construction [24]

3.2.2. Centre Pompidou-Metz, France

Another example of the computing parametric design is the Centre Pompidou-Metz in Metz, France. The Centre Pompidou-Metz is a concrete building with a timber roof structure and it was opened in 2010. The double curved free-form surface has a dimension of $52\,m$ by $104\,m$. The roof has a maximum free span of $50\,m$ and it is supported by different elements [24]. The geometry of the roof was developed using computational form-finding techniques. This geometry is based on a 'minimum surface' and it forms an anticlastic surface geometry with a negative Gaussian Curvature. The cladding is made of pre-stressed PTFE glass fibre membrane for translucency. The area beneath the roof is partially enclosed by a façade, which is self-supporting.

A close collaboration was necessary between the architect and the structural engineer because both were working from a 2D and 3D approach. The form-finding process had many iterations to achieve an architecturally acceptable geometry. This process was performed with the structural software GSA Analysis. GSA was used as an iterative force-density form-finding analysis [24]. All the nodes were given x,y supports, which were only able to move vertically, except for the different supporting positions under the roof surface, which were given pin supports. The tension in each element was made proportional to its length, giving the minimum strain energy for the form of the element.

The structure is categorized as a 'three-way timber gridshell type system' but it is not a real timber gridshell. Since the structure works as a hybrid system with shell action and catenary action but mostly bending action. The structural system was developed as a lattice of simply supported beams. These beams were arranged such that each individual element is supported by the adjacent one. Although the plan was initially to make the beams of the timber material Kerto-S LVL, but due to a low budget this was replaced for standard softwood glulam (GL24h). The beams were joined by timber-to-timber connections with the Vierendeel truss type system of two planks. The thickness of the laths was reduced to avoid reduction of allowable timber strength as given in Eurocode 5.

The fabrication process of the double-curved and twisted glulam planks and node connection was inconvenient for several reasons. First of all, the planks were manufactured as oversized straight sections of glulam. A CNC milling machine was used to provide the required dimensions. The disadvantages of this method are that it gives a high wastage and reduction from the axis at an angle of the timber grain. Secondly for the node connection,

each plank had a predrilled oversized hole through its centre. This was required due to erection tolerance and the planks were connected with M24 bolts [24].

In Summary

The flexibility of modern digital fabrication techniques makes it possible to construct and fabricate other types of structure without the grid shell technique. The Haesley Nine Bridges and Centre Pompidou-Metz have proven that computational modelling can be used from conception to fabrication. An interesting aspect of the Haesley Nine Bridges is that traditional wood joints are used despite the complexity of this roof structure. The parametrisation of the geometry and the automated design steps makes it possible to speed up the whole process till erection of the roof structures. From the Centre Pompidou-Metz it has become clear that there was high wastage of material and reduction from the axis at an angle of timber grain to produce all the different curved and twisted sections.

3.3. Plate Structures

In the recent years, there is a change from grid shell timber structures into shell structures made of plates. In general plates are two-dimensional structures, which can be loaded in two different ways. Multiple planar plates could be combined into a three-dimensional structure. The main important part for a sufficient system of a shell structure is the design of the connections between the plates. Another reason besides the anisotropic properties of timber is that shell structures are not often built in timber is due to the high manufacturing costs. A particular benefit of using timber is the low self-weight of this material. The first timber shell structures have been build, such as the Elephant house in Zürich, Switserland and the Landesgartenschau Exhibition Hall in Schwäbisch Gmünd, Germany.

3.3.1. Elephant House, Switzerland

Figure 3.5: Elephant House, Zoo in Zürich [21]

Figure 3.6: Detail of roof from the Elephant House [18]

The Elephant House is built in 2014 at the Zoo in Zürich, Switserland. A multi-layer lightweight construction is developed for the shallow shell. The free-form timber roof shell has a diameter of 80 m and it covers an area of 6400 m^2. The dome has a maximum height of 18 m in the middle. The waving edge of the dome varies with a distance between 0.8 m and 10 m to the ground [23]. The five lowest points of the edge are the support zones of the roof. The geometry is based on a shell loaded in compression of a reversed suspended membrane model. The shell is supported by the prestressing force of the steel cables. The forces from the shell are transferred to the supports via a reinforced concrete ring beam.

Figure 3.7: Dieter-Paul Pavilion, Schwäbisch Gmünd [20]

It was the first time that a shell structure was made with timber because normally this kind of structure would be made of concrete. The cross-section consists out of three layers of CLT panels for a more uniform load distribution in all directions. The layers are nailed together and screwed on top of these layers, are solid timber ribs with a finishing Kerto-Q panel. On this structure timber blocks are attached to create space for services. The final depth of the cross-section is about 90 cm [23].

Parametric software was used for an iterative form-finding process. Different programmes were needed to create a parametric 3D model. At every stage specific requirements could be integrated into the model. The free-form surface had to be converted into flat strips for the production and erection. Each panel required a separate machine file code and fabrication drawing. The automated panel production produced 200 unique panels for each layer [21]. To produce a linear elastic, composite cross section that could be assembled on site. The double curvature roof shell was erected easily due to panel construction, which made it able to bend about two axes.

3.3.2. Landesgartenschau Exhibition Hall, Germany

The Landesgartenschau Exhibition Hall was built in 2014 in Schwäbisch Gmünd, Germany and this building should stand at least till 2019. Therefore, the experimental hall is not a temporary construction and it should meet the requirements of the design codes. The structure has a height of 6 m, a length of 17 m and a maximum width of 11 m [25]. The whole structure is closed except for the entrance at one side where the glass façade was installed. Especially for this project, local wood is used from the forest of Bäden-Württemberg.

This structure is made of segmental plate shells, which are shell structures composed of planar plates. An advantage of these segmental panels is that they could generate local bending stiffness. Each panel has a dimension of about 1.2 m and a thickness of 50 mm. Beech plywood is used as construction material and it provides structural properties in all directions [26]. A wood finger joint connection is made between two panels, which take the in-plane shear forces. It enables the use of thinner timber plates and thereby increases the efficiency of the entire system as well. For the axial forces and out-of-plane shear forces, crossing screws were needed in the joint connections [26].

The orientation of the segments has an influence on the transfer of the forces. This pattern defines the locations of the connections, which are the weak points in the structure. The trivalent geometry of the panels provides kinematically stability of the segmental plate shell. Therefore the weak points did not need bending stiff connections. ”The global geometry of a segmental plate shell is always a polyhedral surface” [25], which contribute to the structural stability with a triangular mesh.

The segments were produced by a timber construction company with the use of robotic technology. CNC machining made it possible to cut rectangular plywood panels into the polygonal plates. After this the edges of the plates where modified with the help of a robot-arm. The robot-arm produced the milling of finger joints and drilling of the holes for the screws [26]. A temporary construction was built on the building site for assembly of the plates. The plates were built layer by layer, starting from the ground. After this the prefabricated isolation panels, waterproofing and the glass façade were installed to finish the complete structure.

In Summary

A sufficient system of a shell structure comes down to the design of the connections between the plates. Therefore special connections with screws have been developed for the Elephant House and Landesgartenschau Exhibition Hall. A disadvantage for this structural system is that it is made from different plate elements, which makes it difficult to transfer the forces. The Landesgartenschau Exhibition Hall has the advantage with the geometry to solve the problem of transferring the membrane forces. The cross section of the Elephant House is made from multiple layers since the geometry is a shallow shell. The cross section of this structure has a large depth, which is not sufficient due to amount of material.

3.4. Conclusion

An overview of the current state-of-the-art for free-form timber structures has been given. The timber structures have been divided into three different structural systems. Each group contained two complex structures, which are each outstanding on their own. The first and most common structural system for a free-form timber structure is actively bent grid shells. The grid shell technique makes it possible to actively bent the structure into the desired shape. An advantage of this thin structures to transfer the forces is that all the members of these structures are continuous. Therefore it is meaningful to strive for a continuous surface. The increasing advanced computational design tools created new opportunities for the modern use of timber structures. From this point it is interesting to investigate if any kind of shape without the advantage of their geometry could be realised in the future to meet the demand of the architectural design. The grid shell structures composed of segmented members are realised by using their complex digital work flow. The further lies into the development of the parametrisation of the geometry and the automated design steps for a more efficient design process.

The technique for grid shell structures has improved over the years. The development of a structure with a solid timber surface is still open. There has been a change from open grid shell structures into shell structures made of plates. A step in the right direction has been made with the shell structures Elephant house and the Landesgartenschau Exhibition Hall. These structures have only shell behaviour due to their geometry. However the resulting free-form geometries from the architect often combine areas with strong curvature where shell behaviour can be activated, and with flat or shallow regions where the forces need to be transferred in bending moments. It is interesting to explore and develop a structural concept in timber which take both structural behaviours into account. The grid shell structure of the Centre Pompidou-Metz has shown that it is possible to take both behaviours into account.

A disadvantage of this structure is the huge amount of material that was needed and the fabrication process was inconvenient.

As shown in this chapter different systems have been explained for complex timber buildings. The knowledge of this structures will be used for the development of the structural concept. It was found that a double layer timber structure with different height for structural members has not been built, at least not on a large scale. In the next chapter the case study of a timber roof project will contain the different aspects of an architectural design with a smooth, continuous solid surface. The structural system of the Landesgartenschau Exhibition Hall is not applicable for a structure which has shell and bending behaviour. The production of the segmental plate shells is an inspiration for the design of the timber roof project. The structural system of Haesley Nine Bridges is made from segmented members, which generates continuity within the large units. From this structure it can be seen that traditional wood joints can be used, despite the complexity of any structure. The focus will be on the possibilities of using simplified connections. Another interesting structural system is the build-up of the different layers for the Elephant House structure. It is interesting to develop a double-layered structure, which will make efficient use of the material.

4

Design Criteria

This chapter describes the design criteria of the case study; a timber roof project that is relevant for the company Knippers Helbig. The project is located in Sindelfingen, Germany. The load assumptions will be based on the European Standards with accordance to the National Annex of Germany. In this case the shape and the physical boundary conditions of the roof will be given and cannot be changed.

The case study focuses on a one story building with a glass façade and a green roof. The area around the building differs in three directions. At the west side there are trees and a road, the ground is at the same height as the roof surface. At the north side a three story concrete part will be built, which falls outside the scope of the research. At the east/south side a square will be made and this will form a connection with the surrounding existing buildings. The dimensions of the roof for the main part are roughly $40\,m$ by $115\,m$. At the east side the roof will be extended beyond the glass façade. At two areas there will be a maximum span of $35\,m$. The roof is stretched in one direction, as shown in figure 4.1.

4.1. Design Principles

The structural design criteria are based on the European Standards. The EN Eurocodes are a series of ten European Standards in which is specified for the European Union how structural design should be conducted. The basic approach for the design of the building will be according to Eurocode 0: Basis of Design and Eurocode 1: Loading. For Eurocode 1 the general actions on structures are given in EN 1991-1-1:2002, the snow load actions 1991-1-3:2003 and the wind load actions 1991-1-4:2005. The structural design will be based on the European code for the design of timber structures (EN 1995-1-1:2004).

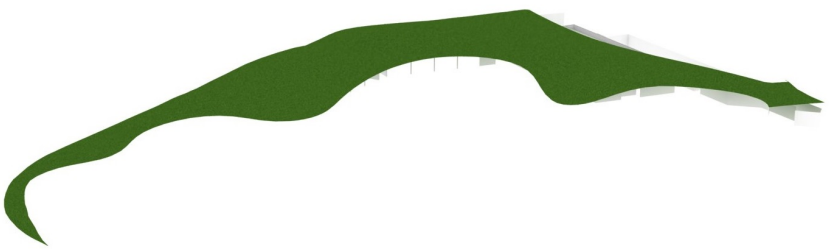

Figure 4.1: Perspective of the timber roof project

Load combinations consist of combinations of design values of the permanent and variable loads in accordance with the Eurocodes. The Ultimate Limit State (ULS) is used to check structural safety according to the Equation (4.1). This equation is the characteristic combination, which is used for those cases where exceeding the limit state causes significant damage or unacceptable deformation. The Serviceability Limit State (SLS) is used to check the usability of the structure on which different combinations of loads are acting. The characteristic combination will be checked according to the Equation (4.2). The frequent combination is of interest in connection with timber structures as well. This combination is intended for use where exceeding the limit state is associated with minor damage or reversible deformations. It will be checked according to the other Equation (4.3). In general a building structure must withstand the most unfavourable combination of loads that could occur in terms of use and structural safety.

Ultimate Limit State

$$E_d = \gamma_G G_k + \gamma_{Q,1} Q_{k,1} + \Sigma \gamma_{Q,i} \psi_{0,i} Q_{k,i} \tag{4.1}$$

Serviceability Limit State

$$E_d = G_k + \gamma Q_{k,1} + \Sigma \psi_{0,i} Q_{k,i} \tag{4.2}$$

$$E_d = G_k + \gamma\_1,1 Q_{k,1} + \Sigma \psi_{2,i} Q_{k,i} \tag{4.3}$$

For the structure differentiation of the actions has to be considered according to the variation of their magnitude in space and with time. The permanent actions (G) are considered as dead load, e.g. self-weight of the construction and superimposed dead load. The variable actions (Q) are considered as live load, e.g. wind load and snow load. The different actions are present in all the load combinations.

Permanent Loads

Dead Load

The self-weight loads are calculated in the analysis model according to the dimensions and material density of each element.

Self-weight and densities	
Concrete	$2500\ kg/m^3$
Glass	$2500\ kg/m^3$
Timber	$5\ kN/m^3$

The elements that are not part of the main structure are not modelled. Therefore, these elements are considered by calculating their effective weight and then applying an equivalent load to the structural elements.

Super Imposed Dead Load

The architectural idea is to have the roof completely covered with vegetation. Therefore an extensive green roof, type ”Nature Roof” will be considered [28]. The self-weight of this type of nature roof is $200\,kg/m^2$ with a depth of $175\,mm$. The built-up of the green roof will be from top to bottom in different layers, as shown in figure 4.2. The first layer consists out of the vegetation mat and a substrate with a combination inspection chamber. The second part of the built up is needed to protect against damage and stores water. This part consists out of filter fleece, drainage board, protection and storage fleece. The load taken into account for the green roof is $1,96\ kN/m^2$.

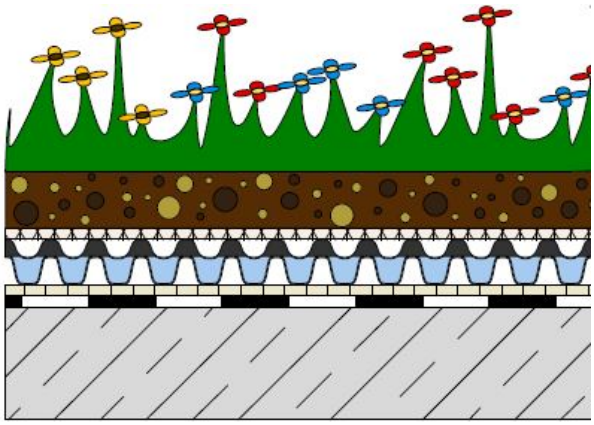

Figure 4.2: Built-up of the Nature Roof system [28]

Variable Loads

The assumptions for the variable loads are made in accordance with the geographical location. Regarding a reference system the height of a location is referred to the standard zero. Normalnull (NN) is an outdated official vertical datum used in Germany. The height of NN is $+439,20\,m$ in Sindelfingen. The influence of the supports of the roof is essential, in this area the soil type is rocks.

Wind Load

Wind load fluctuates with time and these variable actions are related to the short term load duration class. The wind loads are defined using the simplified method as described in the Eurocode. They are represented by static pressures on the surface of the structure and friction wind forces. For the location Sindelfingen the windload zone 1 is valid according to EN 1991-1-4:2005, in figure 4.3.

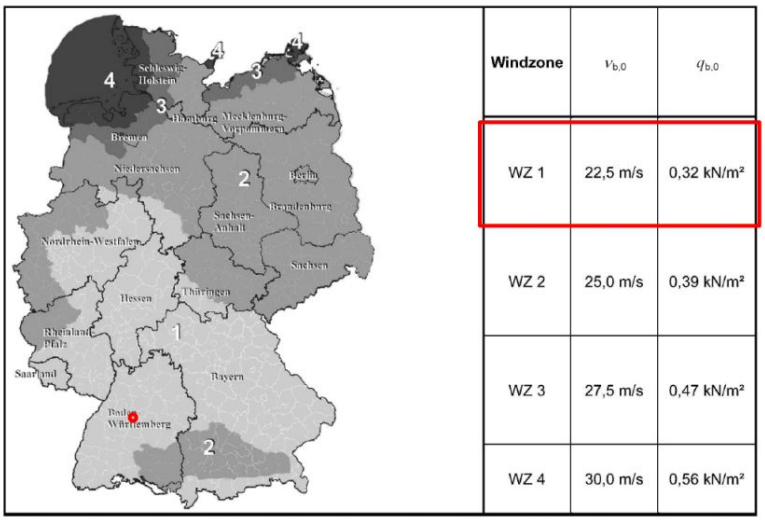

Windzone	$v_{b,0}$	$q_{b,0}$
WZ 1	22,5 m/s	0,32 kN/m²
WZ 2	25,0 m/s	0,39 kN/m²
WZ 3	27,5 m/s	0,47 kN/m²
WZ 4	30,0 m/s	0,56 kN/m²

Figure 4.3: Wind zones map of Germany DIN-EN 1991-1-4:2010-12, 5.1 (Tab 3.26a)

Figure 4.4: Snow zones map of Germany DIN-EN 1991-1-3:2010-12, 3.1 (Tab3.49a)

Table 4.1: Extreme values of wind actions

	$C_{p,net}$			W_k (kN/m^2)
	C_{pe}	$C_{pi} = +0,2$	$C_{pi} = -0,3$	
A	+0,15	+0,05	+0,45	= 0,54 · +0,45 = $+0,24\ kN/m^2$
B	-0,9	-1,1	-0,6	= 0,54 · -1,1 = $-0,59\ kN/m^2$
C	-0,4	-0,6	-0,1	= 0,54 · -0,6 = $-0,31\ kN/m^2$

The wind velocity is $v_{b,O}$ is $22,5\ m/s$ referring to a mean return period of 50 years. The wind pressure q_b is $0,316\ kN/m^2$ with an air density of $1,25\ kg/m^3$. The terrain roughness classification is category III, industrial areas, with a terrain factor (K_r) of $0,22$. The simplified wind calculation can be used for buildings with a height until 25 m. Therefore the assumption for the wind load q_p is $0,5\ kN/m^2$. The roughness coefficient is defined as:

$$c_r(z_w) = K_r ln + [max(\frac{z_w, z_{min}}{z_0})] = 0,22 \cdot ln[max(\frac{10}{0,3}; \frac{5}{0,3})] = 0,76 \quad (4.4)$$

Where the roughness length (z_0) is $0,3\ m$, the reference height (z_w) is $10\ m$ and the height with a constant wind velocity (z_{min}) is $5\ m$. This reference height is defined from:

$$z_w = h + f = 4 + 6 = 10\,m \quad (4.5)$$

The mean wind velocity (v_m) at the reference height of $10\ m$ is calculated with equation 4.6. In this equation the orography factor c_o is taken as $1,0$.

$$v_m(z_w) = c_r(z_w) \cdot c_o(z_w) \cdot v_b = 0,76 \cdot 1,0 \cdot 22,5 = 16,99\,m/s \quad (4.6)$$

The peak velocity pressure (q_p) is defined with equation 4.7, where turbulent intensity (I_v) is $0,29$.

$$q_p(z_w) = [1 + 7 \cdot I_v(z_w)] \cdot 0,5 \cdot \rho \cdot {v_m}^2(z_w) = [1 + 7 \cdot 0,29] \cdot 0,5 \cdot 1,25 \cdot 16,99^2 = 0,54\,kN/m^2 \quad (4.7)$$

The wind load behaviour will be calculated for a simplified curved roof. A positive wind load stands for pressure whereas a negative wind load indicates suction, which denotes uplift of the roof. For the calculation of the wind action the external (C_{pe}) and internal (C_{pi}) pressure coefficients need to be defined. The characteristic wind actions are defined as:

$$w_k = q_p \cdot C_{p,net} = q_p \cdot (C_{pe} + C_{pi}) \quad (4.8)$$

The wind effects on the roof surface result from a constant internal pressure (C_{pi} = $+0,2$ or $-0,3$) combined with the external pressures for each wind direction. The external pressure coefficient is determined from figure 4.5, where $\frac{f}{d} = 0,13$ and $\frac{h}{d} = 0,1$. In the table 4.1 the characteristic wind actions (w_k) are obtained with the different pressure coefficients. A first estimate will be made with the extreme value of these wind actions.

Snow Load

The snow loads are based on historical measurements of snow depths on the ground and snow densities. Snow loading is a variable action of short-term duration. The characteristic snow load on the ground (s_k) is defined for a return period of 50 years. Snowload zone 2 is given from the national loading code DIN EN $1991 - 1 - 4$, in figure 4.4. The characteristic value (s_k) of $1,36\ kN/m^2$ depends on the geographical location and the altitude of the site (A):

$$s_k = 0,25 + 1,91 \cdot (\frac{A + 140}{760})^2 = 1,36\,kN/m^2 \geq 0,85\,kN/m^2 \quad (4.9)$$

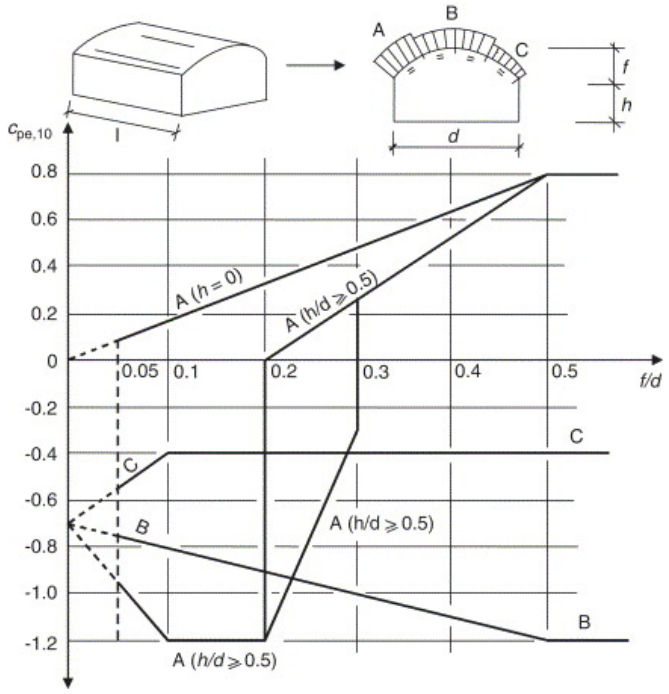

Figure 4.5: Wind load behaviour of a curved roof DIN-EN 1991-1-4:2010-12, 7.2.8 (Tab3.36b)

Table 4.2: Load assumptions

Specification	Dead Load (G)	Variable Load (Q)
Timber (G_0)	0,005 kN/m^2	
Green roof (G_1)	2,0 kN/m^2	
Wind Load (W_A)		+ 0,24 kN/m^2
Wind Load (W_B)		- 0,59 kN/m^2
Wind Load (W_C)		- 0,31 kN/m^2
Snow Load (S)		1,09 kN/m^2
Total	2,005 kN/m^2	1,33 kN/m^2

The characteristic value of the snow load is for ground level. In this case it is important to calculate the value regarding a roof surface. The characteristic value should be multiplied the shape coefficient, which depends on the shape of the roof. The curved roof has an angle between 0 degrees and 30 degrees. Therefore the shape coefficient $\mu_1(\alpha)$ is 0,8. The snow action on the roof surface is determined from:

$$S = \mu_1(\alpha) \cdot s_k = 0,8 \cdot 1,36\, kN/m^2 = 1,09\, kN/m^2 \tag{4.10}$$

Load Assumptions

The dead load implies the self-weight of the structure (G_0) and the permanent load of the green roof (G_1). The live load contains the wind load (W) and the snow load (S). The wind pressure and wind suction will be applied in the x-direction and y-direction, see section 4.2. The values which are used for these loads are shown in the table 4.2.

In the analysis the following load combinations will be considered. The critical load cases are related to the combination of snow load and the wind load. The characteristic will be checked for the ultimate limit state, see table 4.3. In table 4.4 for the serviceability limit

Table 4.3: Ultimate limit state combination of actions

ULS combination of actions	
Load Combination 201:	$1,35 \times G$
Load Combination 202:	$1,35 \times G + 1,5 \times S$
Load Combination 203:	$1,35 \times G + 1,5 \times W_x$
Load Combination 204:	$1,35 \times G + 1,5 \times W_y$
Load Combination 205:	$1,35 \times G + 1,5 \times W_x + 1,5 \times 0,9 \times S$
Load Combination 206:	$1,35 \times G + 1,5 \times W_y + 1,5 \times 0,9 \times S$
Load Combination 207:	$1,35 \times G + 1,5 \times S + 1,5 \times 0,9 \times W_x$
Load Combination 208:	$1,35 \times G + 1,5 \times S + 1,5 \times 0,9 \times W_y$
Load Combination 209:	$1,5 \times S$
Load Combination 210:	$1,5 \times W_x$
Load Combination 211:	$1,5 \times W_y$

Table 4.4: Serviceability limit state combination of actions

SLS combination of actions	
Load Combination 101:	$1,0 \times G$
Load Combination 102:	$1,0 \times G + 1,0 \times S + 0,6 \times W_x$
Load Combination 103:	$1,0 \times G + 1,0 \times S + 0,6 \times W_y$
Load Combination 104:	$1,0 \times G + 0,2 \times S$
Load Combination 105:	$1,0 \times G + 0,5 \times W_x$
Load Combination 106:	$1,0 \times G + 0,5 \times W_y$
Load Combination 107:	$1,0 \times S + 0,6 \times W_x$
Load Combination 108:	$1,0 \times S + 0,6 \times W_y$

state the characteristic combination and the frequent combination will be checked.

- Dead load, permanent
- Dead load + snow, short-term
- Dead load + wind, short-term
- Dead load + snow + wind, combination value, short-term
- Dead load + wind + snow, combination value, short-term
- No dead load + wind + snow, combination value, short-term

Material

The most suitable timber materials are glued laminated timber (Glulam) and laminated veneer lumber (LVL) for the roof project. Glulam is very suitable material for high curvature but after bending the elements, the bottom part still needs to be sawn. Glulam is more expensive than LVL and a ratio of 1/10 is required for the width and height. There are also no thin plates available in Glulam. LVL is a strong and light-weight material. The fabrication of LVL has more benefit of the redistribution of large defects into small ones. An production line of LVL has been developed by Kerto [1], which have the two main products Kerto-Q and Kerto-S. All the veneers are parallel from Kerto-S but Kerto-Q has the advantage that it is

Table 4.5: The modification factor (k_{mod}) according to EN 1995-1-1:2004 Table 3.1

Load-duration Class	Load action	k_{mod} for Service Classes	
		1&2	3
Permanent	self-weight	$0,60$	$0,50$
Long-term	storage	$0,70$	$0,55$
Medium-term	imposed load	$0,80$	$0,65$
Short-term	snow and wind	$0,90$	$0,70$
Instantaneous	accidental load	$1,10$	$0,90$

Table 4.6: The deformation factor (k_{def}) according to EN 1995-1-1:2004 Table 3.2

Laminated lumber veneer (LVL)			
Service Class	1	2	3
k_{def}	0,60	0,80	2,00

cross bonded Kerto. This means that every fifth veneer is glued in the perpendicular direction. This way of build-up increases the lateral bending strength and stiffness of the panel, which increases the shear strength of the material. Cross-bonded veneers give a reduction in moisture-dependent variation across the width of the panel. Therefore this material has a many benefits and will be used for the structure. In section 2.4.1 an overview of the material properties of LVL is given. The material properties of $LVL\ 36\ S\ cross$ are used for structural calculations.

Factors

The actual value obtained from the results should be lower than the allowable strength of the material. The design value X_d of a material property is defined with the characteristic value X_k as:

$$X_d = \frac{k_{mod} \cdot X_k}{\gamma_M} \tag{4.11}$$

For the material properties of Kerto-Q-LVL the partial factor γ_M is $1,2$ and for timber connections γ_M is $1,3$.

The modification factor (k_{mod}) is taking into account the effect on the strength under load action and the moisture content. This factor depends on the Service Class to which the structure belongs and the Load-duration Class. The Service Class 2 will be considered due to the green roof and the cantilever parts of the roof. The Load-duration Classes are characterized by load acting for a certain period of time, as can be seen in table 4.5.

The wood moisture content affects the mechanical properties of the Kerto-Q material. Therefore the deformation factor k_{def} is reflected in the design codes. In k_{def} factor creep behaviour is considered under a constant load at certain ambient relative humidity. In table 4.6 the values for the different service classes are displayed.

The size factor is applied for the following strength properties: bending strength, tension parallel to the grain and tension perpendicular to the grain. Since the failure mechanism is brittle of these properties. The effect of member size k_h on strength is different for the

Table 4.7: Size effect parameter k_h according to EN 14374 Table 3.2

Size effect parameter k_h		
For solid timber:	For glulam:	For LVL:
$min\begin{cases}1,3\\(\frac{150}{h})^{0,2}\end{cases}$	$min\begin{cases}1,15\\(\frac{600}{h})^{0,2}\end{cases}$	$min\begin{cases}1,2\\(\frac{300}{h})^{0,12}\end{cases}$

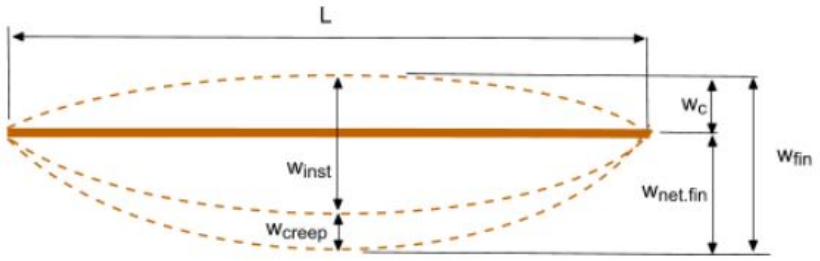

Figure 4.6: Deflection components for a simply supported timber beam

materials of solid timber, glued laminated timber and LVL. In table 4.7 the k_h factor needs to taken into account for these materials.

In the serviceability state the deformations and deflections will be checked according to EN 1995-1-1:2004 7.2. The design values E_{mean}, G_{mean} and K_{ser} are used. The risk of exceeding the deflection limit is kept at a low level. The deflection will be calculated using the characteristic load combinations 102 and 103, see table 4.4.

For design purposes the deflection criteria are based on different deflection scenarios for the various components in the roof structure.In figure 4.6 the different states are displayed. The W_{inst} is the beam deflection due to permanent loads and variable loads immediately after loading. The W_c deflection is the pre camber of the beam in the unloaded state. The W_{creep} due to variable loads plus any time dependent deflection due to permanent loads. The $W_{net,fin}$ is the sagging of the beam relative to the straight line with the supports. The total deflection from pre cambering till time dependent deflection is the W_{fin}.

$$W_{inst} = W_{G,inst} + W_{Q,inst} \tag{4.12}$$

$$W_{fin} = W_{G,fin} + W_{Q,fin} \tag{4.13}$$

where $W_{G,inst}$ is the deflection from the self-weight and the permanent loads, which is Load Combination 101 and where $W_{Q,inst}$ from the separate snow load. For snow load the following values are used; $\psi_0 = 0,6$, $\psi_1 = 0,2$ and $\psi_2 = 0$.

$$W_{Q,fin} = W_{Q,inst} \cdot (1 + \gamma_2 k_{def}) \tag{4.14}$$

$$W_{G,fin} = W_{G,inst} + W_{creep} = W_{G,inst} * (1 + k_{def}) \tag{4.15}$$

where W_{fin} needs to be calculated from the W_{inst} with the different load cases and the time dependent factors needs to be taken into account. From the point of view of appearance the

Table 4.8: The deflection criteria to EN 1995-1-1:2004 7.2 Table 7.2

Deflection criteria	W_{inst}	W_{fin}
Mid span	$\leq \frac{l}{300}$	$\leq \frac{l}{200}$
Cantilever	$\leq \frac{l}{150}$	$\leq \frac{l}{100}$

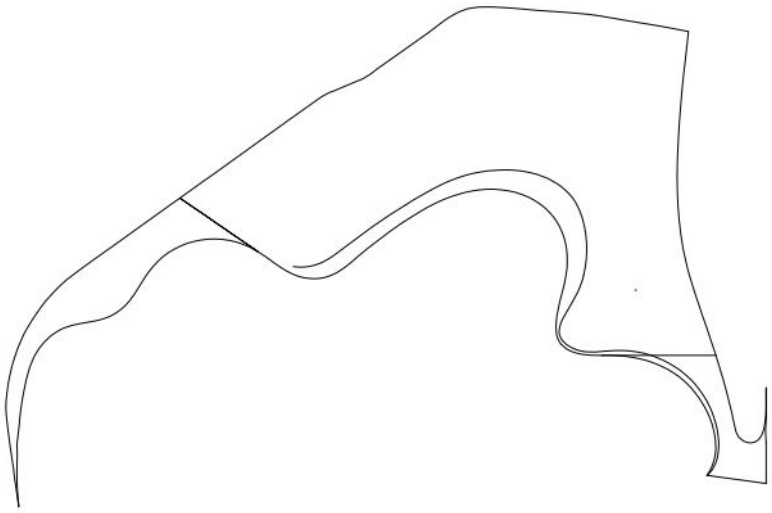

Figure 4.7: The new contour of the adjusted surface

final net deflection is of interest.

For the different deflection components of W_{inst} and W_{fin} needs to meet the design code criterion, which is recommended in EN 1995-1-1:2004 7.2 Table 7.2. In table 4.8 the mid span stands for the deflection between two supporting points and the cantilever stands for the part were the structure is only support at one side. Precaution needs to be taken in the final deflection check for ponding.

In the ultimate limit state the forces, bending moments and stresses will be checked. The dimensions of the structure will be determined on the basis of design in the ultimate limit state. After this the deflection criterion needs to be checked if the dimensions are sufficient.

4.2. Case Study: the Roof Project

The case study focuses on a one story building with a green roof. The design of roof surface has been made by the architects. The tail of the roof has a very limited height and almost equals ground surface. Therefore the surface has been adjusted to the main part. For the scope of this research the adjusted surface will be investigated. In figure 4.7 an extra line shows the contour line of the adjusted surface. The exact dimension values of the adjusted surface are shown in figure 4.8.

Figure 4.8: 2D drawing of the structure with dimensions

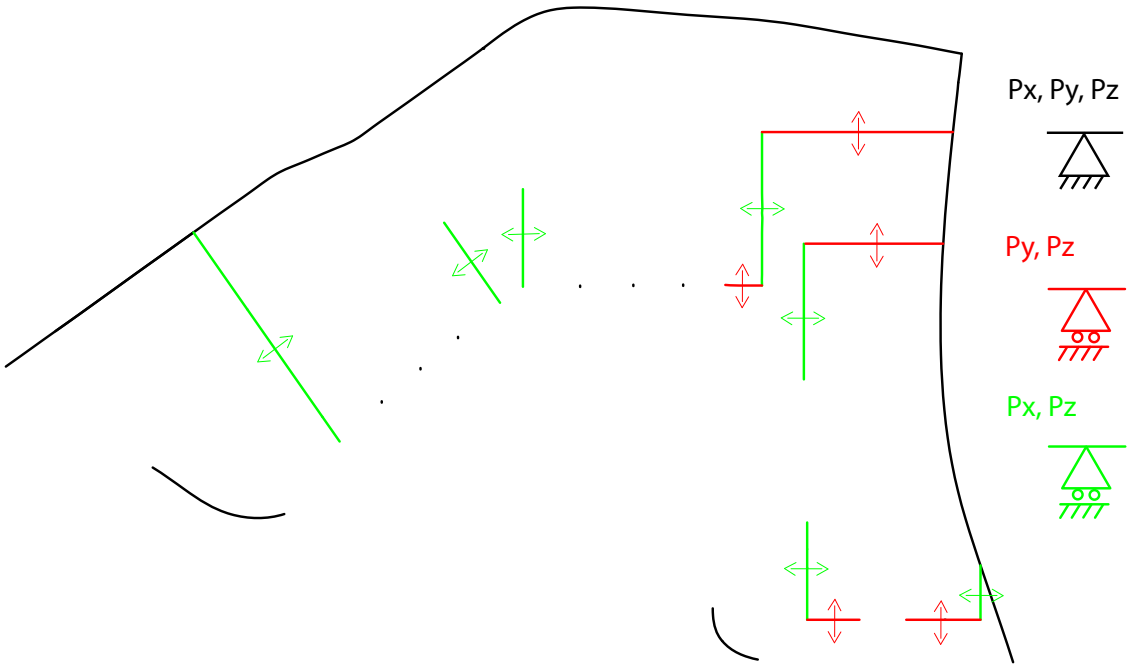

Figure 4.9: The boundary conditions of the roof structure

The roof structure is supported on different ways, as can be seen in figure 4.9. The black points indicated the six columns and these are restrained in all three directions. The outer black lines find their support on the ground or on the concrete building, which are restrained in three directions as well. The green and red lines are restrained in the direction of the line but can move in the perpendicular direction, which presents the concrete walls under the roof. Where two concrete walls met in the corner, this point will be fixed in all directions.

4.2.1. Structural Behaviour

The structural behaviour of the structure should be in equilibrium. It is required that the structural parts should remain stationary for this building to be safe and usable. First the shape of the free-form structure will be discussed for a better understanding of the given problem. The structure will respond when forces are applied. The response of the material under dead load will be explained regarding the first principal stresses.

Gaussian Curvature

The theory behind the Gaussian Curvature is explained in section 2.2. In figure 4.10 the Gaussian Curvature of the roof surface has been shown. The red areas display a lot of curvature with a positive Gaussian Curvature, and the blue areas display a negative Gaussian Curvature. The green areas indicate a flat area or only curvature in one direction. It gives an indication of the form of the roof surface. The Gaussian Curvature analysis shows a clear alternation and transition of the curved and flat parts of the structure.

Radius Curvature

The radius of curvature R has a ratio of $R = \frac{1}{k}$. The larger the radius of curvature is the less the angle of curvature of the surface. The smaller the radius of curvature is the bigger the curvature of the roof surface. In figure 4.11 the radius of curvature of the roof surface has been shown. The red area has a radius of $249,3\,m$, green area of $42,4\,m$ and blue area of $12,5\,m$. Timber has a minimum of radius which the material could be curved into the desired

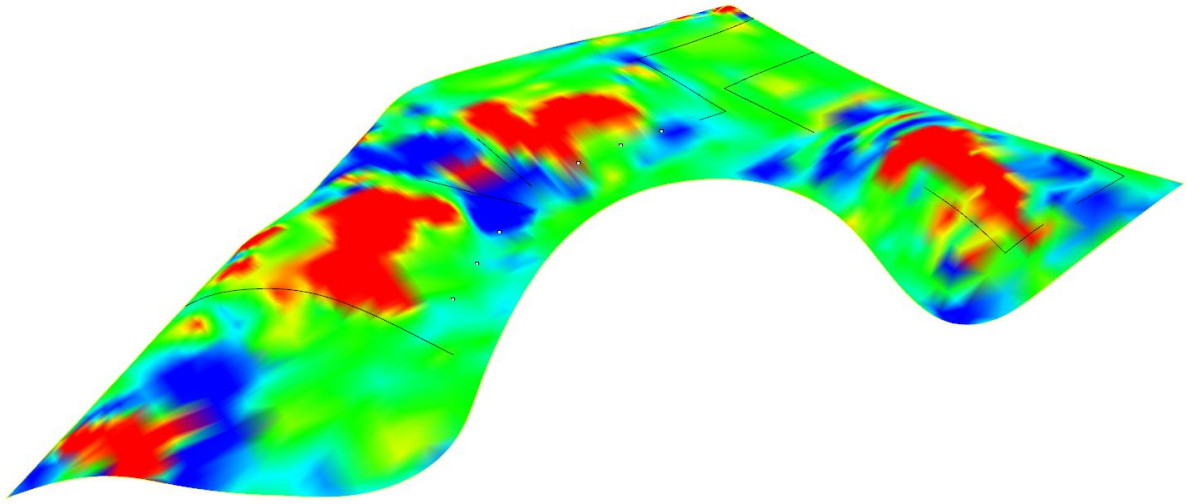

Figure 4.10: The gaussian curvature of the roof surface

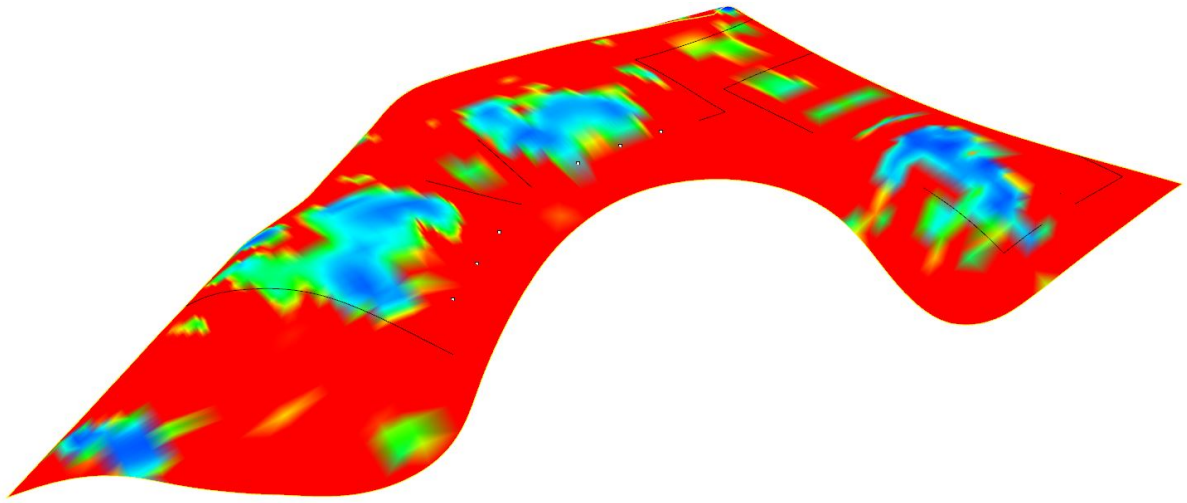

Figure 4.11: The maximum radius of the roof surface

shape.

The lamellas of Kerto-Q could be bended and glued together to form the required curved structure. The maximum thickness of panels is 33 mm. These panels have limitation when it comes down to the required curvature. When bending only in the grain direction of the surface veneers the radius of curvature should meet the requirement; $r \geq 250 \cdot$ panel thickness. The radius of curvature to the surface veneer grain direction should be higher than $600 \cdot$ panel thickness.

Normally after structural analysis the shape of a free-form structure will be further developed to find the balance between structural integrity and design. In this case the shape and the boundary conditions of the roof have been given and cannot be changed. However there are no limitations regarding the height of the roof structure. A principle of smooth height variation will be developed to calculate the required height. For obtaining the results required computer programs and tools will be searched. The timber roof project is a complex structure and computational modelling is needed during the digital design process.

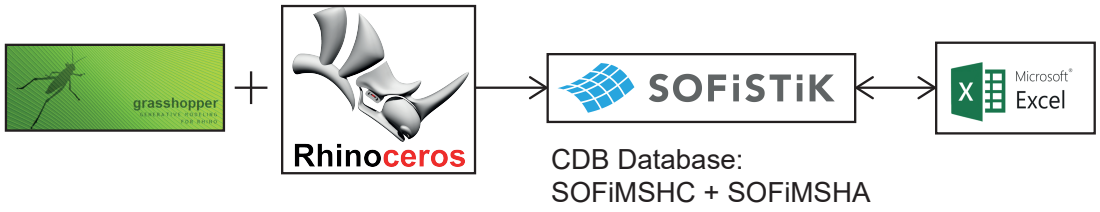

Figure 4.12: The computer programs used with the principle process

4.3. Computational Modelling

In this part the design tools and computer programs for computational modelling will be discussed. Computational Modelling is the use of mathematics, physics and computer science, which will help to study the behaviour of this complex structure. The finite element software and the parametric modelling tools offer many possibilities. A lot of possibilities bring a lot of options with it. Therefore extra care needs to be taken of which input will be given and what kind of output will be obtained.

The following computer programs will be used to perform the structural analysis. The structural design of the roof project will be improved with computer programs like SOFiSTiK, Microsoft Excel and Rhinoceros with Grasshopper and Karamba. These programs will be used from a global analysis till a more detailed one. SOFiSTiK is a Finite Element Analysis program with the use of design software tools. This program offers a detailed structural analysis for buildings to find suitable solutions. This program offers a lot of possibilities with export and import options with different programs and files. For this design research the preprocessor program Rhinoceros will be used. Rhinoceros is a modelling program for designers and architects. Rhino provides tools like Grasshopper to make an accurate model. Grasshopper is a graphical algorithm editor to provide a parametric adjustable geometry.

The program Karamba will be used for global analysis in section 5.1. For this program a more detailed subscription will be given. Karamba works in combination with Grasshopper to provide accurate analysis. Karamba is a parametric structural engineering tool, which could make analyses of 3D beams and shell structures. Elements, supports and load is required as input to make a calculation with Karamba. To get a more accurate result the input of material properties should be applied. The cross section of the elements can be a variable input while generating a loop. The view of results could be numerical in a list or graphical display.

First the free-form structure will be roughly analysed along the surface with the use of Karamba, see section 5.1. As the free-form structure has different structural behaviour, it is necessary to calculate the thickness of the roof structure. The first idea will be to calculate with Karamba the smooth cross sections heights from the obtained bending moments. However the program Karamba uses a simplified version of the material timber which makes the values not accurate. The display of the cross section is kind of arbitrary and therefore these results are not reliable.

In section 5.2 a principle of smooth height variation will be explained. This height variation is applied for a depth optimization of the structure, using different software programs (figure 4.12) to model and analyse the structural behaviour of the roof. The geometry of the roof structure will be set with the CAD tool Rhinoceros and the plug-in Grasshopper. Rhinoceros is used as the preprocessor of SOFiSTiK and a plug-in will be used to convert the geometry into structural elements. First the structure will be analysed by SOFiSTiK. After this the results will be exported to Excel for checking the design of the structure and if needed to generate new data for SOFiSTiK. The different modules of this finite element software will

be for all these steps.

The SOFiSTiK Structural Desktop (SSD) controls the communication between the different programs of the SOFiSTiK software. All the data is stored in a Central Data Base (CDB), which the modules SOFiMSHC and SOFiMSHA are reading from and writing into. SOFiMSHC is a tool for creating and processing geometric models and finite element structures. It can be used as a stand-alone program within Teddy, which is the text input prior for analysis. In this case it is integrated as geometry processing module in the SOFiSTiK program Rhinoceros interface. This module includes all relevant geometric and structural information, which is needed for describing a calculation model. The module SOFiMSHA is used for recreating the geometry with a finite element mesh. This module will be used later on as import data and as modification of a finite element. In this step SOFiMSHC analyses and processes the geometry from Rhinoceros and creates as result a finite element mesh.

4.4. Conclusion

The design criteria and the boundary conditions have been explained. The design principles are based on the European Standards. The load assumptions are obtained on the geographical location and the type of structure. In the scope of this research a general assumption for the wind load has been made for a curved roof. In reality a wind tunnel test should be carried out on a scale model of the building. The loads will be applied according to the load combinations in the serviceability limit state and the ultimate limit state. Further an overview of the material properties and the factors for design values have been given. The structural concept will be applied to the design of the roof project to asses the feasibility. The design principles will be a guide line to check the obtained results.

As explained in this chapter the case study will be a timber roof project. The structural system has been explained and the boundary conditions are set. The roof surface has areas with strong curvature where shell behaviour can be activated, and with flat or shallow regions where the forces need to be transferred in bending moments. The challenge will be to develop an integrated structural concept that can be adapted to the free-form structure to satisfy the local demands of structural timber in an efficient manner. In the following chapter 5 the structural concept will be discussed and the development of the principle of the smooth height variation will be explained. The result of this principle will be shown on the global model in chapter 6.

5

Design approach

In chapter 4 the design criteria for the case study have been discussed. The primary scope of this research is to elaborate a structural concept in timber to cover the free-form surface of the roof. In this chapter different grid structure for the structural concept are described, their suitability for the given problem are discussed and possible improvements for the structural concept are further investigated. One the major points of discussion is the height of the elements in the roof structure, as this is a key contributor to the final roof design, it needs to be determined. A principle of smooth height variation is developed to get the optimal height. The different steps to achieve this will be shown on an example as proof of concept.

5.1. Structural Concept

The challenge is to develop an integrated structural concept that can be adapted in a free-form structure and optimizes the material characteristics of timber. Along different areas in the roof, different mechanism are activated. The surface can divided into shell behaviour, bending behaviour and a combination of both. The most critical areas of the surface are the flat and shallow regions where high bending moments occur. The design of the structural concept takes into account these different zones and with smart selection of shape and thickness of timber in the critical areas of the roof, the structural design is optimized. The structural performance of the three grid layouts will be roughly analysed with the use of Karamba.

Grid Layout 1

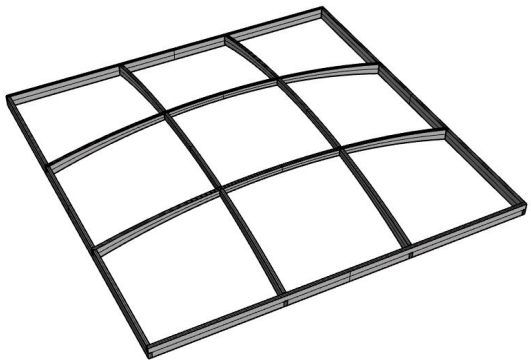

Figure 5.1: Grid layout 1: $2\ m$ by $2\ m$

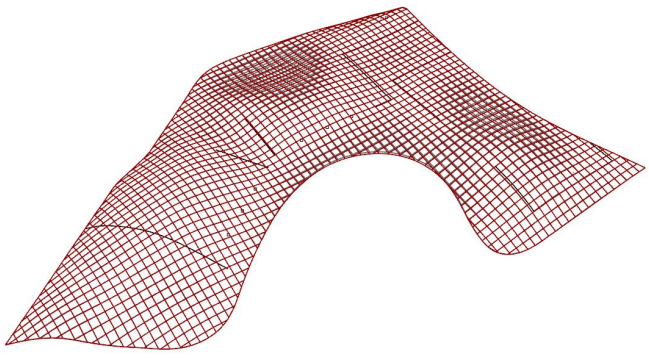

Figure 5.2: Grid 1 structure with deflection

The idea of the first grid layout is to explore and develop prefabricated timber elements to realize the shape of the free-form surface. On site prefabricated timber elements provide an

easy and fast assembly due to the majority of the fabrication in the workshop. The structure will be built from segmented elements that vary in depth. As the surface will be divided into shell behaviour, bending behaviour and a combination of both, the thickness of the elements will vary along the surface. The elements will be thin at areas where pure shell action will occur and the elements will be thicker at areas where bending moments need to be transferred. A smooth height variation will occur at the transfer zone with a combination of both behaviours.

The structural concept consists out of ribbed elements that are covered with plates on the top and the bottom. These plates provide stability for the elements and prevent torsion. The ribbed elements are placed in a rectangular grid, as shown in figure 5.1. A simple connection is made between the ribbed elements. A cut in one direction in the bottom part and a cut in the other direction in the top part are made. The elements will join at the point where they will cross each other. The ribbed elements and the plates will be made out of the timber material Kerto-Q-LVL. The plates are bend to the desired curvature and attached to the ribbed elements by screws.

Grid Layout 2

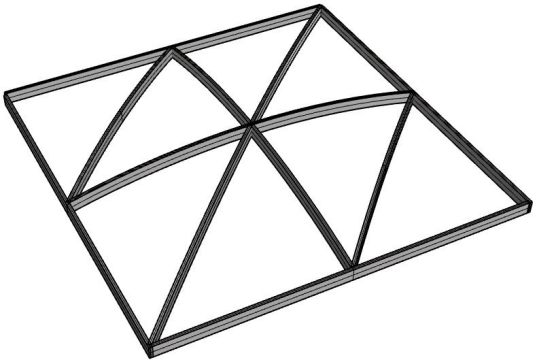

Figure 5.3: Grid layout 2: 3 m by 3 m

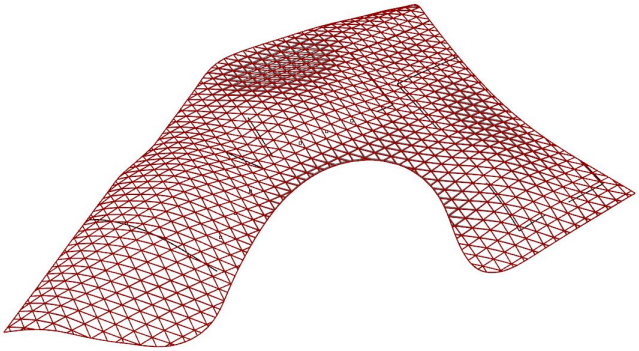

Figure 5.4: Grid 2 structure with deflection

The idea of the second grid layout is built in a triangular grid. In figure 5.3 the diagonals are orientated in one way. The triangles will be smaller and compacter where only forces need to be transferred and the shape of the triangles will be bigger with higher elements where the bending moments need to be transferred.

The advantage of this system is that it provides an in-plane stability due to the triangular geometry. The forces are distributed in three directions and larger spans can be realised. A disadvantage of this system is that the connections are difficult to fabricate, since multiple elements need to be connected. For these connections a big amount of steel is required for the realization. An option to reduce the complexity in the connections is to have continuous beams and the other beams are connected in between.

Grid Layout 3

The idea of the third grid layout stems from the first two grid layouts. The advantage of the thirst grid layout is the easy connection assembly between the ribbed elements. While the advantage of the second grid layout is that it provides in-plane stability. The third grid layout is a combination of these two aspects. The structure will be built with both a triangular and hexagon grid, see figure 5.5. The diagonals have been moved from mid-way span in the square, to cross half way of the ribbed elements. This shift provides a maximum of two ribbed elements in a single joint. Additionally, the built-up grid will provide in-plane stability, which makes the concept stiff and with good interaction between the elements. Where at the same time the forces can be distributed in three directions if needed in certain areas.

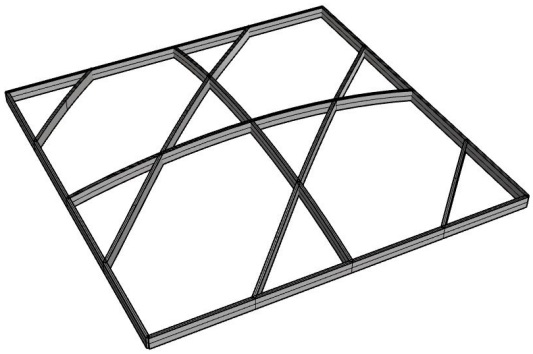

Figure 5.5: Grid layout 3: $3\,m$ by $3\,m$

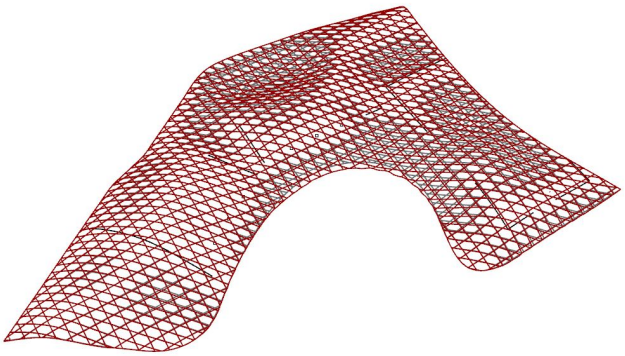

Figure 5.6: Grid 3 structure with deflection

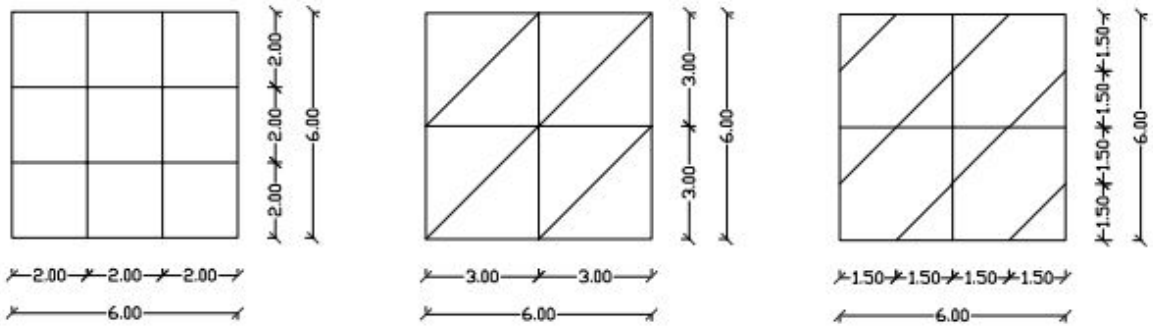

Figure 5.7: The dimensions of the different grid structures in m

Basic Analysis

The build-up of the structural concept are as described above, ribbed elements with plates on the top and the bottom. The ribbed elements are ordered in a unique grid for each grid layout. The segments have the dimensions of $6\,m$ by $6\,m$ for comparison, see figure 5.7. The first grid layout is divided into a grid of $2\,m$ by $2\,m$. The second grid layout is divided into a grid of $3\,m$ by $3\,m$ to get roughly the same mass as the first grid layout. The third grid layout is divided into a grid of $1.5\,m$ by $1.5\,m$.

The grid layouts will be roughly analysed along the surface with the use of Karamba, see section 4.3. The surface will be divided into a grid and modelled as beam elements. Therefore a grid will be drawn by hand and will be projected on the surface. The connections between the elements will be modelled as fully stiff. Although in reality this will not be the case and those connections are difficult to realise with timber. The grid will be supported with pinned connections at the edges and middle parts as subscribed in section 4.2.1. The cross sections of the beams have a width of $90\,mm$ and a height of $400\,mm$. The material properties will be used, which are displayed in table 5.1.

The analysis has been done to get an idea of how the different geometry will behave, see table 5.2. The size of the segments has been chosen such that the grid will have roughly the same mass. However the first grid is lighter than the other two. In figure 5.2 the first grid structure has been shown with the deformed structure. The first grid has a maximum deflection of $1,89\,m$, which is very high considering only dead load. Beams with a height of $400\,mm$ were found not to be sufficient to span up to $35\,m$. The deflection is reduced by half for grid structure 2 and grid structure 3, as can be seen in the overview table below. This analysis is clearly showing that two critical areas occur. The highest bending moments and the maximum deflection occur at the area where the span is $35\,m$. This could be seen

Table 5.1: Characteristic values of wood for grid layout

Characteristic values of Karamba wood		
Bending edgewise	f_{mk}	30 N/mm^2
Mean modulus of elasticity	$E_{0,mean}$	10500 N/mm^2
Average density	ρ_{mean}	470 kg/m^3

Table 5.2: Overview of the results of the different grid structures

Structural concepts	Maximum deflection	Mass
Grid 1	1,89 m	167125 kg
Grid 2	0,85 m	189641 kg
Grid 3	0,84 m	189771 kg

in figure 5.4. The display of the deflections is only a visualisation which could be changed by a factor. In figure 5.6 the other critical area is in the cantilever part with a span of $7-11\,m$.

Conclusion Grid Layouts

All grid layouts have their advantages and disadvantages when it comes down to their structural performance. Only one of the grid layouts will be further developed to cover the free-form surface in the case study. The advantage of the first grid layout is that the connections could easily be assembled between the ribbed elements. The advantage of the other grid layouts is that both could provide stability in their plane. The aim of this research is to develop a structural concept that exhibits both shell and bending behaviour in a smooth, continuous and seamless fashion. Therefore the first grid layout is more suitable to be further developed for the given problem. The assembly advantages for the connections between the ribbed elements are another reason to choose for a rectangular grid. The challenges will be to develop the transition between the curvature and the flat area, as can be seen in figure 5.8, and to develop the connections between the large units. The construction method will be further discussed in section 6.1.

5.2. Principle of smooth height variation

The boundary conditions of the free-form structure are set. There are no limitations regarding the depth of this structure. However the plate width of Kerto-Q is limited till a maximum of $2,5\,m$. The structure can be divided into shell behaviour, bending behaviour and a combination of both. The design of the structural concept takes into account these different zones. Therefore it is efficient to have the material timber there were it is needed for a better distribution. The most critical areas of the surface are flat and shallow regions where a lot of height is needed. At the other areas a slim structure is sufficient. Therefore a smooth height variation is desired for the structure. In this section the principle behind the calculation for a smooth height variation will be explained in more detail.

The computer program Karamba was recommended for calculating a smooth cross section height from bending moments, see section 4.3. A parametric grasshopper set-up was found to be an quick method in determining the height from the moment curves determined with Karamba. The bending moment could be calculated by the program, the height can not be

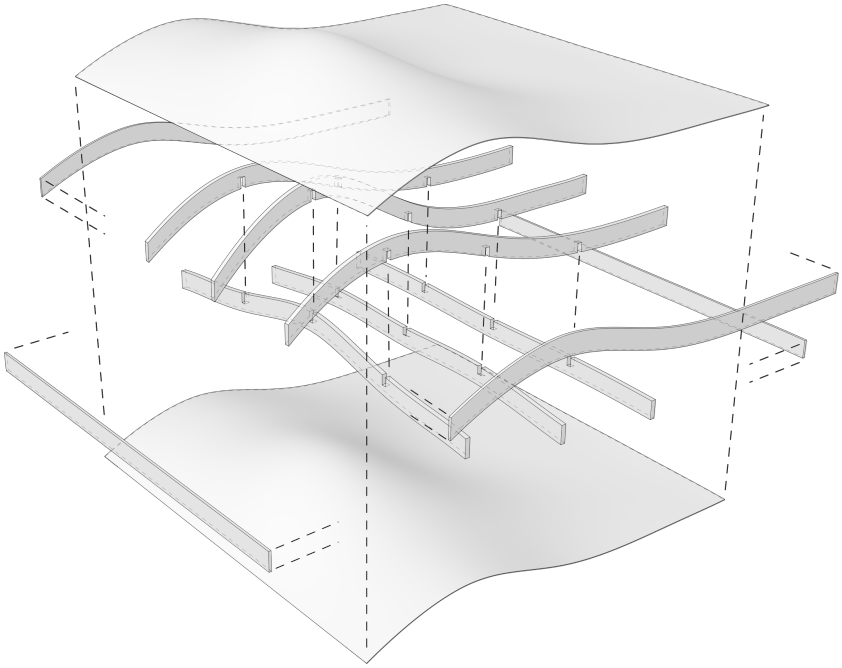

Figure 5.8: Exploded view of the structural concept

directly determined. The desired height can be calculated from the bending stresses. The bending stresses are related to the bending moment and resistance moment, which contains the load on the structure and the dimensions of the cross section. The height of rectangular cross section will be calculated with the following formula

$$\sigma_{m,d} = \frac{M}{W} = \frac{M_y}{\frac{1}{6} \cdot b \cdot h^2} \leq f_{m,d} \tag{5.1}$$

where the bending strength $f_{m,d}$ is determined from

$$f_{m,d} = \frac{k_{mod} \cdot f_{m,k}}{\gamma_M} \tag{5.2}$$

which can be combined with equation 5.1 to calculate the height

$$h = \sqrt{\frac{6 \cdot M_y}{b \cdot f_{m,d}}} \tag{5.3}$$

After this the idea was to obtain the bending moments M_y results by Karamba. The allowable bending stresses will then be determined from the characteristic bending strength $f_{m,k}$, using a fixed value of the width b. The bending moments obtained from Karamba output were average over the element. Therefore it was not possible to obtain the maximum bending moment occurring in one element. For obtaining more accurate results the elements were divided into parts. A beam with a length of 4 m is divided into elements of 1 m each. Each element has a start and end point which will give the beam 5 nodes in total. Since the results could only be obtained from the average of the element, an end or start value is missing.

Another important aspect is that Karamba does not take into account anisotropic material properties, all though it has an option to select different timber materials. The shear modulus of these timber materials is too high for a realistic approach. It was not possible that this value could be adjusted. Therefore it has been decided not to use the program Karamba for the height calculation of the timber structure. After this was found out, a different method was required to calculate the required cross section heights.

The explanation of the process

A principle of smooth height variation is applied for a depth optimization of the structure. In section 4.3 the use of the different software programs have been explained. The geometry of the roof structure will be set with the CAD tool Rhinoceros and the plug-in Grasshopper. First the structure will be analysed after applying the load assumptions with SOFiSTiK. After this the results will be exported to Excel for checking the design of the structure and if needed to generate new data for SOFiSTiK. After this principle the design will be checked according to a checking strategy. Moreover a model with a fine meshing is made to get more accurate results.

The steps of this principle will be shown on an simplified example to make it more understandable. The first step will be to explain the set up of the initial model. In the second step the approximation of the smooth height variation will be discussed. In the third step the design of the structure will be shown and finally the model will be made with a fine mesh for more accurate results. The last step will be to check if the structure has the correct height. If this is not the case, adjustments could be made or all the steps need to be done again. These same steps will be done for the global model, only the final results will be shown in the next chapter 6. The principle of smooth height variation process will be explained according to the diagram, in figure 5.9.

Step 1

The following aspects are taken into account for modelling the initial model:

- Quad elements with a coarse mesh is used to avoid singularity
- Coarse mesh model is less time consuming in stead of using a fine mesh model
- The grain direction of the plates has an influence on the cross section in the different directions. If the main grain direction of the plates will be in the global x-direction, the plates are less stiff in the other direction
- The connection between the plates and the ribbed elements will have an influence. For simplicity and to be on the safe side, the stiffness of the plates will not be included to calculate the height of the cross section

Therefore in this first approximation the plates will not be taken into account. Although the correct way would be to include the plates. First the initial model of the example will be modelled in Rhinoceros (figure 5.10). The geometry will be set up by hand in Rhinoceros. However in a later stage, for the global model, the program Grasshopper will be used to generate the structure in a parametric way. This will speed up the process since the global model has a significant larger size. The elements of the structure are modelled as surfaces and the supports are modelled as point supports. From the SOFiSTiK plug-in in Rhinoceros, the points become structural points and they are fixed in all directions. The surfaces become structural surfaces with material properties and thickness.

Initial model

The example will be made out of timber elements and has the dimensions of $16\,m$ by $8\,m$. The structure will be supported by six columns and with cantilevers in all directions. The columns will be simple supported and they will be pinned in x-, y- and z- direction. The dimensions are divided into a grid of $2\,m$ by $2\,m$. The elements need to span horizontally $6\,m$, vertically $4\,m$ and the dimension of the diagonal will be $7,21\,m$. The dimension of the canopy will be $2\,m$. An overview of the dimension has been given in the figure 5.11.

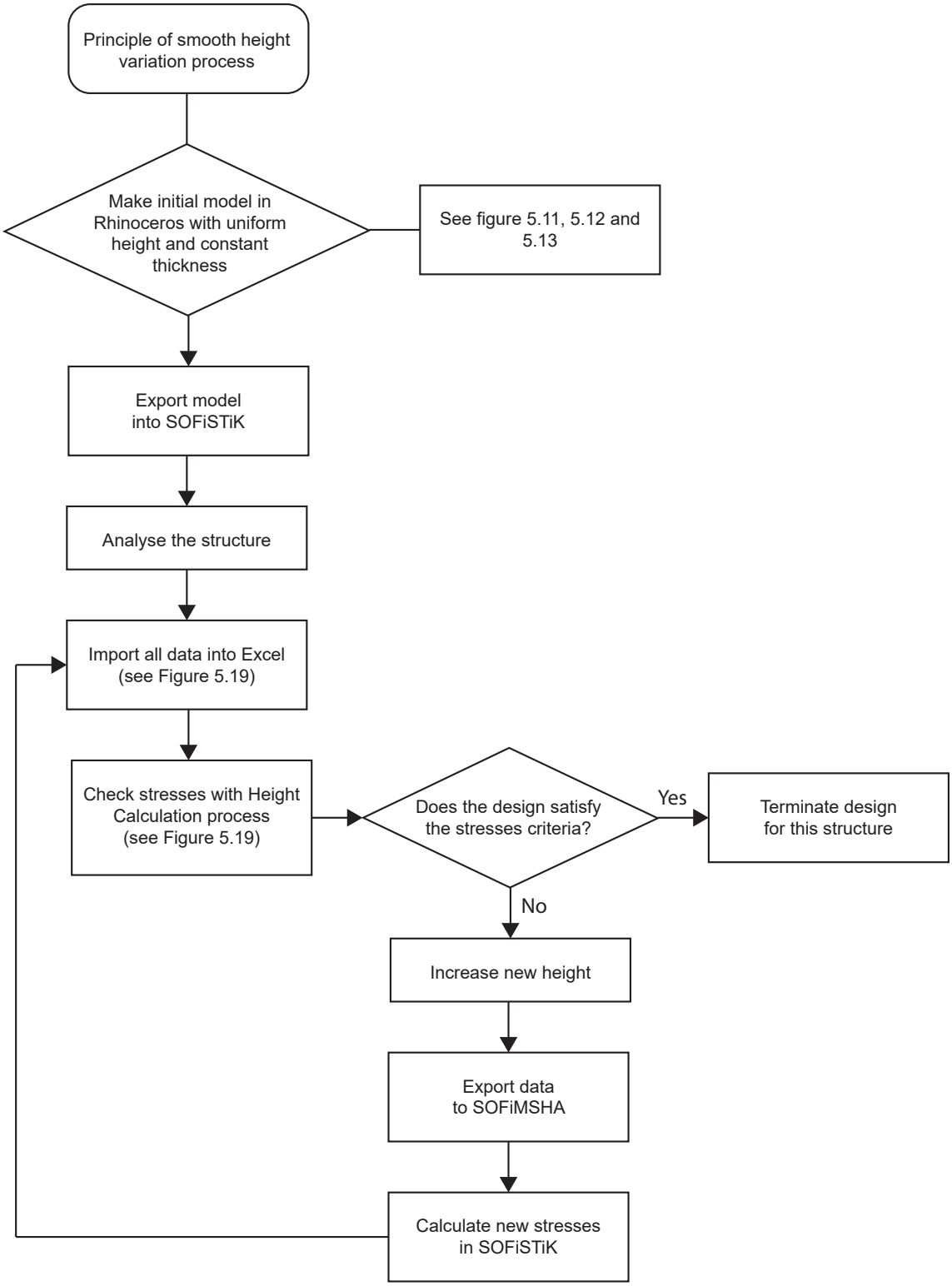

Figure 5.9: The diagram of the principle of the smooth height variation process

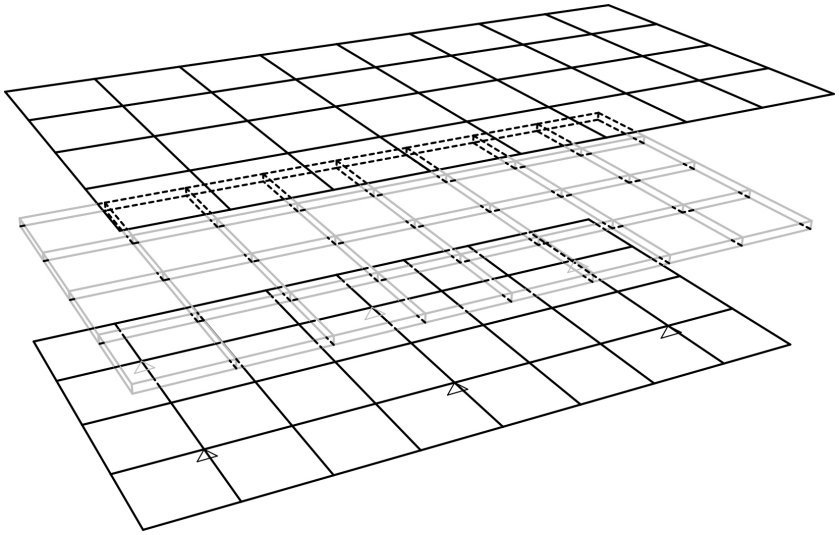

Figure 5.10: The initial model of the example

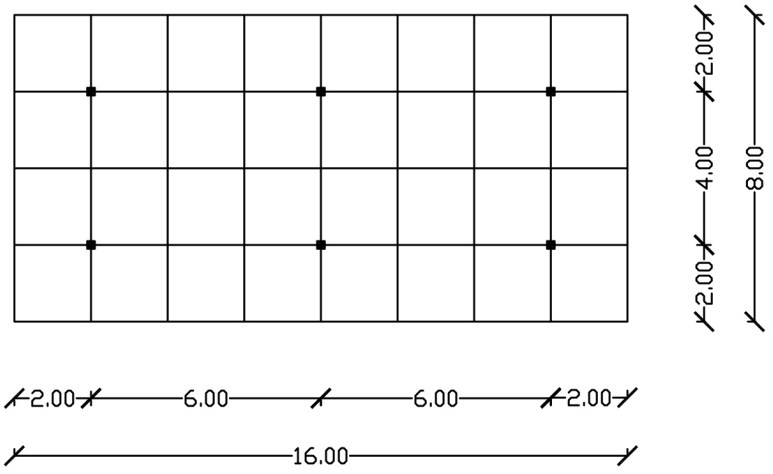

Figure 5.11: The dimensions of the six column example in m

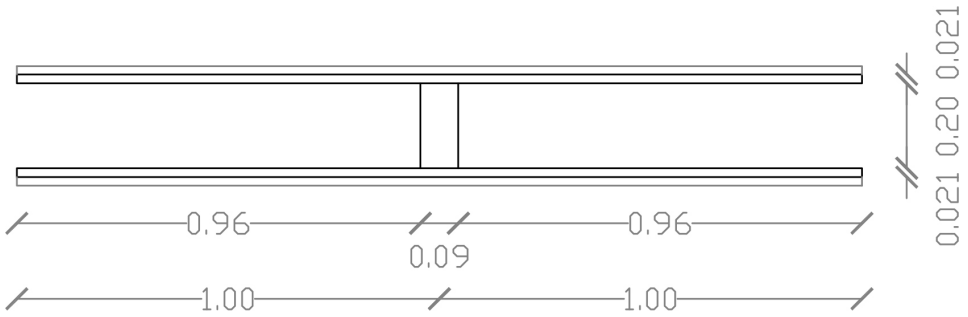

Figure 5.12: The dimensions of the cross section of the example in m

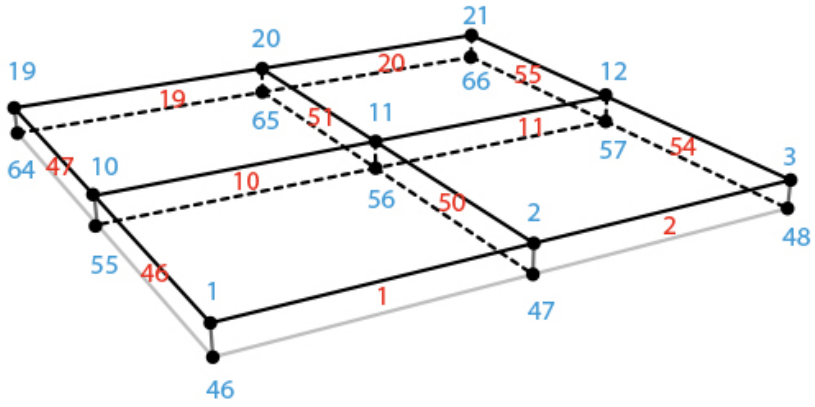

Figure 5.13: A section of the structure with quad numbers and corresponding node numbers

Export data

After this the initial model will be exported to SOFiSTiK. In the Rhinoceros interface, the option has been chosen to use a coarse mesh for the surfaces. Meshing is a discrete representation of the geometry that is involved in differential equations. The structure will have a linear behaviour with the use of single quad elements. A quad element is used in finite element analysis which is used to approximate the exact solution. This is a good approximation since it avoids singularity. Singularity will arise at supports when a fine mesh is used. A pinned connection for the supports is modelled more as a point load, while in reality the support area will be larger.

Build-up initial model

The basic model will have ribbed elements and plates at the top and bottom side. It will start with all ribbed elements having the same cross-sectional size. The cross section of the rectangular ribbed element has a width of $90\,mm$ and a height of $200\,mm$ and the plates have a thickness of $2 \cdot 21\,mm$, see figure 5.12. For calculation the cross section will be approached as a composed I-beam. An important part of this step is to make sure that the surfaces are modelled as one quad element each. A quad will have four nodes, which is displayed in figure 5.13. The red numbers display the quad numbers and the blue numbers display the node numbers. The plates in the build-up beams makes it a stronger cross section than only having a rectangular beam. These plates will help for stability and stiffness. However, to simplify and to be on the safe side for the first approach, the stiffness of the plates will not be included to calculate the height of the cross section.

Coordinate system

Timber has a main grain direction and this needs to be taken into account with modelling the structure. A distinction is made between the global and local coordinate system, see figure 5.14. The local coordinate system of all quad elements is orientated with the local x-axis matches the parallel grain orientation of the timber. Accordingly the local y-axis matches the perpendicular grain orientation. The global coordinate system follows the lay-out of the roof and its boundaries. The local x-axis for the plates could be in the direction of the global x-direction or the global y-direction. If the main grain direction will be in the global x-direction, the plates are less stiff in the other direction. This is another reason for not including the plates, while the stiffness of the I-beams are stronger in one direction than in the other. It has a larger influence on the example model than it will have on the global model. Since the example model has a determined span direction. The main grain direction of the bottom plates could be in the opposite direction to the top plates for a better distribution. However, this is not representative for the global model because it will have different span directions. To define which direction is more suitable is a study on its own.

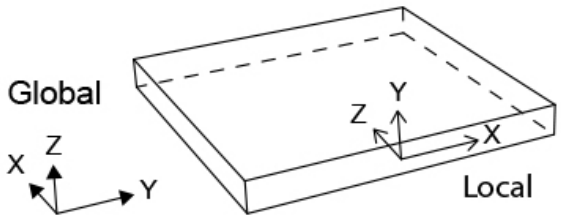

Figure 5.14: The global and local coordinate system

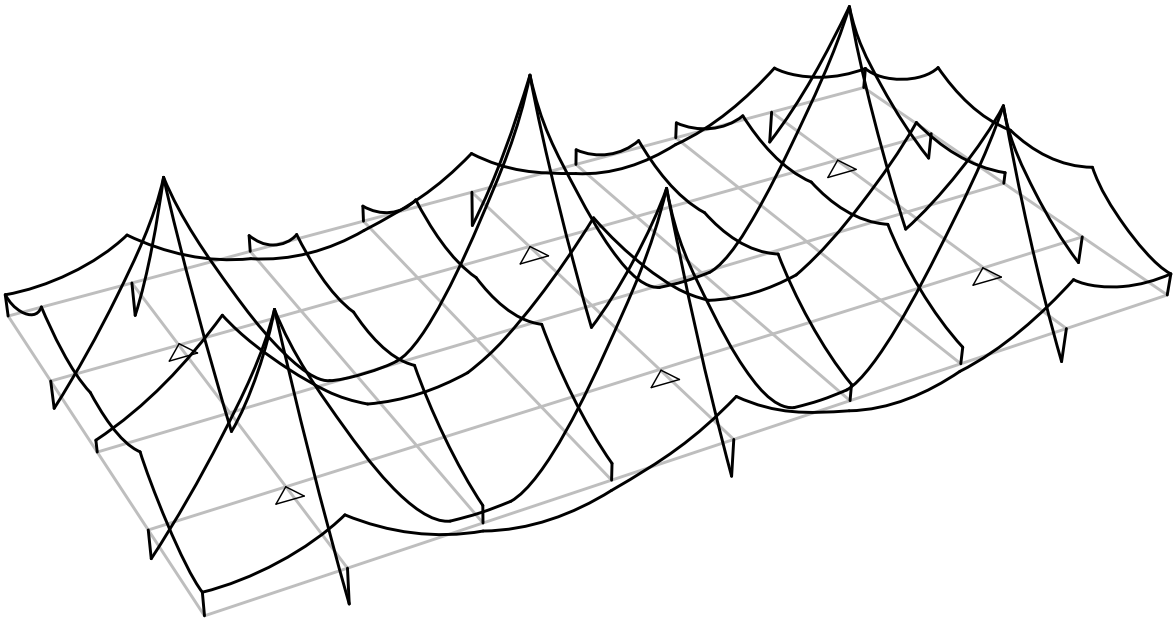

Figure 5.15: The bending moment M_y in both directions

Approach stiffness connection

The plates will be attached to the ribbed elements by screws. For I-beams the amount of screws and the stiffness of the connection should be taken into account, since this will have a influence on the structural behaviour. If the same amount of screws will be used for the calculation example as the global model there will be a difference in stiffness of the connections. The long span of the global model will give stiffer connections than the calculation example. Therefore different material properties will be assigned to the structure. The ribbed elements will have the Kerto-Q properties. The top and bottom plate will have material properties without dead load and stiffness. The stiffness for the connection will be defined in a later stage with a fine mesh.

Load assumptions

The material Kerto-Q has a density of $510\,kg/m^3$ and therefore the self-weight of the structure will be $0,09\,kN/m$. A dead load of $2\,kN/m^2$ will be applied to the structure. The different loads will be applied in combination with simplified load combinations. The deflection will be checked in the serviceability limit state, load combination 101. The dimensions of the cross section will be defined in the ultimate limit state. Therefore the stresses will be checked according to load combination 202. The structure is calculated and the obtained results can be used.

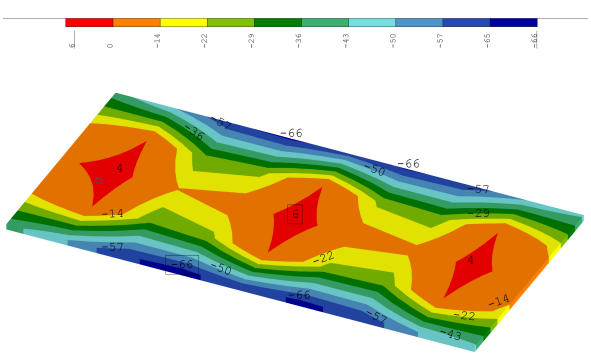

Figure 5.16: The deflection of the initial model in mm

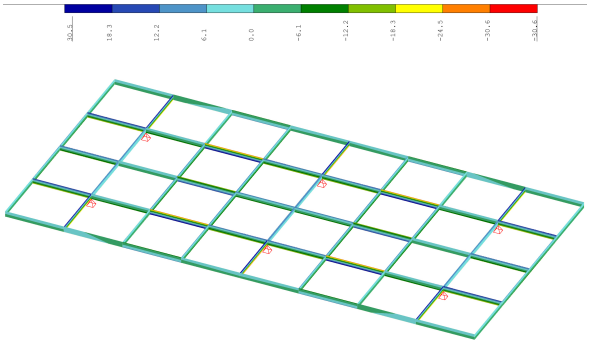

Figure 5.17: The stresses in local x of the initial model in N/mm^2

Analysis of the structure

After the model is exported into SOFiSTiK, the load will be applied and the structure will be analysed. The maximum deflection of the structure is 66 mm, which occurs at the longitudinal cantilever side (figure 5.16). The bending moment M_y in both directions can be shown in figure 5.15. The required height could be calculated from equation 5.3. However the bending moment M_y depends on the dead load and self-weight, which will change when the cross section will change as well. Instead of using this equation with calculating the height from the bending moments, the height will be increased when the actual stresses are above the allowable stresses. The stresses of the initial model are shown in figure 5.17. The maximum tension and compression stresses are $30,6\ N/mm^2$.

Step 2

The initial model has been made and the structure has been analysed. In the second step the approximation of the smooth height variation will be discussed. It will be explained how the data is imported into Excel. The design is compared against the stresses criteria. The height is then increased till this criteria has been met. Further it will be explained how the new geometry and stresses are exported back in SOFiSTiK. All these steps are part of the smooth height variation process, see figure 5.9.

First all the following data will be collected to describe the structure:

- Quad elements with corresponding nodes
- Local coordinate system
- Reaction forces
- Top nodes with their corresponding coordinates
- Bottom nodes with their corresponding coordinates
- Stresses in nodes

The data will be used as import for Excel to get a new height for the design of this structure. This step has been explained in more detail in the diagram of the height variation process, see figure 5.18. The result viewer of SOFiSTiK shows the results in lists which could be used to export to Excel. The first three items will be imported only the first time and it will be used during the whole process, this has been displayed with a dotted line in the figure 5.18. First the quad elements with corresponding nodes will be selected from this list. Each quad number with four node numbers will be imported into a sheet of the Excel file. From each node the coordinates will be taken from the global coordinate system in x, y and z values. The local coordinate system will be imported with the vector orientation of the three directions. The main grain direction will stay orientated upon the top plate and this will not change.

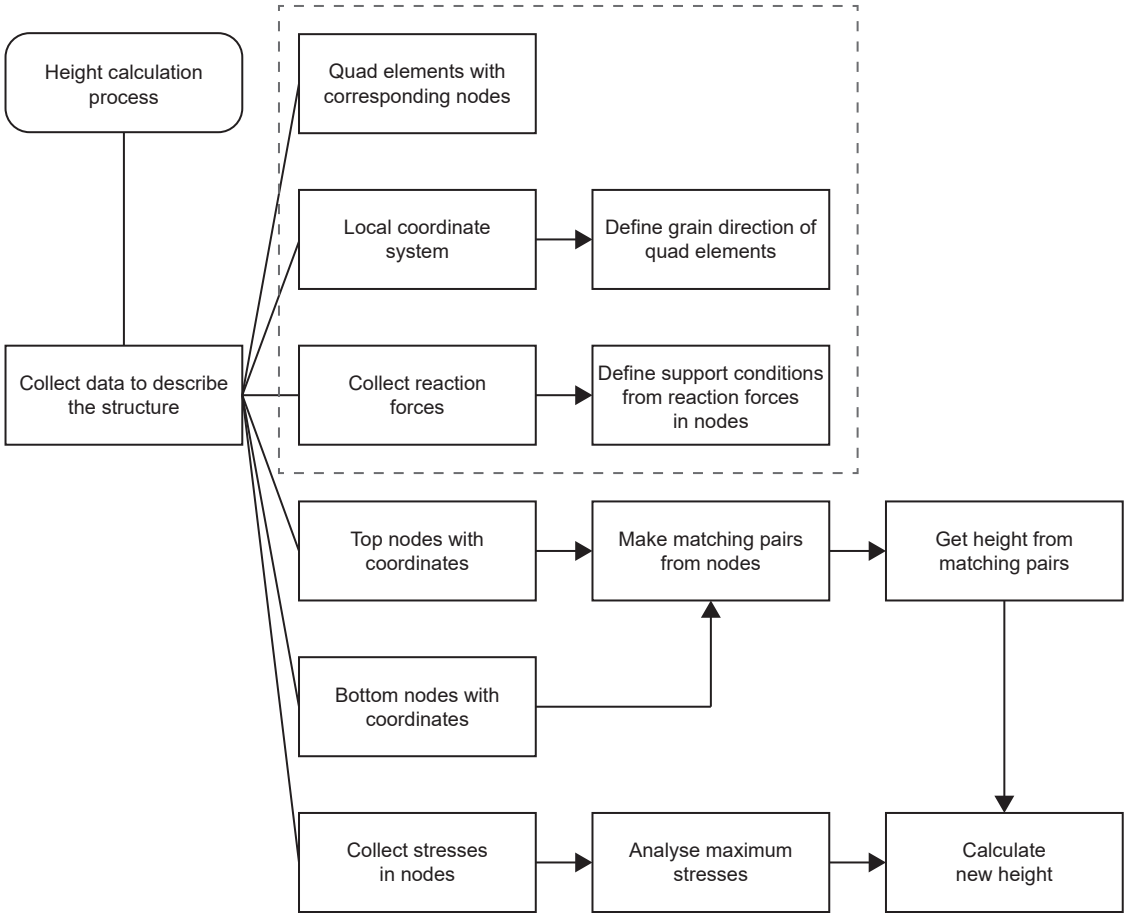

Figure 5.18: The diagram of the height variation process

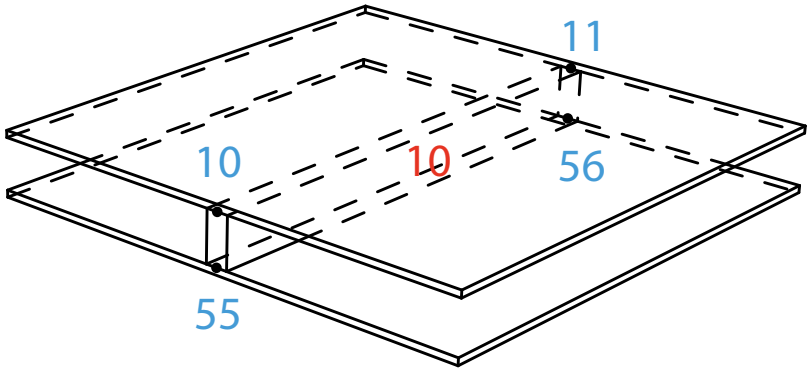

Figure 5.19: The old height between the top and bottom nodes

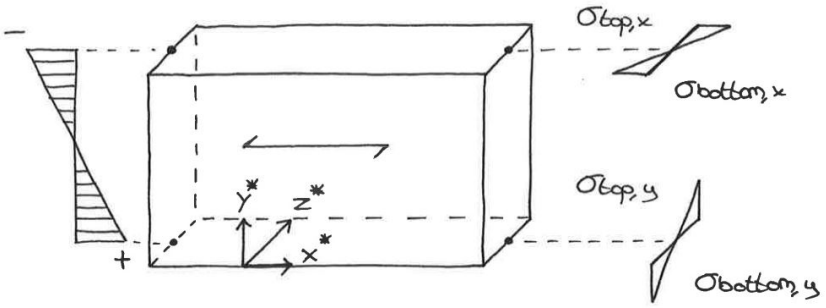

Figure 5.20: Reading out the inplane stresses of the nodes

The reaction forces will be used to define support conditions later on, which bottom nodes are functioning as supports. The reaction forces will be read out of the result viewer and the corresponding node number will be fixed in the desired directions. The node will be fixed in all directions when the forces have no zero values. If P_x is zero then the bottom node should be fixed in y- and z-direction. If P_y is zero then the bottom node should be fixed in x- and z-direction.

Matching pairs

Although the plates will not be used in this approximation, they are helpful to make a distinction between top and bottom nodes. Each quad element for the ribbed elements has two top nodes and two bottom nodes. The top nodes will be unchanged and the bottom nodes will vary when the height needs to be increased. In figure 5.13 an example of numbering elements and node numbers is seen. The top nodes and bottom nodes with their corresponding coordinates will be imported. It is important that the top node and the corresponding bottom node will be matched into a matching pair to get the height. Visual Basic for Applications will be used for this. VBA is a programming language of Excel. In order to find the corresponding bottom node the minimum distance will be searched for in the global coordinate system. For quad element number 10 two matching pairs needs to be made, see figure 5.19. Top node number 10 needs to find the bottom node number 55 and top node number 11 needs to find the bottom node number 56. For the six column example the bottom node could be searched along the global z-direction. In the case that there is a curved surface in the global model, this is not that straight forward. Therefore the following formula will be used for computing the distance between the different nodes:

$$Distance = \sqrt{(x_t - x_b)^2 + (y_t - y_b)^2 + (z_t - z_b)^2} \tag{5.4}$$

In-plane stresses

The strongest axis will be the local x direction which equals the main grain direction.

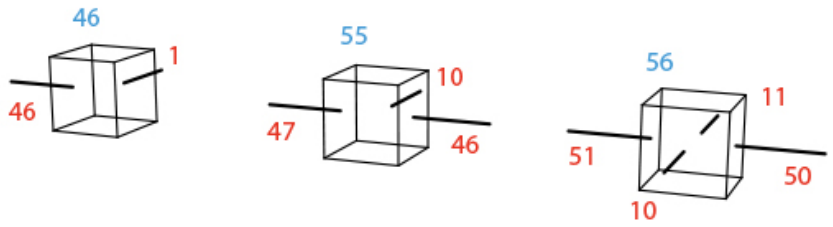

Figure 5.21: The different stresses from ribbed elements in each node

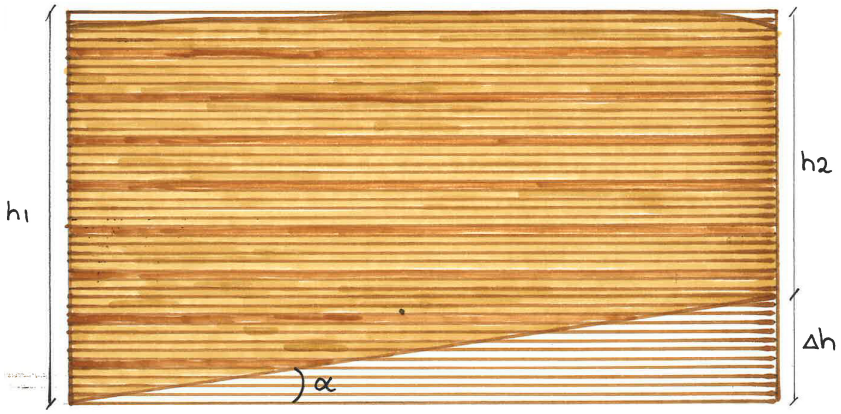

Figure 5.22: The different stresses from ribbed elements in each node

Therefore the normal stresses in x-direction will only be checked. A thickness is assigned to each surface, which will give a distribution in the node. The local z direction will be orientated along the surface thickness. In each node three stresses along the x-direction could be read out. In the positive direction of this axis the first stresses are the bottom stresses, mid plane are the centre stresses and the top are the top stresses. These inplane-stresses and how to read them are displayed in figure 5.20. The absolute maximum from the top and the bottom stresses will be taken. Therefore a list with these values will be created for each node.

Maximum stresses

The surfaces of the ribbed elements and plates are modelled as one quad element each. Each quad element has four nodes in this structure. A quad element for a ribbed element will contain four nodes at each corner, two nodes in the top and two nodes in the bottom. The stresses from different beams will come together in one node. In a corner two elements will come together but in another part of the structure four elements could come together as well, see figure 5.21 . There could be a difference along those elements from different directions. For example the bending moments could be higher in one direction than the other, which makes a difference in stresses. An option could be that from each direction the average stress should be taken. This could generate a difference in height from each direction at the intersection of the beams. It is required to have a smooth transition. Therefore the following decision is made to take the maximum stresses of two, three or four elements. The maximum stress of the quad elements 1 and 46 will be selected. For the other node in figure 5.21, the maximum will be taken of the 10, 46 and 47 elements. For the other node the maximum of one of the four elements will be taken as well. This could generate the fact that the beam will be designed higher than required. It is preferred since this gives a smooth height variation and the plates will have no shift in contrast to the others.

Height difference

In this step it is checked if the design satisfies the stresses criteria. If the actual stresses are not below the allowable stresses the height needs to be increased. The roof surface has

Table 5.3: The reduction factors for elements sawn at an angle [1]

Angle α	0°	2,5°	5°	10°	15°	30°	45°	60°	90°
Bending edgewise	1,00	0,90	0,75	0,55	0,40	0,25	0,20	0,20	0,22
Bending flatwise	1,00	1,00	0,90	0,70	0,50	0,25	0,20	0,20	0,22
Tension ‖ to grain	1,00	1,00	0,90	0,70	0,40	0,25	0,20	0,20	0,23
Compression ‖ to grain	1,00	1,00	0,90	0,70	0,50	0,35	0,25	0,25	0,35
Modulus of elasticity	1,00	0,90	0,80	0,60	0,40	0,15	0,10	0,10	0,23

been predefined by the architect and therefore the top nodes will remain unchanged. If the height needs to be increased the bottom node will be changed. The difference in height which results, that the ribbed elements will be tapered at the bottom sides. In figure 5.22 a ribbed element with difference in height is shown. The top part will be curved but this reduction will be neglected. A reduction factor needs to be taken into account for Kerto-Q when a member is sawn at an angle α to the grain direction [1]. For the example the difference will not be that large and the reduction factors corresponding to an angle of 5° will be taken into account. The difference for the global model will be larger and therefore the reduction factors of an angle of 10° will be taken into account. In table 5.3 the different factors can be found.

Checking stresses criteria

The actual stresses needs to be below the stresses criteria in equation 5.5. In figure 5.17 the maximum stresses are $30,6 N/mm^2$ and the height needs to be increased. For the stresses below $6,1\ N/mm^2$ the height needs to be decreased from the matching pairs.

$$f_{m,d} = \gamma_{reduction} \cdot \frac{k_{mod} \cdot f_{m,k}}{\gamma_M} = 0,75 \cdot \frac{0,6 \cdot 32}{1,2} = 12\ N/mm^2 \tag{5.5}$$

Height approximation

The initial height from the matching pairs is $200 mm$. If the actual stresses are too high the height will be increased. The height will be decreased if the actual stresses are really low. The minimum height is $90\ mm$ for this structure. A minimum height is required since the plates need to be attached by screws and the height should not be smaller than the width of the beam. If the height needs to be increased of decreased, the bottom node will be moved in the vector direction of the matching pairs with the equation 5.3. Each bottom node will have new global x, y and z values. The minimum height step is $10 mm$. In table 5.4 the difference height steps are described for increasing the height, where MAX $f_{m,d}$ is $12\ N/mm^2$. In the case that the stresses are too low, in the table 5.5 the height steps are described for MIN $f_{m,d}$ is $6 N/mm^2$.

The new height between the two matching pairs 10 & 55 and 11 & 56 has been defined on the stresses. In figure 5.23 the change in height of the ribbed element is shown, the bottom plate is deformed as well. After the new height for each matching pair has been defined a new structure will be generated. All the quad elements, node topology and support conditions are required for the new structure as input for SOFiSTiK. From Excel all the data will exported into SOFiMSHA and the new stresses will be calculated.

In figure 5.24 the new stresses are depicted. The middle columns take up more bending moments than the other columns and therefore the height is higher at those supports. It can be seen that the height will be reduced at all the cantilever parts. The maximum stress is $16,6\ N/mm^2$ which is not lower than the allowable stress of $12\ N/mm^2$. Therefore the data of these stresses will be imported again into Excel.

The bottom nodes with their corresponding coordinates will be imported and the matching pairs will get the new height. The new stresses will be imported as well. The stresses will be

Table 5.4: Increasing the height by steps for max $f_{m,d}$

If $\sigma_{m,d}$ ≥max $f_{m,d}$		
$\sigma_{m,d} \geq 1,15 \cdot f_{m,d}$	then	$H_{new} = H_{old} + 2 \cdot H_{step}$
$\sigma_{m,d} \geq 1,2 \cdot f_{m,d}$	then	$H_{new} = H_{old} + 3 \cdot H_{step}$
$\sigma_{m,d} \geq 1,3 \cdot f_{m,d}$	then	$H_{new} = H_{old} + 4 \cdot H_{step}$
$\sigma_{m,d} \geq 1,4 \cdot f_{m,d}$	then	$H_{new} = H_{old} + 5 \cdot H_{step}$
$\sigma_{m,d} \geq 1,5 \cdot f_{m,d}$	then	$H_{new} = H_{old} + 6 \cdot H_{step}$
$\sigma_{m,d} \geq 2 \cdot f_{m,d}$	then	$H_{new} = H_{old} + 8 \cdot H_{step}$
$\sigma_{m,d} \geq 3 \cdot f_{m,d}$	then	$H_{new} = H_{old} + 10 \cdot H_{step}$
$\sigma_{m,d} \geq 4 \cdot f_{m,d}$	then	$H_{new} = H_{old} + 14 \cdot H_{step}$
$\sigma_{m,d} \geq 5 \cdot f_{m,d}$	then	$H_{new} = H_{old} + 18 \cdot H_{step}$

Table 5.5: Decreasing the height by steps for min $f_{m,d}$

If $\sigma_{m,d}$ ≤min $f_{m,d}$		
$\sigma_{m,d} \leq 0,5 \cdot f_{m,d}$	then	$H_{new} = H_{old} - 1,5 \cdot H_{step}$
$\sigma_{m,d} \leq f_{m,d}$	then	$H_{new} = H_{old} - 0,7 \cdot H_{step}$

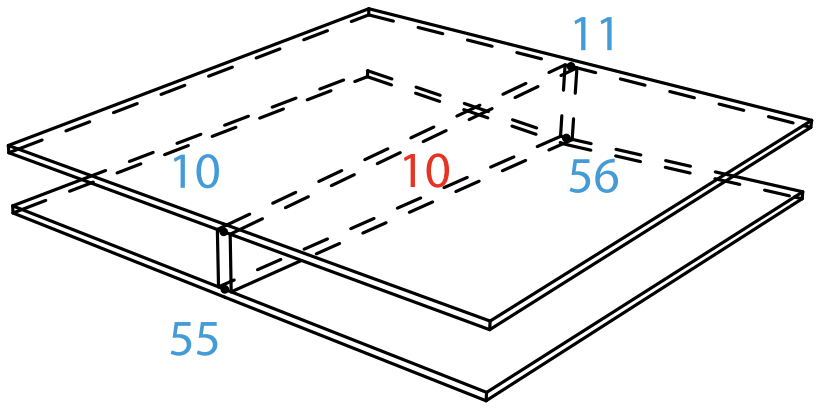

Figure 5.23: The new height between the top and bottom nodes

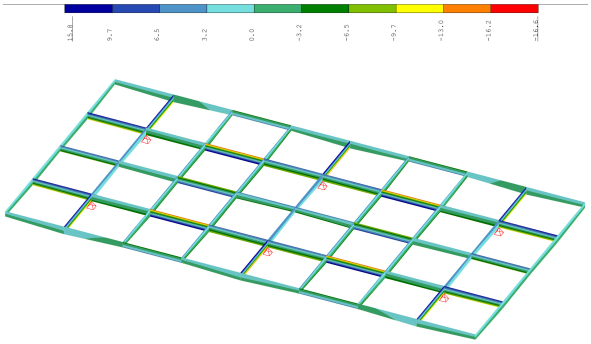

Figure 5.24: The stresses in local x of the structure with the new height N/mm^2

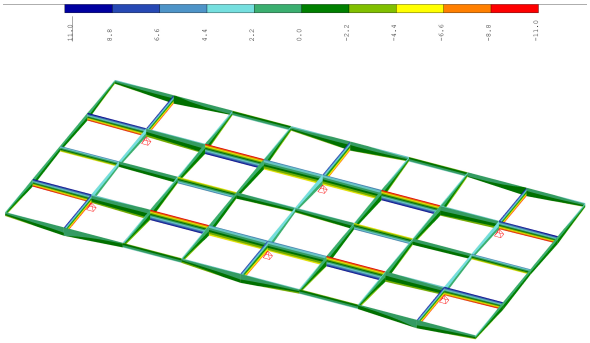

Figure 5.25: The stresses after multiple iterations in N/mm^2

checked in each node and the design might not satisfy the stresses criteria in some nodes. Therefore the height will be increased or decreased where necessary. Multiple iterations will be done to increase the height by steps till the stresses are met. After the iterations the design criteria needs to satisfy the equation 5.5. Then the iterations are terminated and the design has been completed for this structure.

In figure 5.25 the end stresses are shown for this step. The maximum stress is $11.0 N/mm^2$ which is lower than the allowable stress of $12 N/mm^2$. Therefore the height for these stresses is known from the iterations. It is expected that the stresses are equal among the structure. However, in figure 5.25 a couple of ribbed elements show the colours of low stresses. This is cause by using the maximum stress for a smooth height variation, resulting in unequal stress distribution.

Step 3

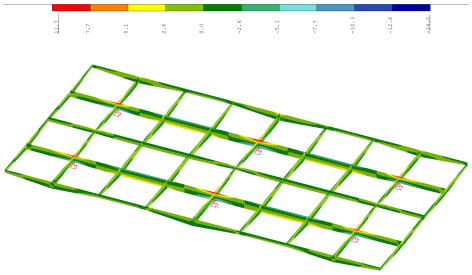

Figure 5.26: The stresses (N/mm^2) of the structure with a fine mesh of $0,09\ m$

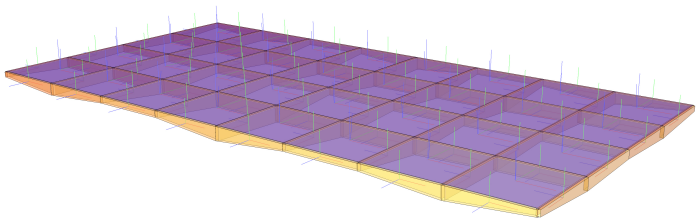

Figure 5.27: The local x-direction of the plates and ribbed elements, displayed by the red line

In the third step the design of the structure will be shown and the model will be made with a fine mesh for more accurate results. In step 2 a new height has been defined for the structure. The top and bottom points from the database will be imported into Rhinoceros. From these points a new geometry is made. This geometry is set up by hand in Rhinoceros. However in a later stage, for the global model, the program Grasshopper will be used to generate the structure in a parametric way as well. The finite element meshes are made for this structure.

In this step the plates will be included for a better approximation. The plates will be attached to the ribbed elements by screws. For I-beams the amount of screws and stiffness of the connection should be included since this will have an influence on the structural behaviour. The stiffness of connection has been calculated and it is approximately 50 percent. The incision of the ribbed elements gives a reduction of 7 percent stiffness. The reduction in stiffness will be taken into account for the calculation example and the global model.

Therefore the material properties of the plates will have only 40 percent stiffness. All these calculations will be shown in more detail in chapter 6. The proof of the approximation for reduction of the material properties of the plates will be given in section 6.2.2.

The grain direction of the ribbed elements are orientated in the strongest axis. The local x-direction is in the span direction of the ribbed elements. The grain direction of the plates are orientated in the global x-direction. The red line displays the local x-direction of the top plates in figure . The bottom plates have the same direction as the top plates. Therefore the cross section in the global x-direction is stronger than in the global y-direction.

Fine mesh model

The finite element meshes are made for this structure. Only rectangular elements are used if possible and a density of $0,09\,m$ with the mesh is used. The ribbed elements width has been taken for this density for the current results.

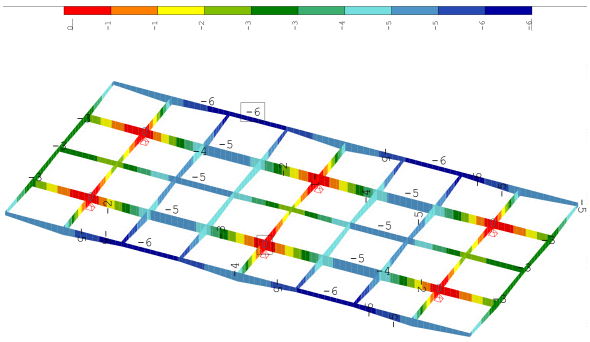

Figure 5.28: The deflection (mm) of the structure from the ribbed elements

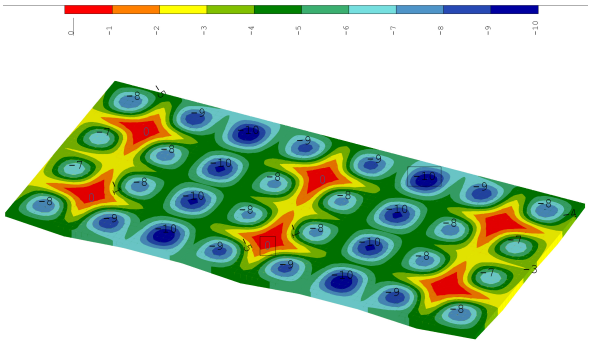

Figure 5.29: The deflection (mm) of the structure with a fine mesh of $0,20\,m$

In figure 5.26 the stresses are displayed with a fine mesh of $0,09\,m$, where the maximum stress is $14\,N/mm^2$. At some points the stresses are too high. The stresses are locally as they occur at the supports. The support conditions are modelled as pin supports. A pin support could be seen as a point load under the structure. Therefore singularities could occur and this needs to be solved by a more realistic approach. Therefore rectangular elements of a density of $0,20\,m$ with the mesh is used. Approximately two times the ribbed elements width has been taken for the current results.

The maximum deflection of the structure is $6\,mm$ for the ribbed elements, which occurs at the longitudinal cantilever side (figure 5.28). The maximum deflection with the plates included is $10mm$, see figure 5.29 . The stresses are depicted in the figure 5.30 with a maximum of $10,4\,N/mm^2$.

Step 4

The fourth and last step will be to check if the structure has the correct height. If this is not the case, adjustments could be made by hand or step 2 and 3 need to be done again. The checks are done for the different groups of the ribbed elements, top and bottom plates. However the design check for the ribbed elements will only be displayed in detail in section 5.3. The strength verification for the cross section dimensions need to be checked with the following equations from EN 1995-1-1: 2004, 6.1 and 6.2. If the values will exceed the design values, the elements should be made higher.

For combined bending and axial tension stresses will be checked with equation 5.6 and equation 5.7.

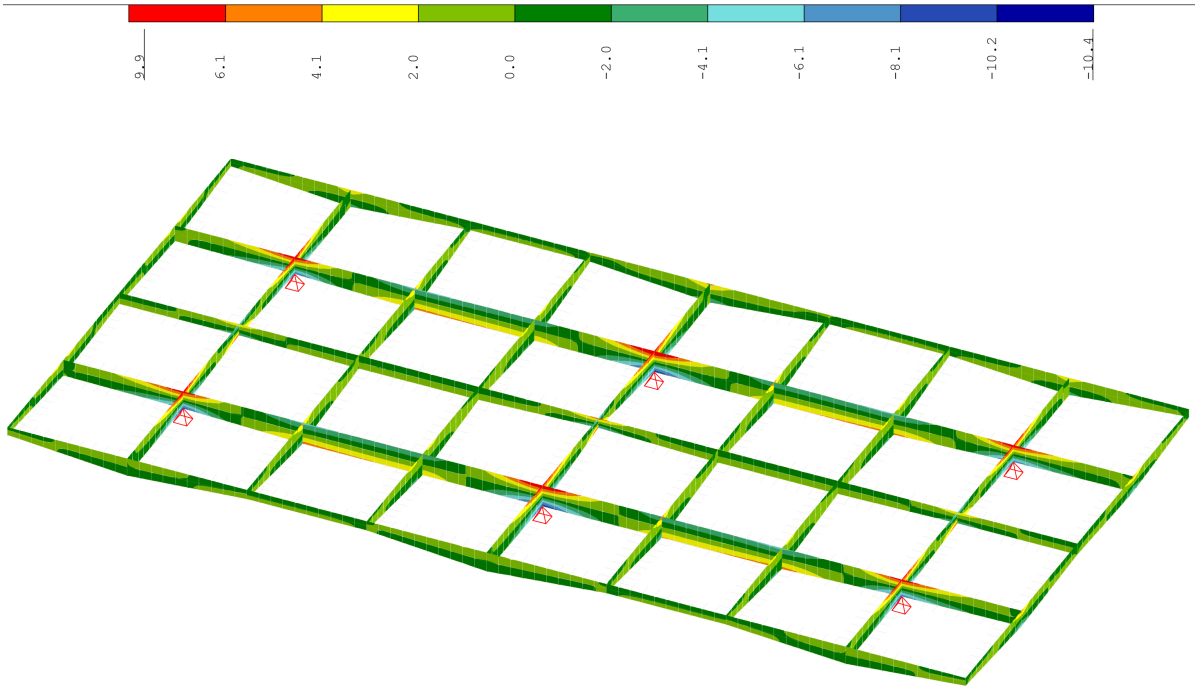

Figure 5.30: The stresses (N/mm^2) of the structure with a fine mesh of $0,20\ m$

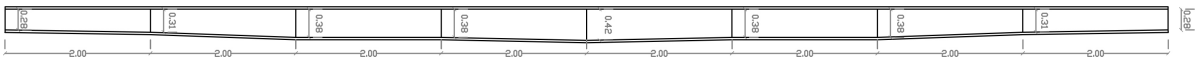

Figure 5.31: The dimensions of the beam on supports in the global x direction (m)

$$\frac{\sigma_{t,0,d}}{f_{t,0,d}} + \frac{\sigma_{m,y,d}}{f_{m,y,d}} + k_m \frac{\sigma_{m,z,d}}{f_{m,z,d}} \leq 1 \tag{5.6}$$

$$\frac{\sigma_{t,0,d}}{f_{t,0,d}} + k_m \frac{\sigma_{m,y,d}}{f_{m,y,d}} + \frac{\sigma_{m,z,d}}{f_{m,z,d}} \leq 1 \tag{5.7}$$

The equation 5.8 and equation 5.9 shall be satisfied for combined bending and compression stresses.

$$\left(\frac{\sigma_{c,0,d}}{f_{c,0,d}}\right)^2 + \frac{\sigma_{m,y,d}}{f_{m,y,d}} + k_m \frac{\sigma_{m,z,d}}{f_{m,z,d}} \leq 1 \tag{5.8}$$

$$\left(\frac{\sigma_{c,0,d}}{f_{c,0,d}}\right)^2 + k_m \frac{\sigma_{m,y,d}}{f_{m,y,d}} + \frac{\sigma_{m,z,d}}{f_{m,z,d}} \leq 1 \tag{5.9}$$

The equation 5.10 shall be satisfied for shear and transverse forces.

$$\left(\frac{\tau_{y,d}}{f_{v,d}}\right)^2 + \left(\frac{\tau_{z,d}}{f_{v,d}}\right)^2 \leq 1 \tag{5.10}$$

For shear and torsion interaction will be checked with equation 5.11.

$$\left(\frac{\tau_{tor,d}}{k_{shape} \cdot f_{v,d}}\right) + \left(\frac{\tau_{y,d}}{f_{v,d}}\right)^2 + \left(\frac{\tau_{z,d}}{f_{v,d}}\right)^2 \leq 1 \tag{5.11}$$

The section forces are read from the program SIR of SOFiSTiK, which will be explained in section 5.4. The height of the long beam and short beam can roughly be checked from the bending moments. The dimensions of the long beam are displayed in figure 5.31. The

Table 5.6: Beam on supports in global x direction 5.31

Height h $\cdot 10^3$ (mm)	Bending moment M_y $\cdot 10^6$ (Nmm)	Bending stresses $\sigma_{m,d}$ (N/mm^2)	Unity check
0,28	- 0,5	- 0,43	0,04
0,31	- 17,5	- 12,14	1,01
0,38	+ 16,1	+ 7,43	0,62
0,38	+ 9,4	+ 4,34	0,36
0,42	- 32,3	- 12,21	1,02
0,38	+ 11,7	+ 5,40	0,45
0,38	+ 14,7	+ 6,79	0,57
0,31	-17,5	- 12,14	1,01
0,28	-0,5	-0,43	0,04

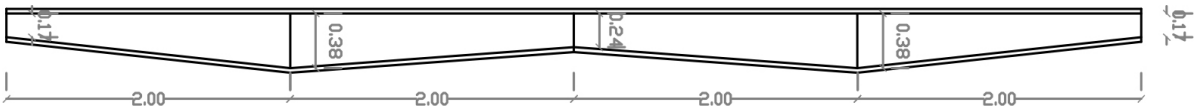

Figure 5.32: The dimensions of the middle beam in the global y direction (m)

bending moments along this beam are compared with the bending stresses, if the determined height is correct from the allowable stresses. An overview of these results has been given in table 5.6. The same has been done for the short beam, see figure 5.32. In table 5.7 the rough check for the short beam is shown. For the correct way of calculating the stresses in comparison with the forces, see equation 5.19. In the following section the height of the ribbed elements will be checked in detail on bending and shear stresses.

5.3. Checking strategy

The material properties of Kerto-Q are used for the ribbed elements. The reduction factors are taken into account for $f_{m,0,d}$, $f_{m,90,d}$, $f_{t,0,d}$ and $f_{c,0,d}$. For the plates 40 percent of the material properties of Kerto-Q has been assigned. The local coordinate system has been explained in section 5.1 of this chapter. A distinction has been made between the different loads as different factors need to be applied for long or short time loading. Considering the service class and the actual duration class, all the material design values are calculated with the factors (table 5.8).

Table 5.7: Middle beam in global y direction 5.32

Height h $\cdot 10^3$ (mm)	Bending moment M_y $\cdot 10^6$ (Nmm)	Bending stresses $\sigma_{m,d}$ (N/mm^2)	Unity check
0,17	+ 0,1	+ 0,23	0,02
0,38	- 6,7	- 3,09	0,26
0,24	+ 0,2	+ 0,23	0,02
0,38	- 6,8	- 3,14	0,26
0,17	+ 0,1	+ 0,23	0,02

Table 5.8: Factors load-duration class

Service class:	2					
Load-duration class:	Permanent	LC 201	k_{mod}	0,6	γ_m	1,2
Load-duration class:	Short-term	LC 203	k_{mod}	0,9	γ_m	1,2

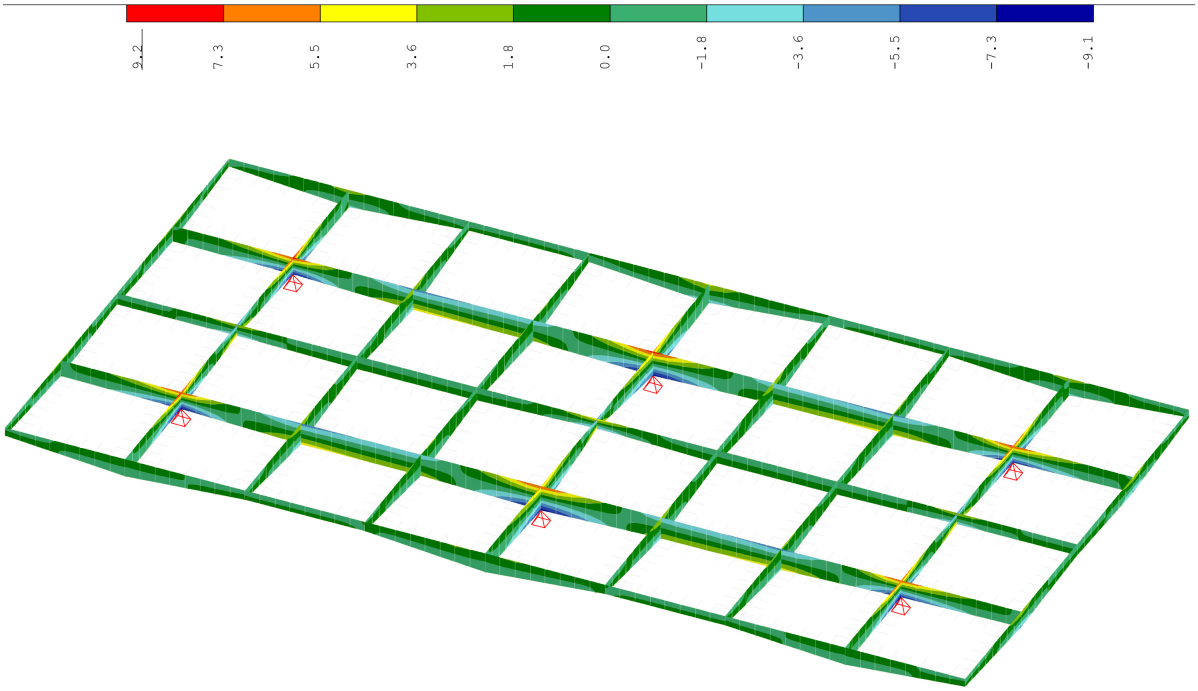

Figure 5.33: The stresses in local x of the end structure in N/mm^2

The results of checking the ribbed elements will be shown below. From SOFiSTiK the maxima and minima internal forces and stresses have been obtained. The stresses have been divided into three parts; top, bottom and middle. The set-up of these three layers has been explained in the section 5.1. The top stresses are mentioned as S_{xu}, S_{yu} and S_{xyu}. The bottom stresses are mentioned as S_{xl}, S_{yl} and S_{xyl}. The stresses in the middle plane are mentioned as S_x, S_y and S_{xy}. The x-axis stands for parallel to the grain. The y-axis stands for perpendicular to the grain. The combination of XY stands for the shear stress edgewise. These stresses could be read from SOFiSTiK along the edge. The shear stresses flatwise are not provided by the program. Therefore the shear forces V_x and V_y along the plate thickness are used instead. The stress resultants having the dimension force per unit length.

In the case for the global model that local stresses occur, they need to be solved with the required connection details. For example where a support occur, there the high load needs to be transferred into the plate. This is ignored during the check if the stresses are high at the support conditions. These local stresses needs to be resolved in detail. The local issues for the calculation example where solved by a mesh density of two times the ribbed element thickness. However the middle columns still had problems with the bending stress flatwise and therefore the height has been increased from $400\,mm$ to $420\,mm$. This maximum height is shown in figure 5.31 for the beam in global x-direction. In the other direction the maximum height is $380\,mm$ and the minimum height is $170\,mm$, see figure 5.32. In figure 5.33 the top stresses in local x (S_{xu}) of Loadcase 202 are displayed.

Table 5.9: Design values - LC 201

Design values:	Permanent				
Flatwise		N/mm^2	**Edgewise**		N/mm^2
Bending ∥ to grain	$f_{m,0,d}$	16,20	Bending	$f_{m,d}$	12,00
Bending ⊥ to grain	$f_{m,90,d}$	4,00	Tension ∥ to grain	$f_{t,0,d}$	10,80
Compression	$f_{c,90,d}$	1,10	Tension ⊥ to grain	$f_{t,90,d}$	2,5
Shear	$f_{v,d}$	0,65	Compression ∥ to grain	$f_{c,0,d}$	11,70
			Compression ⊥ to grain	$f_{c,90,d}$	4,5
			Shear	$f_{v,d}$	2,25

The maximum stresses and forces for the load case 201 are shown in table 5.10. The minimum and maximum stresses and forces are taken, which cells have an extra border. For example the minimum top stress in local x, S_{xu} is $-6,09\ N/mm^2$ and the maximum top stress in local x, S_{xu} is $6,17\ N/mm^2$. The material design values for the permanent load case are shown in table 5.9. In the following steps the checks for shear and in-plane stresses, edge and flatwise are done.

The design check will be done for the shear flatwise and edgewise. The shear stresses flatwise are not provided by the program SOFiSTiK. Therefore the maximum shear force $v_{max,ed}$ is taken from min/max v_x, min/max v_y. $V_{max,ed}$ is $3,05\ N/mm$ and it is used to calculate the maximum shear stress $\tau_{xy,ed}$ with equation 5.12. The maximum shear stress $\tau_{xy,ed}$ is lower than the allowable shear flatwise stress, see equation 5.13.

The maximum shear stress interaction is considered with equation 5.10, where $\tau_{y,d}$ is min/max v_x and $\tau_{z,d}$ is the corresponding v_y. The combination of where $\tau_{y,d}$ is min/max v_y and $\tau_{z,d}$ is the corresponding v_y is checked as well. From these values the absolute maximum has been taken, which is $0,01 N/mm^2$ and smaller than 1.

The maximum is taken of min/max s_{xyu}, min/max s_{xyl} and min/max s_{xy} for the maximum shear edgewise stress $\tau_{xy,ed}$. The shear edgewise stress $\tau_{xy,ed}$ is $0,79 N/mm^2$ and it is smaller than the $f_{v,d}$, see equation 5.14.

$$\tau_{xy,ed} = 1,5 * \frac{v_x}{b * h} = 0,05\ N/mm^2 \tag{5.12}$$

$$\frac{\tau_{xy,ed}}{\tau_{xy,rd}} = \frac{0,05}{0,65} = 0,08\ N/mm^2 < 1 \tag{5.13}$$

$$\frac{\tau_{xy,ed}}{f_{v,d}} = \frac{0,79}{2,25} = 0,35\ N/mm^2 < 1 \tag{5.14}$$

All internal forces causes stresses at the top, the middle and the bottom layer of the finite element elements. The design values of bending ($f_{m,0,d}$) have a higher capacity than for tension ($f_{t,0,d}$) and compression ($f_{c,0,d}$). Therefore all stress checks are done by only considering the tension and compression values. In the table 5.11 the maximum values are checked if the utilization is below 1.

The linear superposition of the in-plane stresses in the x-axis and y-axis are checked. The maximum value is taken and the corresponding stress value for the other directions as well. The stresses are checked if they are below the bending stresses edgewise $f_{m,edge,d}$ and flatwise $f_{m,90,flat,d}$ for the top and bottom layer, see equation 5.15. This check is executed for eight times, the top values are 0,82, 0,82, 0,78, 0,14 and the bottom values are 0,82, 0,82, 0,78,

Table 5.10: Max stresses and forces - Permanent - LC 201

	nr	v_x	v_y	s_{xu}	s_{yu}	s_{xyu}	s_{xl}	s_{yl}	s_{xyl}	s_x	s_y	s_{xy}
min v_x	1002	-1,77	0,49	-5,75	-1,1	0,47	-6,09	-1,24	0,52	-5,92	-1,17	0,5
max v_x	1001	1,77	0,49	-5,75	-1,1	-0,47	-6,09	-1,24	-0,52	-5,92	-1,17	-0,5
min v_y	1842	0,03	-3,05	0,53	0,04	0,05	0,23	-0,06	0,07	0,38	-0,01	0,06
max v_y	1590	0,03	3,05	0,23	-0,06	-0,07	0,53	0,04	-0,05	0,38	-0,01	-0,06
min s_{xu}	1004	1,77	-0,49	-6,09	-1,24	0,52	-5,75	-1,1	0,47	-5,92	-1,17	0,5
max s_{xu}	1090	1,77	0,49	6,17	-1,22	-0,47	5,14	-1,13	-0,52	5,65	-1,17	-0,5
min s_{yu}	1078	0,98	0,02	4,9	-1,48	0,7	5,55	-1,46	0,69	5,23	-1,47	0,69
max s_{yu}	1948	0,05	-2,79	-0,04	0,53	0,06	0,12	-0,55	0,11	0,04	-0,01	0,08
min s_{xyu}	1553	-0,71	-0,01	-4,51	0,3	-0,79	-4,51	0,3	-0,77	-4,51	0,3	0,78
max s_{xyu}	1503	0,71	-0,01	-4,51	0,3	0,79	-4,51	0,3	0,77	-4,51	0,3	0,78
min s_{xl}	1002	-1,77	0,49	-5,75	-1,1	0,47	-6,09	-1,24	0,52	-5,92	-1,17	0,5
max s_{xl}	1029	1,77	-0,49	5,14	-1,13	0,52	6,17	-1,22	0,47	5,65	-1,17	0,5
min s_{yl}	1017	-0,98	-0,02	5,55	-1,46	0,69	4,9	-1,48	0,7	5,23	-1,47	0,69
max s_{yl}	2053	-0,05	2,79	0,12	-0,55	0,11	-0,04	0,53	0,06	0,04	-0,01	0,08
min s_{xyl}	1735	0,71	0,01	-4,51	0,3	-0,77	-4,51	0,3	-0,79	-4,51	0,3	-0,78
max s_{xyl}	1706	-0,71	0,01	-4,51	0,3	0,77	-4,51	0,3	0,79	-4,51	0,3	0,78
min s_x	1002	-1,77	0,49	-5,75	-1,1	0,47	-6,09	-1,24	0,52	-5,92	-1,17	0,5
max s_x	1010	1,77	-0,49	6,17	-1,22	0,47	5,14	-1,13	0,52	5,65	-1,17	0,5
min s_y	1017	-0,98	-0,02	5,55	-1,46	0,69	4,9	-1,48	0,7	5,23	-1,47	0,69
max s_y	1454	0	0	3,86	0,38	0,43	3,86	0,38	0,43	3,86	0,38	0,43
min s_{xy}	2022	-0,71	-0,01	4,16	0,3	-0,78	4,23	0,3	-0,77	4,2	0,3	-0,78
max s_{xy}	2245	-0,71	0,01	4,23	0,3	0,77	4,16	0,3	0,78	4,2	0,3	0,78

Table 5.11: Tension and compression values - LC 201

Tension and Compression		N/mm^2		N/mm^2		
Max tension ∥ to grain	$f_{t,0,ed}$	6,17	$f_{t,0,d}$	10,80	= 0,57	< 1
Max tension ⊥ to grain	$f_{t,90,ed}$	0,53	$f_{t,90,d}$	2,50	= 0,21	< 1
Max compression ∥ to grain	$f_{c,0,ed}$	6,09	$f_{c,0,d}$	11,00	= 0,52	< 1
Max compression ⊥ to grain	$f_{c,90,ed}$	1,48	$f_{c,90,d}$	4,50	= 0,33	< 1

Table 5.12: Design values - LC 209

Design values:	Variable				
Flatwise		N/mm^2	**Edgewise**		N/mm^2
Bending ∥ to grain	$f_{m,0,d}$	24,30	Bending	$f_{m,d}$	18,00
Bending ⊥ to grain	$f_{m,90,d}$	6,00	Tension ∥ to grain	$f_{t,0,d}$	16,20
Compression	$f_{c,90,d}$	1,65	Tension ⊥ to grain	$f_{t,90,d}$	3,75
Shear	$f_{v,d}$	0,98	Compression ∥ to grain	$f_{c,0,d}$	17,55
			Compression ⊥ to grain	$f_{c,90,d}$	6,75
			Shear	$f_{v,d}$	3,38

Table 5.13: Max stresses and forces - Variable - Lc 209

	nr	v_x	v_y	s_{xu}	s_{yu}	s_{xyu}	s_{xl}	s_{yl}	s_{xyl}	s_x	s_y	s_{xy}
min v_x	1002	-0,91	0,24	-2,78	-0,54	0,23	-2,97	-0,61	0,26	-2,87	-0,57	0,24
max v_x	1001	0,91	0,24	-2,78	-0,54	-0,23	-2,97	-0,61	-0,26	-2,87	-0,57	-0,24
min v_y	1842	0,03	-1,62	0,28	0,04	0,02	0,13	-0,06	0,04	0,21	-0,01	0,03
max v_y	1590	0,03	1,62	0,13	-0,06	-0,04	0,28	0,04	-0,02	0,21	-0,01	-0,03
min s_{xu}	1004	0,91	-0,24	-2,97	-0,61	0,26	-2,78	-0,54	0,23	-2,87	-0,57	0,24
max s_{xu}	1090	0,91	0,24	3,00	-0,60	-0,23	2,49	-0,55	-0,25	2,75	-0,57	-0,24
min s_{yu}	1078	0,44	0,01	2,42	-0,73	0,34	2,73	-0,72	0,34	2,57	-0,72	0,34
max s_{yu}	1948	0,03	-1,48	-0,04	0,30	0,03	0,04	-0,32	0,05	0,00	-0,01	0,04
min s_{xyu}	1553	-0,32	0,00	-2,22	0,15	-0,39	-2,22	0,15	-0,38	-2,22	0,15	-0,38
max s_{xyu}	1503	0,32	0,00	-2,22	0,15	0,39	-2,22	0,15	0,38	-2,22	0,15	0,38
min s_{xl}	1002	-0,91	0,24	-2,78	-0,54	0,23	-2,97	-0,61	0,26	-2,87	-0,57	0,24
max s_{xl}	1029	0,91	-0,24	2,49	-0,55	0,25	3,00	-0,60	0,23	2,75	-0,57	0,24
min s_{yl}	1017	-0,44	-0,01	2,73	-0,72	0,34	2,42	-0,73	0,34	2,57	-0,72	0,34
max s_{yl}	2053	-0,03	1,48	0,04	-0,32	0,05	-0,04	0,30	0,03	0,00	-0,01	0,04
min s_{xyl}	1735	0,32	0,00	-2,22	0,15	-0,38	-2,22	0,15	-0,39	-2,22	0,15	-0,38
max s_{xyl}	1706	-0,32	0,00	-2,22	0,15	0,38	-2,22	0,15	0,39	-2,22	0,15	0,38
min s_x	1002	-0,91	0,24	-2,78	-0,54	0,23	-2,97	-0,61	0,26	-2,87	-0,57	0,24
max s_x	1010	-0,91	-0,24	3,00	-0,60	0,23	2,49	-0,55	0,25	2,75	-0,57	0,24
min s_y	1078	0,44	0,01	2,42	-0,73	0,34	2,73	-0,72	0,34	2,57	-0,72	0,34
max s_y	1454	0,00	0,00	1,87	0,19	0,21	1,87	0,19	0,21	1,87	0,19	0,21
min s_{xy}	2022	-0,32	0,00	2,04	0,15	-0,38	2,07	0,15	-0,38	2,05	0,15	-0,38
max s_{xy}	1972	0,32	0,00	2,04	0,15	0,38	2,07	0,15	0,38	2,05	0,15	0,38

$0,14$ as well. In equation 5.16 the tension stresses edgewise $f_{t,0,d}$ and flatwise $f_{t,90,d}$ for the middle layer are checked. This check is executed for four times, the middle values are $0,77$, $0,78$, $0,81$, $0,44$ From these values the maximum is taken for the utilization check, which is $0,82$ and it lower than $1,0$. Therefore the combined bending and tension stress are satisfied, equation 5.6 and equation 5.7.

$$\left(\frac{s_{x,u}}{f_{m,edge,d}}\right)+\left(\frac{s_{y,u}}{f_{m,90,flat,d}}\right) \tag{5.15}$$

$$\left(\frac{s_x}{f_{t,0,d}}\right)+\left(\frac{s_y}{f_{t,90,d}}\right) \tag{5.16}$$

The permanent design values have been checked and the variable design are checked as well. The maximum stresses and forces for the load case 209 are shown in table 5.13. The material design values for the permanent load case are shown in table 5.12. In the same steps as for the permanent design values the checks for shear and in-plane stresses, edge and flatwise are done. All the values are satisfied and below the allowable stresses of the material.

5.4. Proof of Equivalence of Forces and Stresses

The equivalence of forces and stresses between beams modelled with 2D FE-elements and linear FE-elements will be discussed. All beams as above modelled as build-up beams, which consists out of plate and web, with quad elements as 2D FE-elements. From these models, reading out internal forces and moments is not as straight forward as for line models with beam elements as 1D element. This could be determined with the program SIR from SOFiSTiK, which stands for Sectional Results by making cuts locally. In this section it will be explained how the real stresses are matching the inner forces.

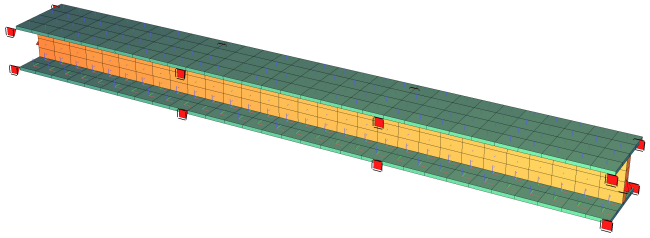

Figure 5.34: Beam modelled with 2D FE-elements with a span of 6 m

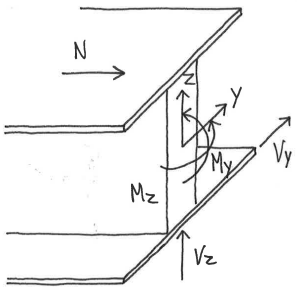

Figure 5.35: The section forces in a cross section by making a cut locally

For checking the equivalence, a simple supported I-beam will be modelled as with plate elements and line element. The I-beam has a span of 6 m and the models will be divided in six sections. In figure 5.34 the beam is modelled with plate elements and line element. The other beam will be modelled as a line with an I-section. The web has a height of 400 mm and a width of 90 mm. The flanges has a thickness of 21 mm and width 2000 mm but modelled with the effective width of 570 mm.

To illustrate this, the following loads are applied on the I-beam. The self weight of the cross section is $0,61\,kN/m$, with for plates $0,43\,kN/m$ and the ribbed element $0,18\,kN/m$. The dead load is $2,0\,kN/m^2$ over an area width of $2,0\,m$. The total distributed load q of the beam is $4,61\,kN/m$. A horizontal line load is applied of $10,0\,kN/m$ in the span direction.

The design bending moment for this simple support beam has been calculated with equation 5.17. The shear forces at the support conditions has been calculated with equation 5.18.

$$M_{gd} = 1,35 \cdot \frac{1}{8} \cdot q \cdot l^2 = 1,35 \cdot \frac{1}{8} \cdot 4,61 \cdot 6^2 = 28,0\,kNm \tag{5.17}$$

$$V_z = 1,35 \cdot \frac{q \cdot l}{2} = 1,35 \cdot \frac{4,61 \cdot 6}{2} = 18,7\,kN \tag{5.18}$$

At three locations a cut has been made for the beam modelled with the plate elements. The three locations are at $x = 1\,m$, $x = 3\,m$ and $x = 5\,m$. In figure 5.35 the different forces are displayed along the cross section. An overview of the section forces is given in table 5.14. The forces from the line element are compared with the section forces from the plate elements. The section forces are displayed in figures 5.37, 5.39 and 5.41. The forces are equal to the forces of the line element in figures 5.36, 5.38 and 5.40. The deflection from the line element is $8,91\,mm$ and from the plate elements is $8,86\,mm$. The forces from the line element are the same as the section forces from the plate elements, which are equal to the calculated values from equation 5.17 and 5.18.

$$\sigma_x = \frac{M}{W} + \frac{N}{A} = \frac{28 \cdot 10^6}{6,98 \cdot 10^6} + \frac{30 \cdot 10^3}{59940} = 4,51\,N/mm^2 \tag{5.19}$$

$$W_y = \frac{2 \cdot I_y}{H} = \frac{2}{442} \cdot \left(\frac{570442^3 - 480400^3}{12}\right) = 6975869,6\,mm^3 \tag{5.20}$$

The stresses from the plate elements are compared with the forces. The stresses are calculated from equation 5.19 in the middle of the beam with a bending moment M_y of $28,0\,kNm$ and a normal force N_x of $30,0\,kN$. The resistance moment is calculated In equation 5.20, which is $6,98 \cdot 10^6\,mm^3$. The stresses σ_x is equal to $4,51\,N/mm^2$. In figure 5.44 the stresses from the model are displayed. For this example the stiffness of the connection has been taken

into account, which will be explained in more detail in section 6.2.2. The stresses in web are $6,51\,N/mm^2$ and in the flanges $2,73\,N/mm^2$, which gives an average of $4,60\,N/mm^2$. The forces from the line element match with the stresses from the plate elements.

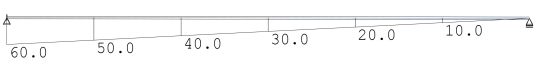

Figure 5.36: The normal forces N_x (kN) of the line element

Figure 5.37: The normal forces N_x (kN) of the plate elements

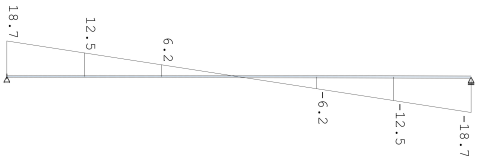

Figure 5.38: The shear forces V_Z (kN) of the line element

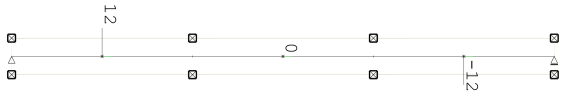

Figure 5.39: The shear forces V_z (kN) of the plate elements

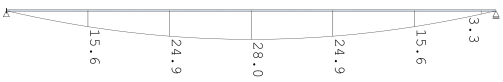

Figure 5.40: The bending moment M_y (kNm) of the line element

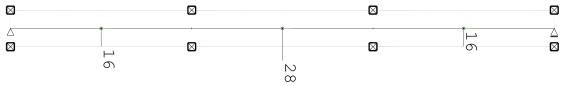

Figure 5.41: The bending moment M_y (kNm) of the plate elements

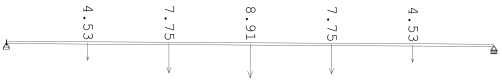

Figure 5.42: The deflection w (mm) of the line element

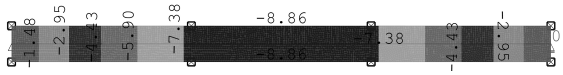

Figure 5.43: The deflection w (mm) of the plate elements

5.5. Conclusion

In this chapter different structural concepts are described, their suitability for the given problem are discussed. Only one of the structural concepts will be further developed. This will be structural concept 1 because the connections could easily be assembled between the ribbed elements and it is most suitable to generate a smooth and continuous double-curved surface.

One of the major points of discussion is the height of the elements in the roof structure, as this is a key contributor to the final roof design, this has been calculated. Therefore the principle of smooth height variation has been explained to get the optimal height. The different steps to achieve this has been shown on an example as proof of concept. The first step has been to make an initial model. In the second step the approximation of the smooth height variation has been discussed. In the third step a more accurate model has been made with a fine mesh and the results have been shown. The fourth and final step the strength verification of the cross section dimension has been checked and therefore the checking strategy has been explained. Proof of equivalence of forces and stresses between beams modelled with 2D FE-elements and linear FE elements has been given. The approach and the difference at some points with the global model have been discussed. The height optimisation for the roof structure has been proved. The final results of the global model will be shown in chapter 6.

Table 5.14: Section forces of plate elements example with a span of $6\ m$

Section Forces	$N_x\ kN$	$V_y\ kN$	$V_Z\ kN$	$M_t\ kNm$	$M_y\ kNm$	$M_z\ kNm$
1	$50,40$	$-0,00$	$12,37$	$-0,00$	$15,53$	$0,00$
2	$30,70$	$-0,00$	$0,05$	$-0,00$	$27,95$	$0,00$
3	$10,30$	$-0,00$	$-12,42$	$0,00$	$15,54$	$0,00$

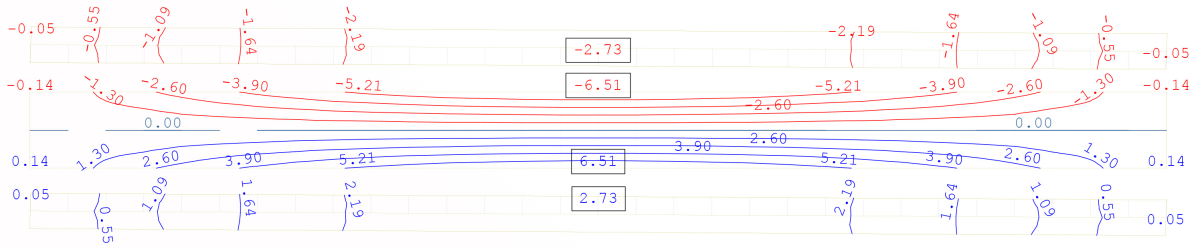

Figure 5.44: The stresses from the beam modelled with quad elements

Timber structures depend on structural requirements and the different types of constrains related to fabrication, transportation and assembly. Therefore it is important to take the production technology of timber into account during the design process. From this point the structural concept needs to be further developed. In section 6.1.2 of the next chapter the design of the connections and the supports will be developed. The structural concept will be applied to the design of the roof project to test the feasibility in detail.

6

Structural Design

In chapter 5 the structural concept with its suitability for the given problem has been discussed. A principle of smooth height variation has been developed to get the optimal height and it has been proved on the example. The structural concept will be applied to the design of the roof project to asses the feasibility. In this chapter the construction method for this project will be discussed. The approximation for the simulation of the global model will be given. The structural analysis of the global model will be discussed, in which the design of connections will be included.

6.1. Construction Method

The roof structure will be supported on different ways, by six columns, the ground and the walls. The structural concept will be further developed on how to actually built it. The development of an appropriate construction method for manufacturing and assembly of the structure. The difficulties associated for making a decision between prefabrication and building on site with timber will be discussed. The solutions and techniques that led to completion of the roof project will be given. The consequences and possibilities of the structural concept with regard to fabrication, manufacturing, and assembly will be assessed.

In this section the integrated structural concept will be discussed in more detail. The following connections needs to be further developed. The structural concept consists out of ribbed elements that are covered by plates on the top and the bottom. These plates provide stability and will be attached to the ribbed elements by screws. A simple connection will be made between the ribbed elements. A cut in one direction in the bottom part and a cut in the other direction in the top part are made. The elements will join at the point where they will cross each other.

6.1.1. Manufacturing and Assembly

Timber structures are associated with difficulties with its construction. The development of an appropriate technique and methods to monitor and assist the construction process is important. The first idea was to built prefabricated box elements of $6\,m$ by $6\,m$. The structural concept would be mostly prefabricated timber elements to realize the shape of the free-form surface. On site prefabricated timber elements provide an easy and fast assembly due to the majority of the fabrication in the workshop. However due to transportation the prefabricated elements should be limited to certain dimensions.

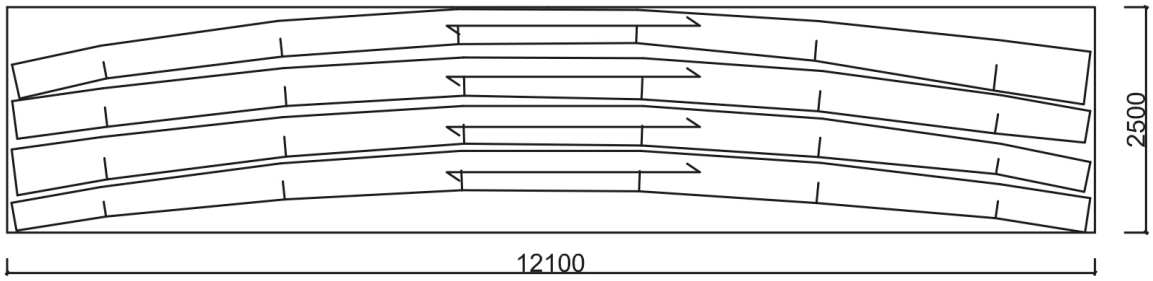

Figure 6.1: Four curved elements will be cut-out from one plate

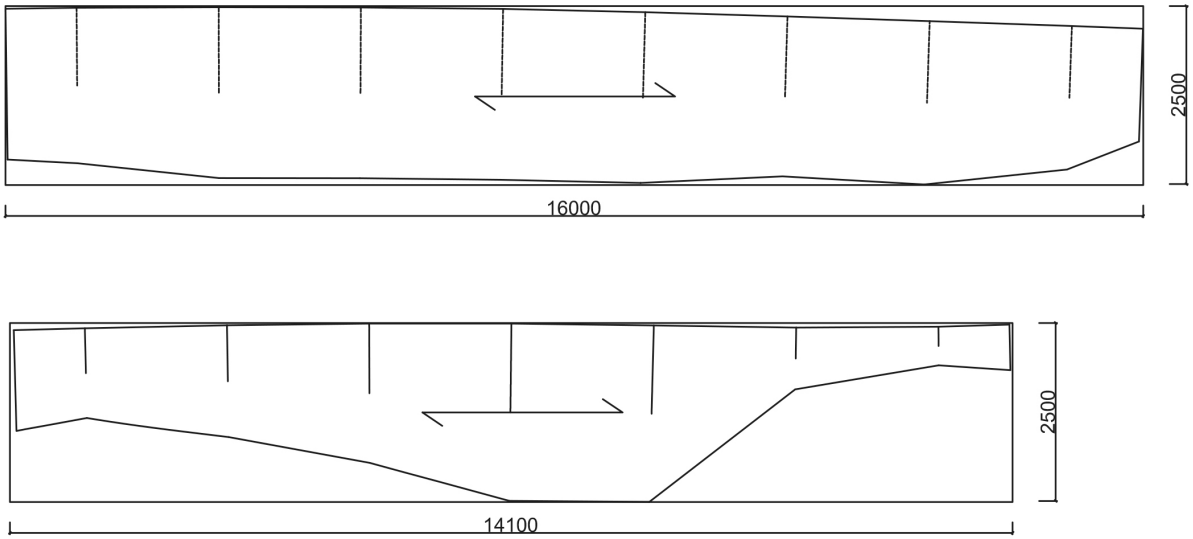

Figure 6.2: The large depth elements will be cut-out from plates

Prefabrication or building on site

For the construction method a decision needs to be made whether the construction will be prefabricated or made in-situ. However a combination of both is also possible. Kerto-Q elements are available in the maximum sizes: a thickness of 90 mm, a width or a height of 2.500 mm and a length of 25.000 mm. The height of the ribbed elements is not preferred to be larger than 2.500 mm.

It is preferred to prefabricate as much as possible. Prefabrication has an advantage due to the ability to have a constant climate in the fabric. The preferred climate for timber could be easily maintained. The products will be made under a temperature of 20° and a relative humidity of 65 %. Another advantage is that the prefabricated elements are quick to erect on site. A disadvantage for building on site is that the elements will be vulnerable for weather conditions and insect attack. To protect the timber elements, a tent is needed on the building site. An advantage is that in the workshop tent the elements could be pre-assembled.

Different ribbed elements should be prefabricated due to the curved nature of the structure. The bottom part of the ribbed elements will be tapered under an angle to the grain direction. The fabrication of the curved elements will be cut-out from plates. The chosen sizes from the ribbed elements will be explained later on. Multiple shallow curved elements can be made out of one plate, see figure 6.1. The ribbed elements with the larger depth will be cut out of one plate, see figure 6.2. It is mainly flat at the critical area where the larger depth of $2,5\ m$ is required. However one part is slightly curved and it is not possible to cut

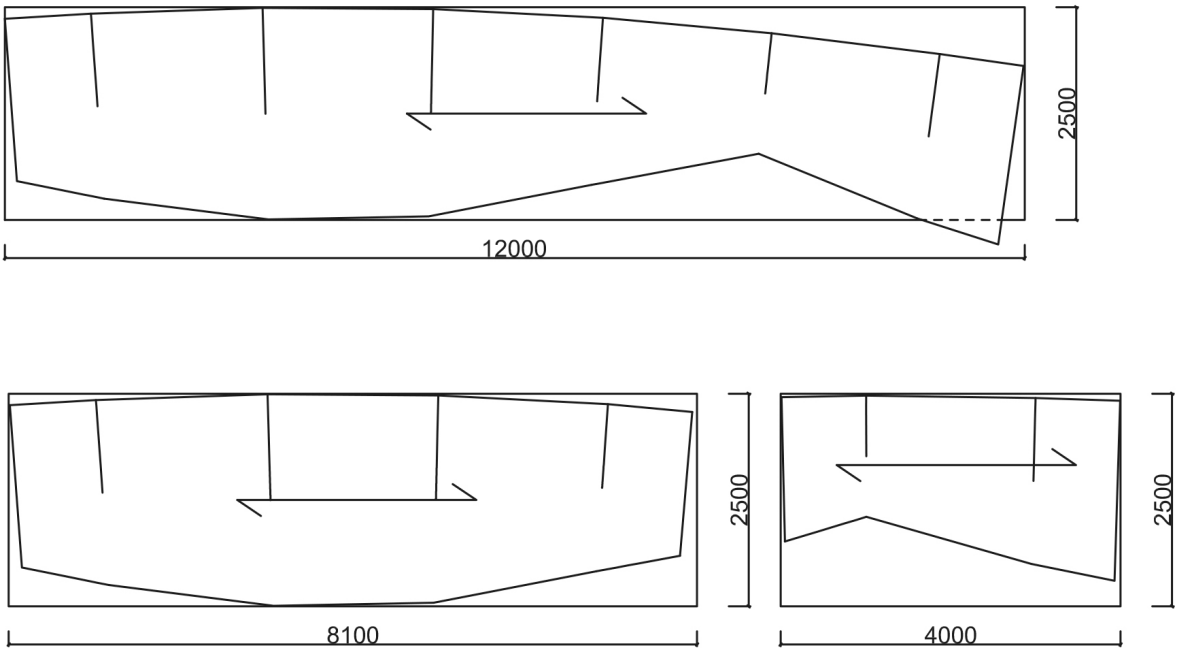

Figure 6.3: An extra connection will be made to solve this cut-out problem

out the preferred size from one plate. Therefore this element will be divided into two and an extra connection will be made, see figure 6.3.

Transportation

The regular way of transporting the timber elements from the fabric to the building site is by trucks. A combination of tractor and trailer has a maximum width of $2,55\,m$, height of $4\,m$ and length of $16\,m$ [5]. For the box elements of $6\,m$ by $6\,m$ special transportation is needed. The depth of the boxes could vary from $0,5\,m$ to $2,5\,m$, which makes that due to the curvature a total depth of more than $2,5\,m$ could be achieved. The sizes of elements for the structural concept are limited due to sizes of a truck. Although it is not preferred to assemble on the building site, the elements will be transported by pieces.

Manufacturing

The plates and the ribbed elements will be transported separately to the building site. The ribbed elements are limited to a height of $2,5\,m$ and a length of $16\,m$. The ribbed elements will be prefabricated with the desired height for every element. The incision for the simple connection between the ribbed elements will already be made in the fabric. In these elements the holes for the screws will be pre drilled. The top plates will have a length of $16\,m$ and a width of roughly $2\,m$. The bottom plates will have a length of $6\,m$ and a width of roughly $2\,m$. All the elements will be numbered beforehand for a better overview on the building site.

The roof structure of $90\,m$ by $140\,m$ needs to made from all those elements. The roof structure needs to be divided into segments since the ribbed elements are limited up to a length of $16\,m$. The advantage of this large units is that a significant amount of simple connections can be made between the ribbed elements. The structure is divided into a puzzle of segments by cutting the grid of $2\,m$ by $2\,m$. The connections will me made at the position with the lowest bending moment. It is not preferred to choose a location where high moments or hogging moments occur. Therefore the locations has been chosen to avoid the support locations as much as possible. In figure 6.4, the location of the connections for the segmentation is displayed by the black lines.

Assembly

All the elements are brought to the building site. From these elements the assembly of the structure will be made. This is the phase when the structure will actually be made. On the building site there will be a tent, where there will be worked to pre assemble the elements. A scaffolding will be used to support the structure temporary. A crane will be used to lift the elements into position on the scaffolding. The structure will be built up in different steps. This will be displayed by one segment of the whole structure, see figure 6.5.

The first step will be to connected the ribbed elements. The ribbed elements for the global x direction will be at the bottom. These ribbed elements will have their incision at the top part. The ribbed elements for the global y direction step will be placed in the other direction. The ribbed elements in the other direction will have an incision at the bottom part. A crane will be used to lift the ribbed elements into position on the scaffolding. The ribbed elements will be connected into each other, see figure 6.6. The system will be stiff after the ribbed elements will be combined together.

All the ribbed elements of the structure in both directions are in place. First the top plates will be attached to the ribbed elements. These plates will be placed over the ribbed element connections such that the forces can be transferred trough the plates. After this the scaffolding will be moved to be able to attach the bottom plates. Although the bottom plates have been limited to length of $6\,m$, this will be critical step. It is very difficult to screw these plates from the bottom. In figure 6.7 an exploded view of the build-up of the structure is shown. In terms of organisation of the project, it should comply the Construction (Design & Management) Regulations (CDM). The CDM 2017 are the main set of regulations for managing the health, safety and welfare of construction projects. However these regulations are outside the scope of this research.

The strongest axis of the plates is the main grain direction. Therefore the direction of the plates will be in one direction, which makes the cross section in this direction stiffer than the other one. Since it is not clear in which direction the roof structure spans it is hard to choose the correct direction. Therefore the top plates and the bottom plates will consist out of two plates, each of the two plates orientated in the another direction. The different layers of the top plates are shown on page 74. The first layer of plates will be in the global y-direction. The second layer will be placed on top, in the global x-direction. This build-up contributes to a more continuous surface. In section 6.2.2 it will be explained how this will be modelled in the structural model.

Before the structure can be build the plates need to pre assembled. For the plates there are limitations on the tightness of curvature to which it could be bent into the desired shape. The top and the bottom plates will be cold bent to the desired curvature. However there are limitations to the tightness of the curvature can be bent, which has been discussed in section 4.2.1. The radius of curvature for the top plates has been investigated.

The shape of the bottom plates has been changed due to the change in height of the ribbed elements. In figure 6.8 the radius of curvature for the bottom plates is depicted. The dark blue areas have a radius of curvature above $20\,m$. The light green and light blue areas have a radius of curvature around $12,5\,m$. The red areas have a curvature below $12\,m$, these are critical and a closer look should be made if these could be bent into the desired shape without breaking the timber plate.

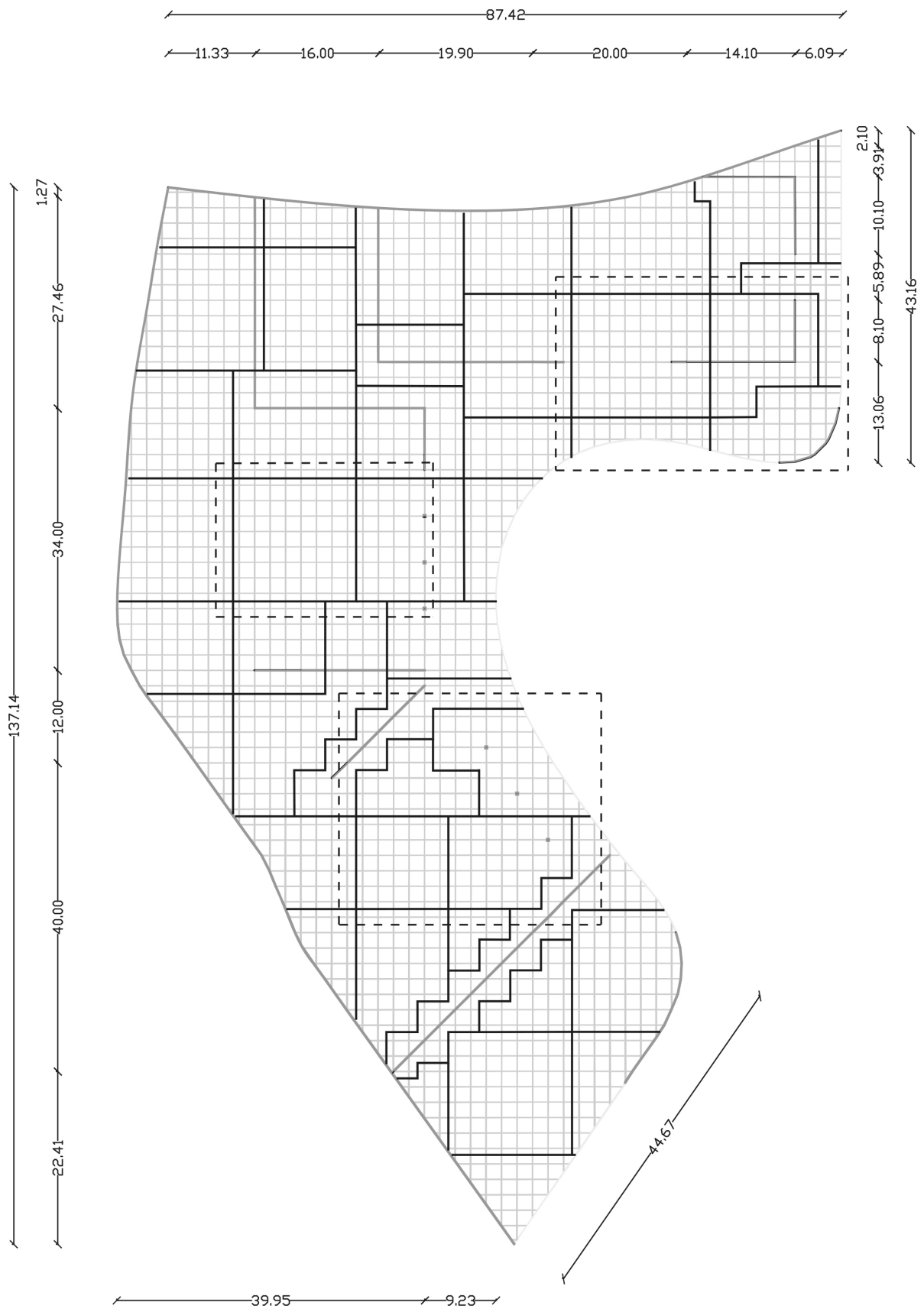

Figure 6.4: The division of the ribbed elements for a maximum size of $16\ m$, see black line. The areas in the striped lines will be checked for the calculation of connections.

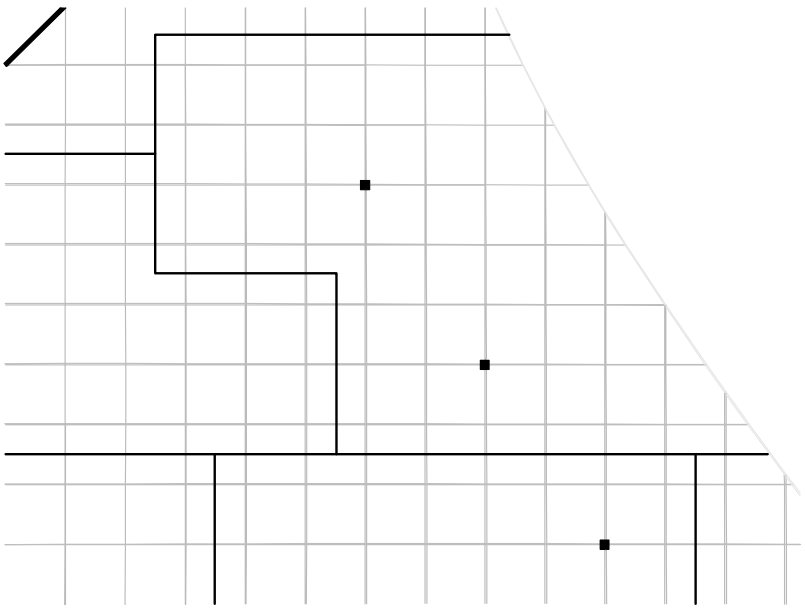

Figure 6.5: One segment of the whole structure, which the build-up will be shown in more detail

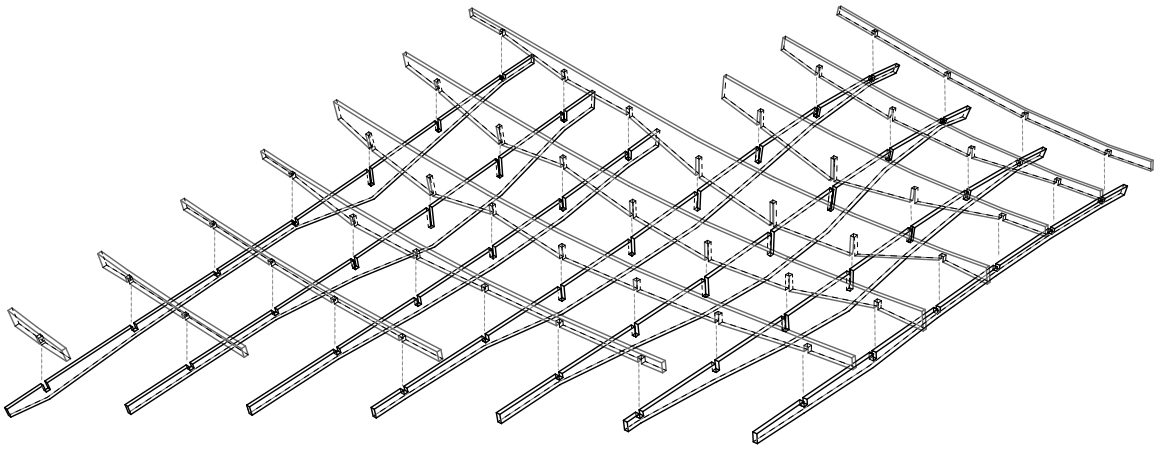

Figure 6.6: The ribbed elements with their incisions are connected into each other

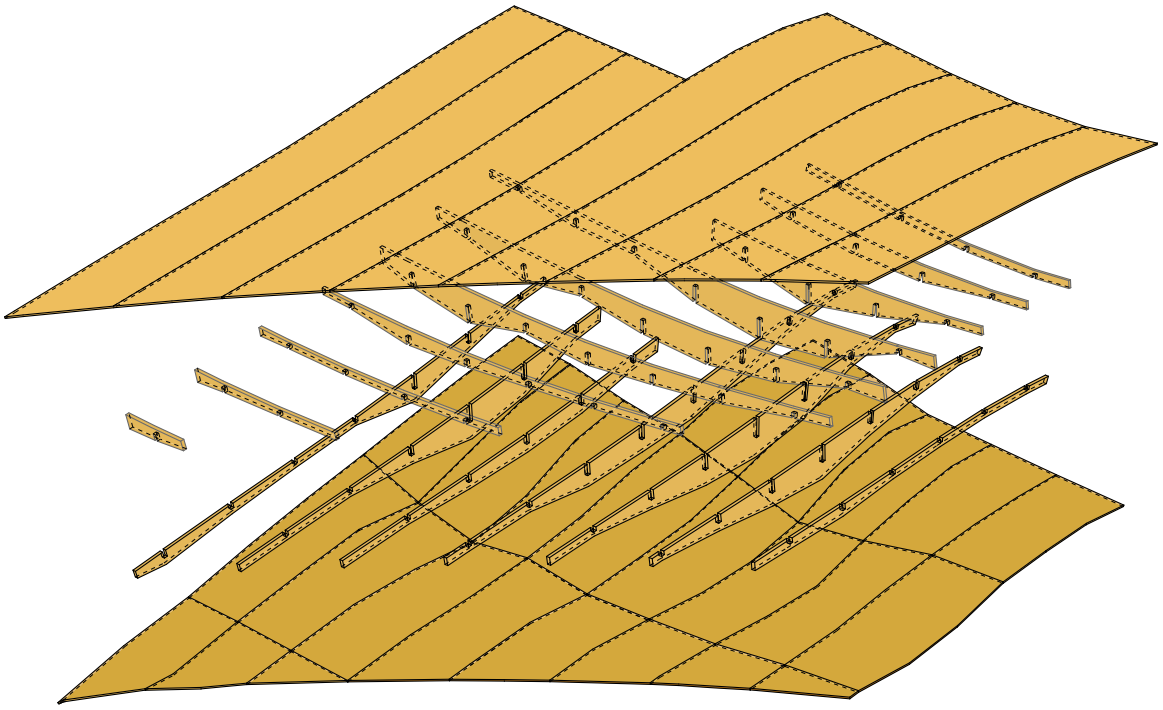

Figure 6.7: Exploded view of one segment from the roof structure

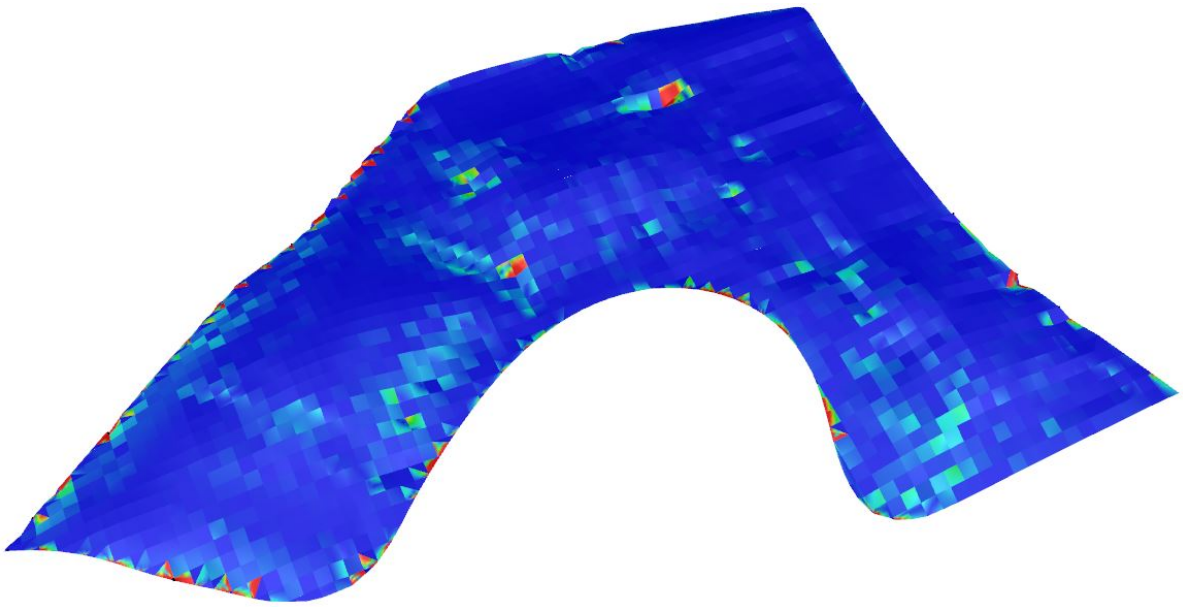

Figure 6.8: The radius of curvature of the bottom plates

Overview plate orientation

First layer of plates
into the global y-direction

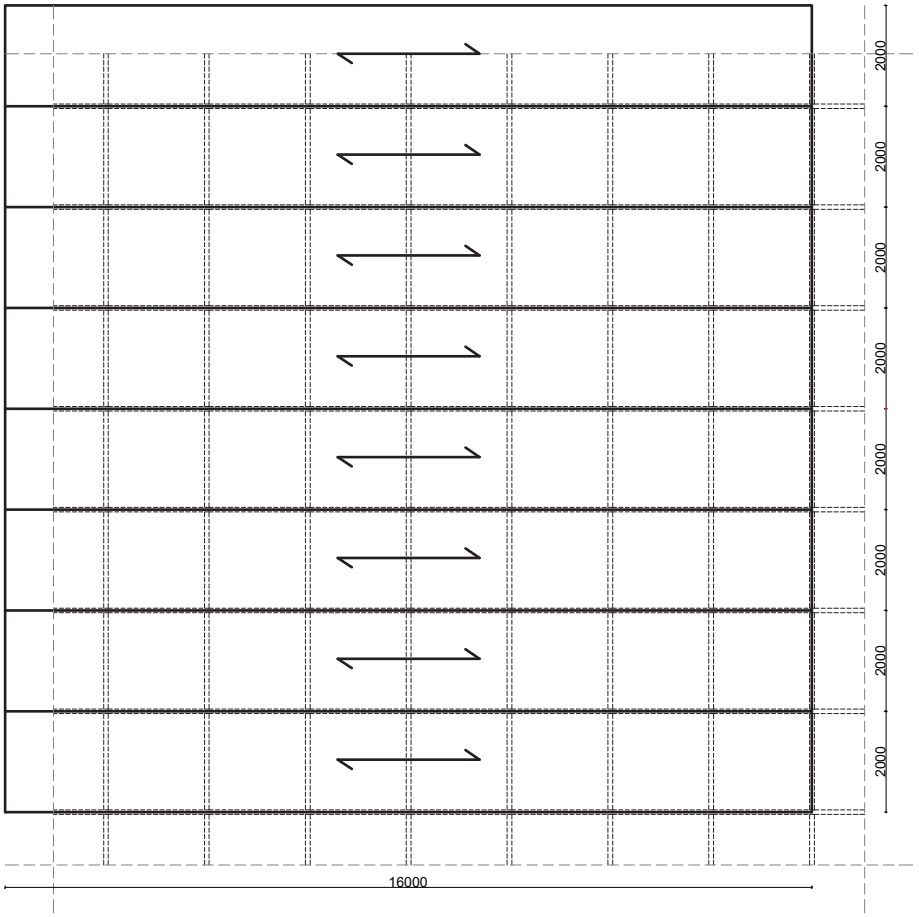

Second layer of plates
into the global x-direction

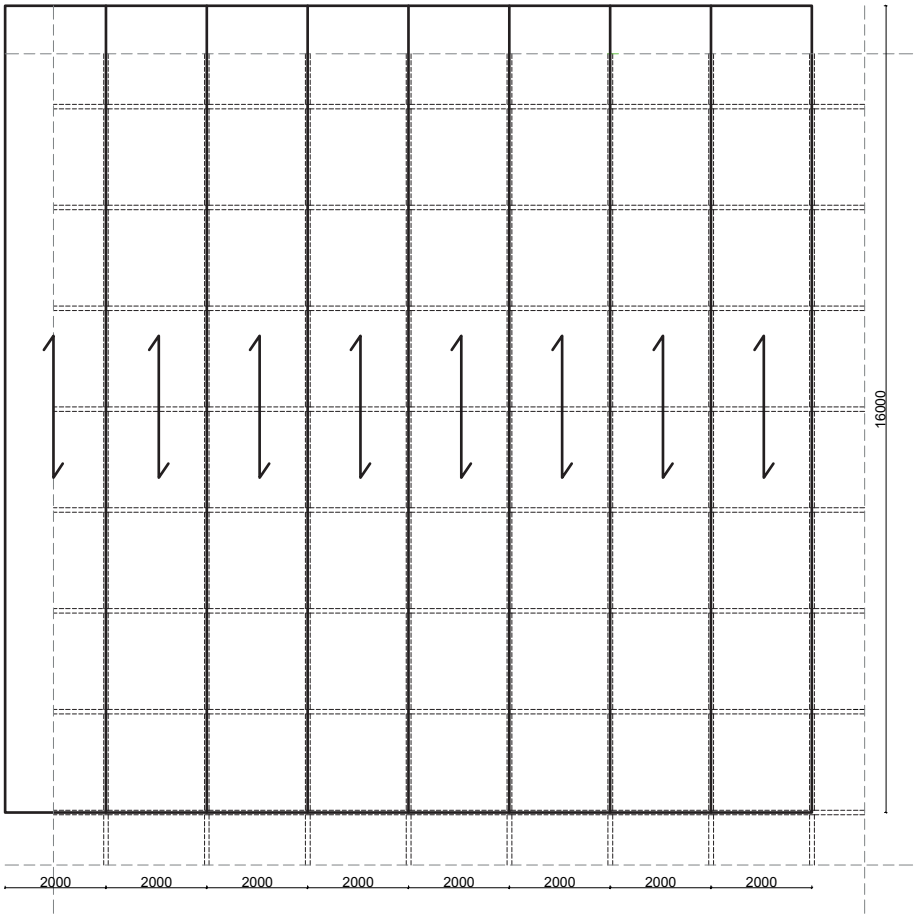

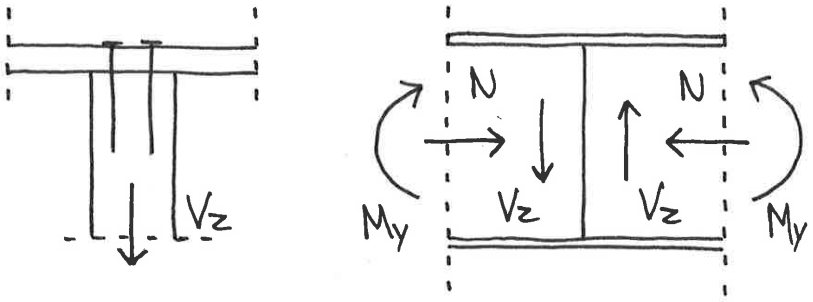

Figure 6.9: The section forces for connection calculation

6.1.2. Connection Design and Detail

The idea behind the construction method for the roof structure has been discussed. For making this possible connections are needed. Connections will be made between the elements and for the segmentation of the large units. The structural concept of the ribbed elements and the plates will primarily resists bending, shear and torsion. At the following pages the details will be explained and shown. For the calculation of the connections the forces have been extracted from SOFiSTiK. At several locations the middle point from the cross section has been taken, from this position a cut has been made. The several locations are displayed by areas in the striped lines in figure 6.4. The section forces has been extracted from each cross section with a local coordinate system. In figure 6.9 the different section forces are displayed. The structure has a height difference from $0,2\ m$ till $2,5\ m$. In table 6.1 the forces from different heights are depicted, which are present as an average of the structure.

Connection 1: Plates to Rib

The highest stresses will occur at the top and bottom of the ribbed element. The height of the structure is calculated that the higher the bending stresses the higher the ribbed element is. The cross section will be stronger by attaching plates and provides later torsional stiffness. The idea behind the structural concept is that material is present where it should be and in the right quantities. This design will contribute for maximum strength in bending. The plates will be screwed to the ribbed elements. The plates will contribute to transfer mainly the tension and compression forces.

At page 81 an overview of the different sections for the connections between the plate and the ribbed element is shown. For the height of the ribbed elements an average of all the heights is taken, which is roughly $1\ m$. In the drawing Section A-A the first layer of the top plates will be screwed into the ribbed elements in the global y-direction.

At the other page 82 the other sections are displayed. In the drawing Section B-B, a section has been made at the position of the incision of the ribbed element in y-direction. The incision will be half the height of the ribbed element, which is in this case $500\ mm$. The first layer of the bottom plates will be screwed into the ribbed elements in the global y-direction. The plates will contribute to transfer the forces at the location where an incision in the ribbed element is.

In the drawing Section C-C the second layer of the top plates will be screwed, trough the first layer and into the ribbed elements in the global x-direction. The top plates consists out of two layer, which are each $21\ mm$. The total thickness of the top plates are $42\ mm$.

In the drawing Section D-D, a section has been made at the position of the incision of the ribbed element in other direction. The second layer of the bottom plates will be screwed into the ribbed elements in the global y-direction. The total height of the plates and the ribbed element is $1084\ mm$.

At page 83 the details of the screw connection are displayed. The Eurocode has a requirement that it is only allowed to screw from the plates into the main element and not the other

Table 6.1: Section forces (see section 5.4)

Load-case	$N_x\ (kN)$	$V_y\ (kN)$	$V_z\ (kN)$	$M_t\ (kNm)$	$M_y\ (kNm)$	$M_z\ (kNm)$
$Height$ 0,49 m						
$1,35 \cdot G$	-3,9	+8,73	+2,4	-2,32	+8,41	+1,58
$1,5 \cdot S$	-1,6	+4,24	+1,27	-1,12	+4,27	+0,76
$1,35 \cdot G + 1,5 \cdot S$	-5,5	+12,97	+3,67	-3,44	+12,68	+2,34
$Height$ 1,14 m						
$1,35 \cdot G$	+23,5	-3,29	+9,09	-1,57	-11,71	-0,46
$1,5 \cdot S$	+11,7	-1,38	+4,11	-0,76	-5,17	-0,2
$1,35 \cdot G + 1,5 \cdot S$	+35,2	-4,67	+13,2	-2,33	-16,88	-0,66
$Height$ 1,61 m						
$1,35 \cdot G$	-13,3	+2,91	-12,2	-4,32	+206,31	+0,31
$1,5 \cdot S$	-5,3	+1,22	-5,72	-1,85	+85,35	+0,12
$1,35 \cdot G + 1,5 \cdot S$	-18,6	+4,13	-17,92	-6,17	+291,66	+0,43
$Height$ 2,07 m						
$1,35 \cdot G$	-74,9	-11,83	-36,38	-2,78	+52,71	-3,9
$1,5 \cdot S$	-23,7	-5,08	-15,16	-1,27	+22,59	-1,71
$1,35 \cdot G + 1,5 \cdot S$	-107,6	-16,91	-51,54	-4,05	+75,3	+5,61

way around. In the screwed connections part from EN 1995-1-1: 8.7 the distances have been checked. The required minimum distance for the end is $3\,d$ and the minimum spacing is $5\,d$. The plates will be screwed by 2 screws with a diameter of $6\,mm$. The minimum edge distance is $18\,mm$ and the minimum spacing is $30\,mm$. In detail 1.1 and 1.2 the edge distance is $24\,mm$ and the spacing is $30\,mm$. The spacing along the grain direction is $250\,mm$, every $2\,m$ there will be 16 screws. See section 6.2.1 for the stiffness calculation for the different layers.

Calculation Connection 1

The screw connection between plates and ribbed element is timber-to-timber joint. The screws have a diameter of $6\,mm$, which is greater than $5\,mm$ and the holes should be pre-drilled to prevent splitting of the wood. The screwed joints will be axially loaded by V_z, see left picture in figure 6.9. It needs to be checked whether the shear force can be taken by the capacity of the screws. It is not possible to design each location individual but the different locations are relevant for the whole structure. These locations are present to show how it will work for all the other connections.

The characteristic load-carrying capacity for screws per single shear per fastener should be taken as the minimum value found from the following expressions EN 1995-1-1:2004 8.2.2 (8.6).

$$F_{v,Rk} = min\begin{cases} f_{h,1,k}\cdot t_1\cdot d \\ f_{h,2,k}\cdot t_2\cdot d \\ \dfrac{f_{h,1,k}\cdot t_1\cdot d}{1+\beta}\left[\sqrt{\beta+2\beta^2\left[1+\dfrac{t_2}{t_1}+\left(\dfrac{t_2}{t_1}\right)^2\right]+\beta^3\left(\dfrac{t_2}{t_1}\right)^2}-\beta\left(1+\dfrac{t_2}{t_1}\right)\right]+\dfrac{Fax,Rk}{4} \\ 1{,}05\cdot\dfrac{f_{h,1,k}\cdot t_1\cdot d}{2+\beta}\left[\sqrt{2\beta(1+\beta)+\dfrac{4\beta(2+\beta)M_{y,Rk}}{f_{h,1,k}\cdot d\cdot {t_1}^2}}-\beta\right]+\dfrac{Fax,Rk}{4} \\ 1{,}05\cdot\dfrac{f_{h,1,k}\cdot t_2\cdot d}{1+2\cdot\beta}\left[\sqrt{2\beta^2(1+\beta)+\dfrac{4\beta(1+2\beta)M_{y,Rk}}{f_{h,1,k}\cdot d\cdot {t_2}^2}}-\beta\right]+\dfrac{Fax,Rk}{4} \\ 1{,}15\cdot\sqrt{\dfrac{2\cdot\beta}{1+\beta}}\sqrt{2\cdot M_{y,Rk}\cdot f_{h,1,k}\cdot d}+\dfrac{Fax,Rk}{4} \end{cases} \tag{6.1}$$

In equation 6.1 t_1 is $21\,mm$ and t_2, which length of the screw minus t_1 is $129\,mm$. The rope effect should be taken into account for screws as a contribution of 100 percent. The characteristic fastener yield moment will be taken from Z.9.1-449 Table 3 for SPAX screws, which $M_{y,Rk}$ is 10.900 Nmm for diameter of $6\,mm$.

The characteristic embedment strength of the plate ($f_{h,1,k}$) will be determined with equation 6.2 Z.9.1-847 3.2.1 since it is screwed flatwise. The ribbed element is screwed edgewise and the characteristic embedment strength ($f_{h,2,k}$) will be determined with equation 6.3 (Z.9.1-847 3.2.2).

$$f_{h,1,k} = 37(1-0{,}01d) = 37(1-0{,}01\cdot 6) = 34{,}8\,N/mm^2 \tag{6.2}$$

$$f_{h,2,k} = 37\cdot(1-2\cdot d)\cdot(1-0{,}01\cdot d) = 37\cdot(1-2\cdot 6)\cdot(1-0{,}01\cdot 6) = 23{,}2\,N/mm^2 \tag{6.3}$$

In equation 6.4 the ratio between the embedment strength of the two members will be determined, EN 1995-1-1:2004 8.2.2 (8.8).

$$\beta = \frac{f_{h,2,k}}{f_{h,2,k}} = \frac{23{,}2}{34{,}8} = 0{,}67 \tag{6.4}$$

Table 6.2: Screw capacity check for connection plates to rib

Height (m)	Load-case	V_z (N)	$F_{v,Rd}$ (N)	$\frac{F_{v,Ed}}{F_{v,Rd}}$
0,49 m	$1,35 \cdot G$	2.400	693,02	0,12 ≤ 1
	$1,5 \cdot S$	1270	1.059,75	0,12 ≤ 1
1,14 m	$1,35 \cdot G$	9.090	2624,83	0,45 ≤ 1
	$1,5 \cdot S$	4.110	3.811,63	0,43 ≤ 1
1,61 m	$1,35 \cdot G$	-12.200	3.522,87	0,60 ≤ 1
	$1,5 \cdot S$	-5.720	5.174,58	0,59 ≤ 1
2,07 m	$1,35 \cdot G$	-36.380	10.505,08	1,79 ≥ 1
	$1,5 \cdot S$	-15.160	14.882,68	1,69 ≥ 1

The characteristic axial withdrawal capacity of the fastener will be depicted with equation 6.5 (Z.9.1-449 3.2.2).

$$Fax, Rk = k_{ax} \cdot f_{1,k} \cdot d \cdot t_{pen} = 1,0 \cdot 18,21 \cdot 6 \cdot (150 - 21) = 14092\,N \tag{6.5}$$

The minimum value for the load-carrying capacity for screws is determined from equation 6.1 (d), which is $5393,3\,N$. For permanent load case $F_{v,Rd,G}$ is $2941,8\,N$ with k_{mod} is 0,9 and variable load case $F_{v,Rd,S}$ is $4412,7\,N$ with k_{mod} is 0,6, both divided by γ is $1,1$ for steel.

The load on a fastener should be taken from equation 6.6 (EN 1995-1-1:2004 Annex B (B.10)) . All the values for this equation will be determined in section 6.2.1 and 6.2.2.

$$F_{v,Ed} = \frac{\gamma_u \cdot E_{eff} \cdot A_{plate} \cdot a \cdot s}{(EI)_{eff}} \cdot V_z = 0,2887 \cdot V_z \tag{6.6}$$

In table 6.2 the capacity of the screws are checked for the different forces from table 6.1. In these calculations the capacity for each fastener has been taken two times, since there are two screws every joint. This is for permanent load case $F_{v,Rd,G}$ is $5883,65\,N$ and variable load case $F_{v,Rd,S}$ is $8825,48\,N$. The three locations with the different height and structural behaviour are present for the structure. The connection between the plates to rib works mainly for the entire structure. However the shear forces were too high at the location for the span of $35\,m$ and there the amount of screws needs to be increased.

Connection 2: Rib to Rib

The ribbed element connections are two different connections. The simple connection between the ribbed elements from different direction is made by an incision. The ribbed elements will mainly transfer axial forces. The incision will make the ribbed elements less stiff, the reduction for the global model will be calculated in section 6.2.2. The incision will be made half of the height of the ribbed element. In figure 6.6 how this connection will be made is shown.

The simple connection between the ribbed elements makes different segments. For completing the segmentation the ribbed elements will be connected by each end. This connections needs to be stiff and moment resistant. These connections are not visible since the plates will cover the ribbed elements.

The location has been chosen where the lowest bending moment will occur. At page 83 two connections are shown and the other connection is shown at page 84. However at some locations it was unavoidable to make a connection where the bending moment is low. This is

due to the limited length of $16\,m$, especially at the critical area with a span of $35\,m$. In detail 2 the bending moment and shear forces needs to be transferred. The height will differ among the surface and different locations have been checked. The connections will be made where also no hogging moments will occur and looks mainly like detail 3 with a height of $390\,mm$.

Calculation Connection 2

The characteristic load-carrying capacity for thick steel plates as the outer members of a double shear connection should be taken as the minimum value found from the following expressions EC5: Part 1-1: 8.2.3 (8.13). The timber ribbed elements will be connected by two outer steel plates with a thickness of $10\,mm$. A dowel connection will be made with each a diameter of $10\,mm$ and characteristic tensile strength (f_u) of $360\,N/mm^2$. The characteristic fastener yield moment will be depicted from equation 6.8, EN 1995-1-1:2004 8.5.1.1 (8.30). The rope effect should not be considered for bolted connections.

$$F_{v,Rk} = min\begin{cases} 0,5 \cdot f_{h,2,k} \cdot t_2 \cdot d \\ 2,3\sqrt{M_{y,Rk} \cdot f_{h,2,k} \cdot d} \end{cases} \tag{6.7}$$

$$M_{y,Rk} = 0,3 \cdot f_u \cdot d^{2,6} = 0,3 \cdot 360 \cdot 10^{2,6} = 42995,6\,Nmm \tag{6.8}$$

$$f_{h,0,k} = 0,082(1 - 0,01d)\rho_k = 0,082(1 - 0,01 \cdot 10)480 = 35,4\,N/mm^2 \tag{6.9}$$

The minimum value for the load-carrying capacity for bolts is determined from equation 6.7 (b), which is $8973,1\,N$. For permanent load case $F_{v,Rd,G}$ is $4894,4\,N$ and variable load case $F_{v,Rd,S}$ is $7341,6\,N$. In table 6.3 the connections are checked for the different forces from table 6.1. The load carrying capacity $F_{v,Rd}$ has been multiplied by two shear planes and the amount of bolts. The bending moment has been multiplied by lever arm, to apply it as a tension or compression force.

The forces that needs to be transferred by the rib-to-rib connection are displayed in the right picture in figure 6.9. Detail 3 is the first type of connection with height of $0,49\,m$ transfers the normal force, shear force and small bending moment by one steel plate. Detail $2a$ is the second type of connection with height of $1,14m$ transfers the normal force and shear force by the middle plate. The bending moment M_y has been multiplied by a lever arm of $0,8m$. The tension and compression forces are transferred by the top and bottom steel plates. Detail $2b$ is the third type of connection with height of $1,61\,m$ transfers mainly bending moment, which is transferred by the top and bottom steel plates with a large amount of bolts. The bending moment M_y has been multiplied by a lever arm of $1,2\,m$.

Support connections

The roof structure is supported on different ways, which is by six columns, the walls, the concrete building and the ground. The support conditions are outside the scope of this research. However an idea will be described of how the connections could be made. The design behind the connections from the structure with the columns and the walls will be given, see page 84.

Column connection

The six columns are restrained in all three directions of the global coordinate system. The forces from these directions needs to be transferred from the structure into the concrete column. A round steel tube with four steel plates will be welded together, see detail 4. The steel plates with a thickness $10\,mm$ will be placed in the middle of each timber ribbed element. The steel-timber connection will be connected with $20\,dowels$ with a diameter of $12\,mm$. The steel connection will be connected on a steel plate, which is connected with the concrete column.

Table 6.3: Capacity check for steel plates - Ribbed element

Height (m)	Load-case	$N_x\ (N)$	$V_z\ (N)$	$M_y \cdot 10^6$ (Nmm)	n	$F_{v,Rd}$	$\frac{F_{v,Ed}}{F_{v,Rd}}$
0,49 m	$1,35 \cdot G$	-3900	2400	8,41	12	117465,6	0,41 ≤ 1
	$1,5 \cdot S$	-1600	1270	4,27	12	176198,4	0,14 ≤ 1
1,14 m	$1,35 \cdot G$	23500	9090		8	78310,4	0,62 ≤ 1
	$1,5 \cdot S$	11700	4110		8	117465,5	0,13 ≤ 1
	$1,35 \cdot G$			-11,71	6	58732,8	0,50 ≤ 1
	$1,5 \cdot S$			-5,17	6	88099,2	0,15 ≤ 1
1,61 m	$1,35 \cdot G$	-13300	-12200	206,31	60	587328,0	0,65 ≤ 1
	$1,5 \cdot S$	-5300	-5720	85,35	60	880992,0	0,17 ≤ 1

The characteristic load-carrying capacity for a steel plate as the central members of a double shear connection should be taken as the minimum value found from the following expressions EC5: Part 1-1: 8.2.3 (8.11). The rope effect should not be considered for bolted connections.

$$F_{v,Rk} = min \begin{cases} f_{h,1,k} \cdot t_1 \cdot d \\ f_{h,1,k} \cdot t_1 \cdot d \left[\sqrt{2 + \frac{4M_{y,Rk}}{f_{h,1,k} \cdot d \cdot {t_1}^2}} - 1 \right] \\ 2,3\sqrt{M_{y,Rk} \cdot f_{h,1,k} \cdot d} \end{cases} \tag{6.10}$$

$$M_{y,Rk} = 0,3 \cdot f_u \cdot d^{2,6} = 0,3 \cdot 360 \cdot 12^{2,6} = 69070,9\,Nmm \tag{6.11}$$

$$f_{h,1,k} = 0,082(1 - 0,01d)\rho_k = 0,082(1 - 0,01 \cdot 12)480 = 34,6\,N/mm^2 \tag{6.12}$$

The minimum value for the load-carrying capacity for bolts is determined from equation 6.7 (b), which is $9206\,N$. For permanent load case $F_{v,Rd,G}$ is $5021,5\,N$ and variable load case $F_{v,Rd,S}$ is $7532,2\,N$. For a correct calculation the capacity of the steel tube should also be considered. However the rough design of the column connection is only given for an idea of how it could be made.

Wall connection

The support conditions from the walls are rolled supports. The roof structure is able to move perpendicular on the walls but the structure is restrained in the direction of the walls. The forces needs to be transferred through the connection to the concrete wall. Slotted holes are made to make it able to move in the perpendicular direction of the wall. In detail 5 the slotted holes are displayed by an arrow for the movement direction. The characteristic load-carrying capacity for thick steel plates as the outer members of a double shear connection should be taken as the minimum value found from equation 6.7. For a correct calculation the steel plates attached to the wall should also be considered but this is behind the scope of this research.

Overview of sections

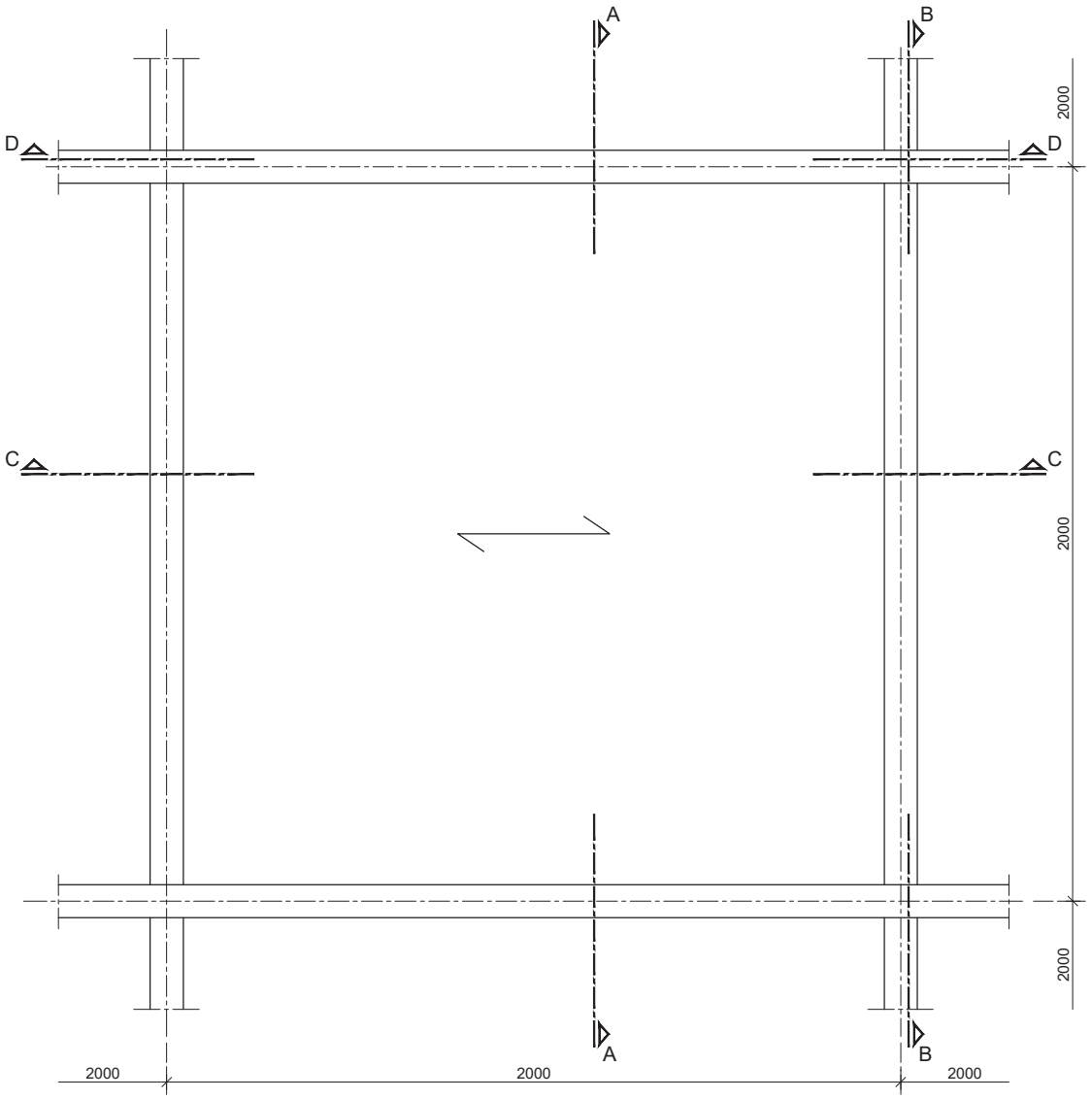

Scale 1:20

Section A - A

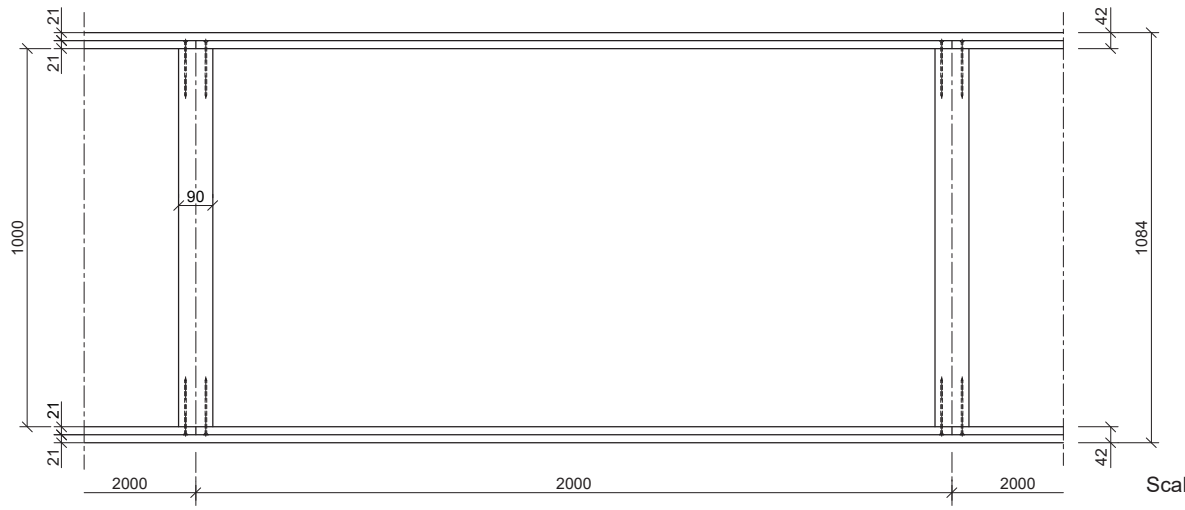

Scale 1:20

Section B - B

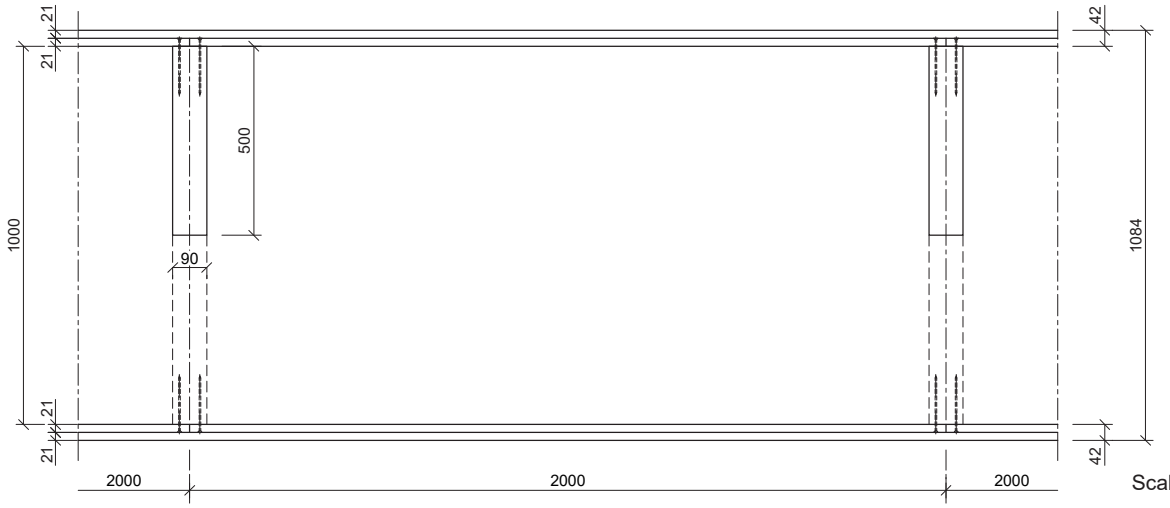

Scale 1:20

Section C - C

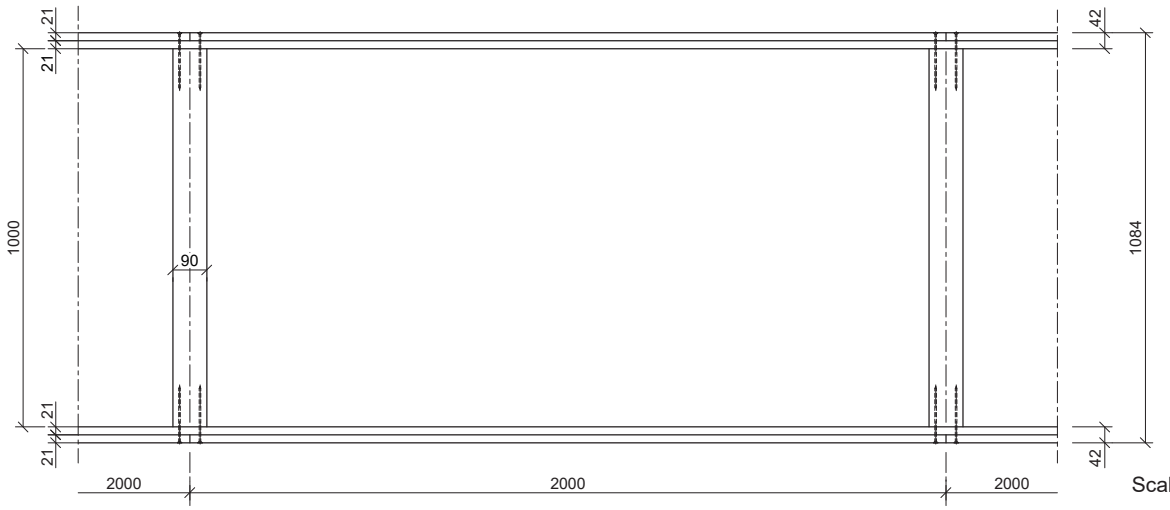

Scale 1:20

Section D - D

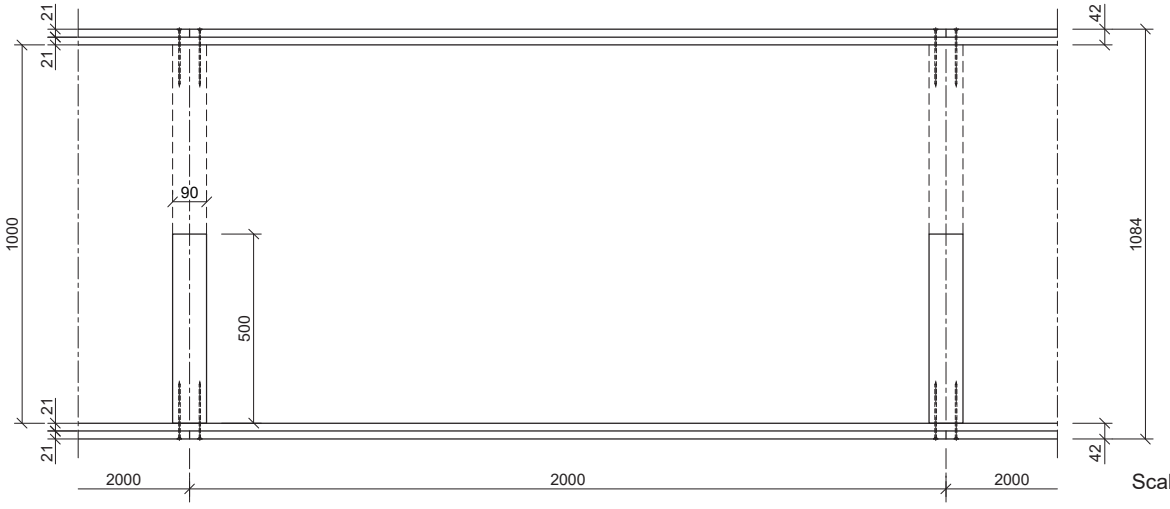

Scale 1:20

Detail 1.1

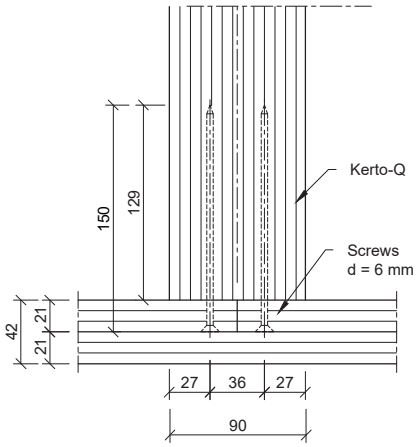

Detail 1.2

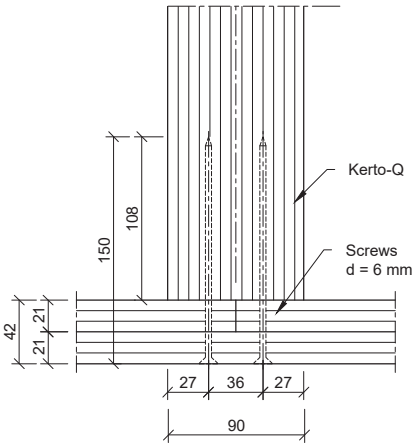

Scale 1:5

Detail 2a

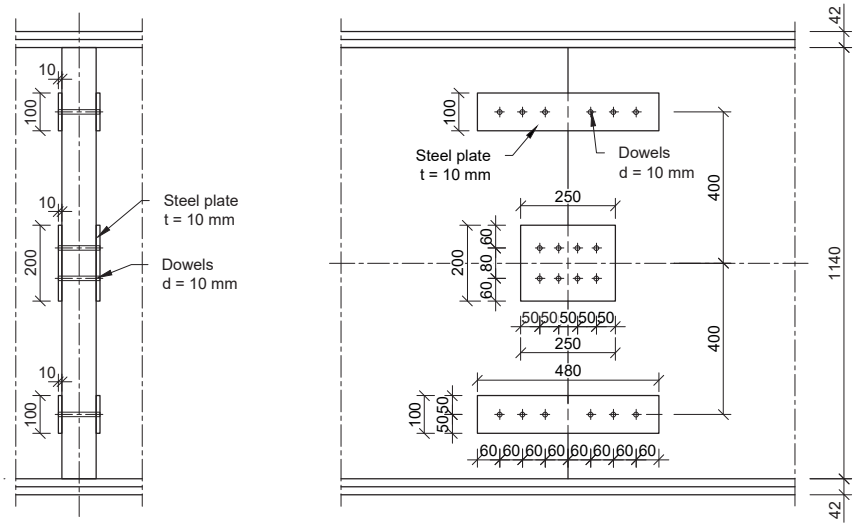

Scale 1:20

Detail 2b

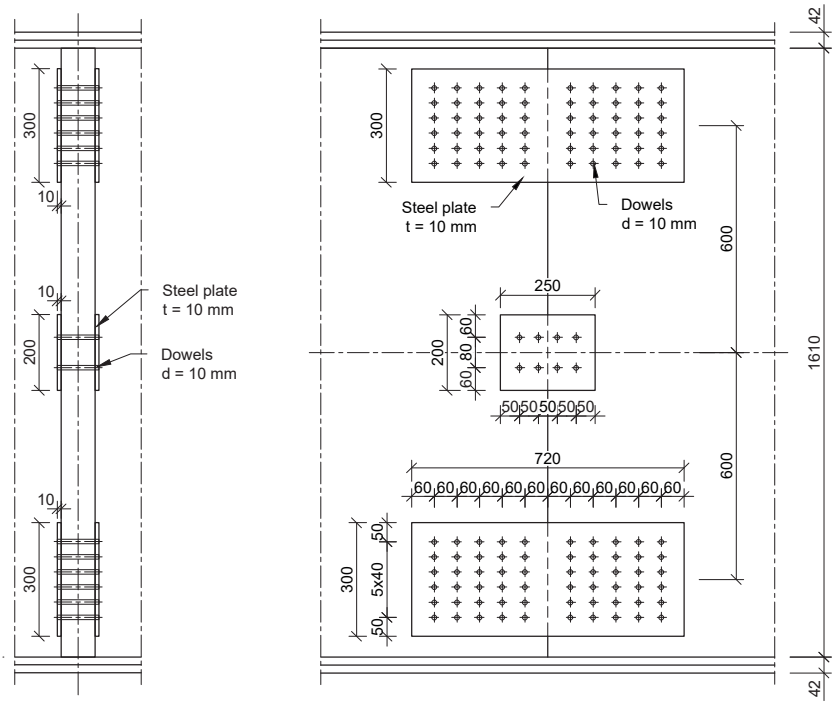

Scale 1:20

Detail 3

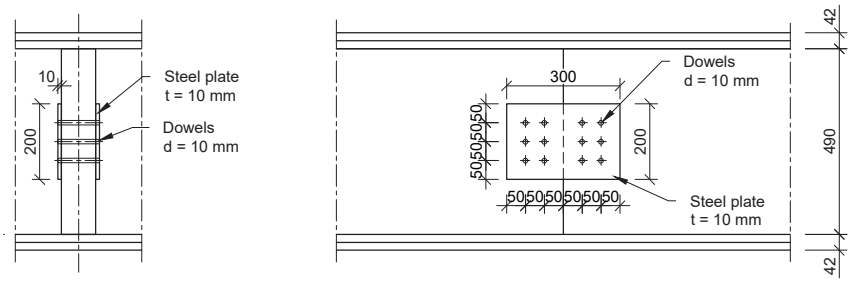

Scale 1:20

Detail 4

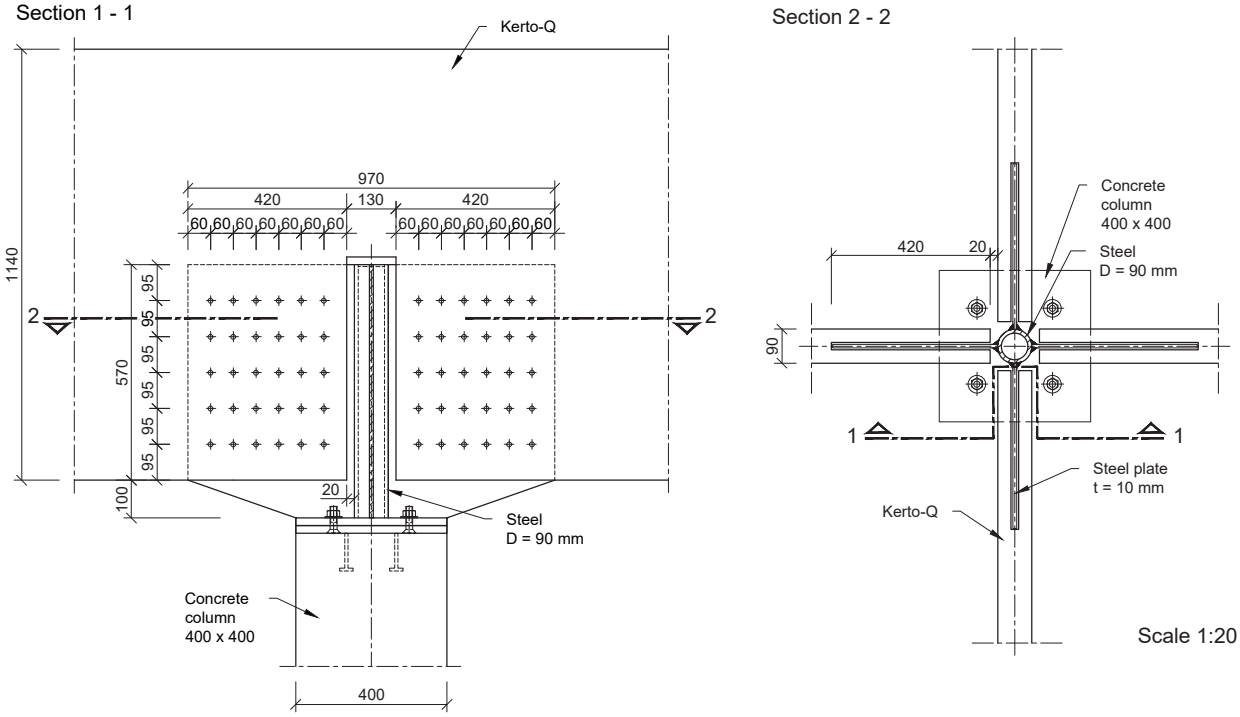

Scale 1:20

Detail 5

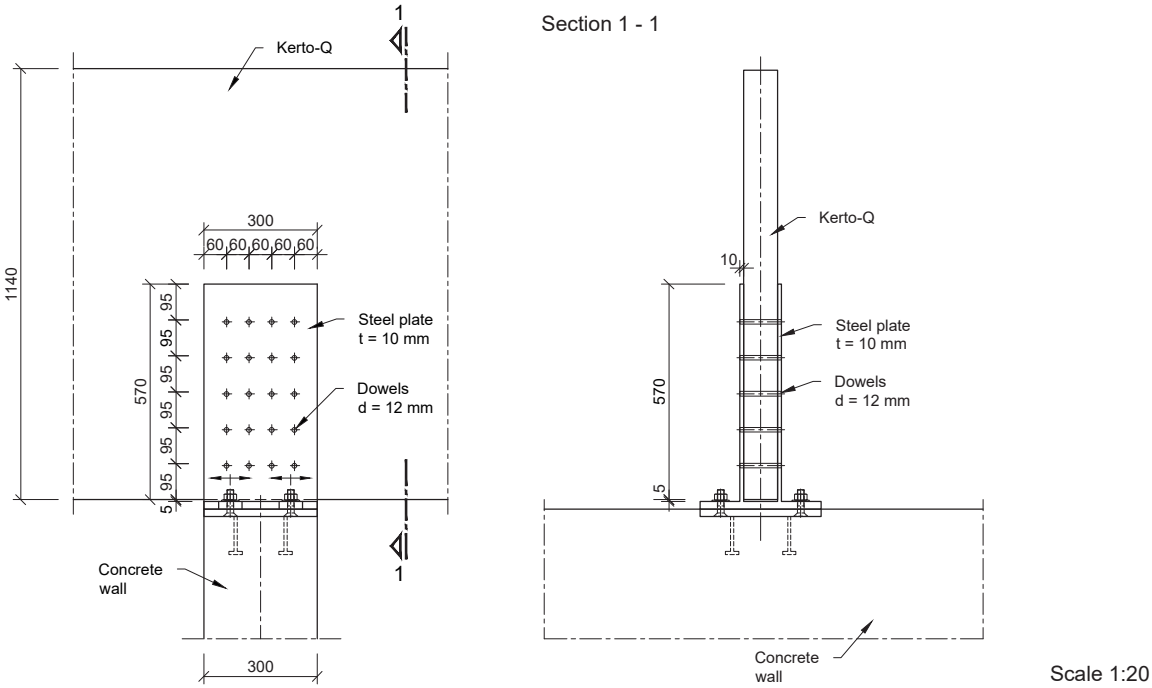

Scale 1:20

6.2. Global Model

In this section the approximation for the simulation of the global model will be given. The global model is complex and large, which makes it difficult to approach exact each different connection type. Therefore it has been chosen to have a more general approach which applicable for the whole structure. The structural analysis of the global model will be discussed, in which the design of connections will be included.

6.2.1. Built-up Beam

In this part the stiffness approximation for the global model will be discussed. The plates will be attached to the ribbed elements by screws. For I-beams the amount of screws and stiffness of the connection should be included since this will have an influence on the structural behaviour. A simplified approximation will be made since the global model is complex and too large to make individual connections. First as proof of concept a simply supported beam will be calculated and compared with a model in SOFiSTiK. The reduction of bending stiffness for the simple connection between the ribbed elements will be calculated. The approximation for the global model will be given. Therefore a cross section from the global model with a height of $400\,mm$ is considered for the stiffness calculation.

Stiffness approximation

A simply supported beam with a span of $6\,m$ will be considered. The composite cross section of the ribbed elements with the plates will be approached as an I-beam. In figure 6.10 the dimensions of the cross section are displayed. Due to shear deformations, the normal stresses in the centre plane of the flanges are not uniformly distributed. The contributions of the flanges due to the bending stiffness and bending capacity of the composite cross section consequently decreases. Therefore the following approximation for the effective flange width b_{eff} will be given.

The effective width will be calculated with equation 6.15 with b_w is $90\,mm$. The value of $b_{c,eff}$ and $b_{t,eff}$ should not be greater than the maximum value for shear lag, EN 1995-1-1, 9.1.2 (Tab. 9.1). The effective flange width due to the effect of shear lag is $0,1 \cdot length$, see equation 6.13 . In equation 6.14 the value of $b_{c,eff}$ should also not be greater than the maximum value of plate buckling, which is $20 \cdot t_{plate}$ for plywood parallel to the webs.

$$b_{t,eff} = min(0,1 \cdot l; b) = min(0,1 \cdot 6000; 2000) = 600\,mm \tag{6.13}$$

$$b_{c,eff} = min(0,1 \cdot l; 20 * t_{plate}; b) = min(0,1 \cdot 6000; 20 * 21; 2000) = 420\,mm \tag{6.14}$$

$$b_{eff} = b_{c,eff} + b_w\,(or\ b_{t,eff} + b_w) = 420\,mm + 90\,mm = 510\,mm \tag{6.15}$$

The composite cross section will be modelled with a width of $510mm$ and a height of $442mm$. The self weight of the entire cross section will be taken into account. The composite beam will be supported by pinned connections. In the serviceability limit state the deflection will be calculated. The stresses will be calculated in the ultimate limit state. The simulation of the model will be made with quad elements according to the plate theory.

The results will be compared with hand calculations, which are based on the Euler-Bernoulli beam theory. This beam theory is a simplification of the linear theory of elasticity. It provides a means of calculating the characteristics of beams. It covers the case for small deflections caused by lateral forces. For the Timoshenko beam theory those deflections are taken into account. The Kirchhoff-Love theory of plates is used to determine the stresses and deformation in plates subjected to forces and moments. This theory is an extension of

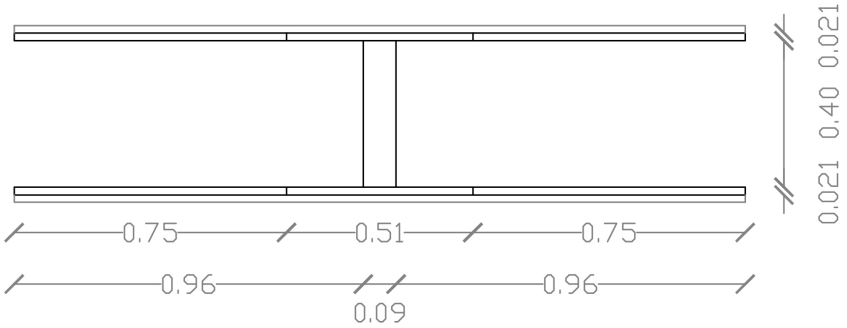

Figure 6.10: The dimensions of the cross section for the simply supported beam in m

the Euler-Bernouilli beam theory. The Mindlin theory of plates takes into account the shear deformation through the thickness of a plate. Therefore the Mindlin theory is often called the first-order shear deformation theory of plates. The SOFiSTik program calculates with the Timoshenko beam theory for beams and with the Mindlin theory for plates. For simplicity no detailed investigation has been done for the hand calculations. Normally shear deformation has not a large influence but it was found out that for composite beams it certainly had. Therefore the shear modulus of the material properties has been increased significantly in SOFiSTiK.

Connection plates to rib

The stiffness connection between the plates and the ribbed elements will be calculated. If this connection is glued it is assumed that the connection will be fully stiff and the cooperation factor γ will be $1,0$. The plates will be attached with screws to the ribbed elements. For the strength verification the cooperation factor γ needs to be calculated. The top and bottom plates will have a thickness of $2 \cdot 21\ mm$ and the ribbed elements a thickness of $90\ mm$, see figure 6.10. It will be assumed that the screws have a diameter of $6\ mm$, which are spaced $250\ mm$ over the length of the beam. The final slip modulus K_{ser} of the screws will be determined using equation 6.16 according EN 1995-1-1:2004-7.1.

$$K_{ser} = \frac{\rho^{1.5} \cdot d}{23} = \frac{510^{1.5} \cdot 6}{23} = 3004,5 \tag{6.16}$$

The final slip modulus K_{ser} will be multiplied by the amount of screws every $1\ m$. There will be two screws and n factor will be $2 \cdot 4$ is 8, which will give a K_{ser} of $24036,4$.

$$K_u = \frac{2}{3} \cdot \frac{K_{ser}}{(1 + 2 \cdot k_{def})} = \frac{2}{3} \cdot \frac{24036,4}{(1 + 2 \cdot 0,8)} = 6163,2 \tag{6.17}$$

The stresses will be calculated with the following ultimate limit state calculations. The stiffness for the screws will be different than in the serviceability limit state. The slip modulus K_u can be determined with equation 6.17 by using 6.16. For connections the creep factor needs to be taken into account twice. The cooperation factor will be calculated equation 6.18 from EN 1995-1-1, B.2 (B.5).

$$\gamma = \frac{1}{1 + p} \tag{6.18}$$

The cooperation factor will be calculated with equation 6.18. Using this equation, the cooperation factor γ_u can be determined with equation 6.19 (EN 1995-1-1:2004 Annex B (B.5)) for the ultimate limit state. In this equation the length l is the span of simply supported beams. For continuous beams l is equal to $0,8$ of the relevant span and for cantilevered beams l is equal to twice the cantilever length. For the global model the minimum span is

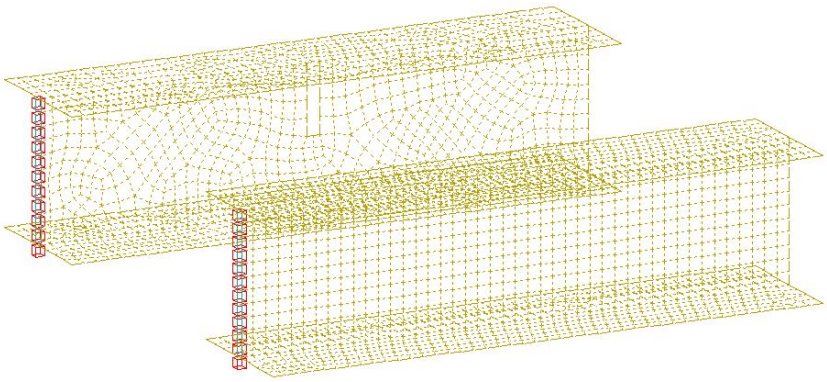

Figure 6.11: Two ribbed elements with an incision and without an incision

$6\,m$, in this case the length l will be taken as $4,8\,m$.

$$p_u = \frac{\pi^2 \cdot E_{eff} \cdot A \cdot s}{K_u \cdot l^2} = \frac{\pi^2 \cdot 4487,18 \cdot (33 \cdot 690) \cdot 100}{1943,8 \cdot (6000)^2} = 1,44 \tag{6.19}$$

In equation 6.19 the effective modulus of elasticity has been determined with equation 6.20.

$$E_{eff} = \frac{E}{(1 + k_{def})} = \frac{10.500}{(1 + 0,8)} = 5833,33\ N/mm^2 \tag{6.20}$$

The cooperation factor γ is $0,48$. This gives an indication of 50 percent stiffness. More screws and or less spacing between them could be increased to increase the stiffness.

Simple connection

A simple connection will be made for intersecting the different ribbed elements. In the ribbed elements an incision will be made of half the length and width of $90\,mm$. The bending stiffness will be reduced by taking away some material of the element. Two ribbed elements with an incision and without an incision are compared, see figure 6.11. A simplified calculation is made to check the loss of stiffness with the equation from figure 6.14. The ribbed elements have a length of $4\,m$ and a load of $10kN$ is applied.

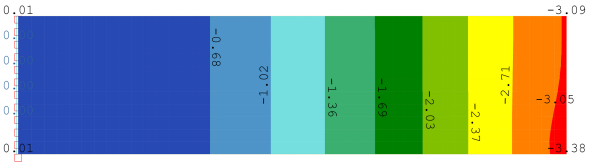

Figure 6.12: Ribbed elements without incision

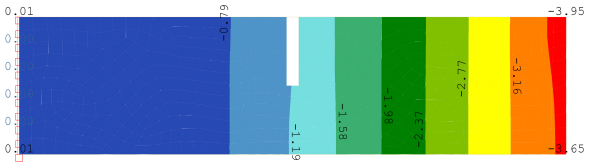

Figure 6.13: Ribbed elements with incision

The maximum deflection of the ribbed elements without an incision is $3,38\,mm$, see figure 6.12. In figure 6.13 the deflection under the point load of the ribbed elements with an incision is $3,65\,mm$. The bending stiffness is calculated with equation 6.27. In table 6.4 both bending stiffness are displayed. The difference is $\frac{5,845}{6,312} = 0,93$. The incision gives a reduction of 7 percent stiffness.

$$EI = \frac{F \cdot l^3}{3 \cdot u} = \frac{10.000 \cdot 4.000^3}{3 \cdot u} \tag{6.21}$$

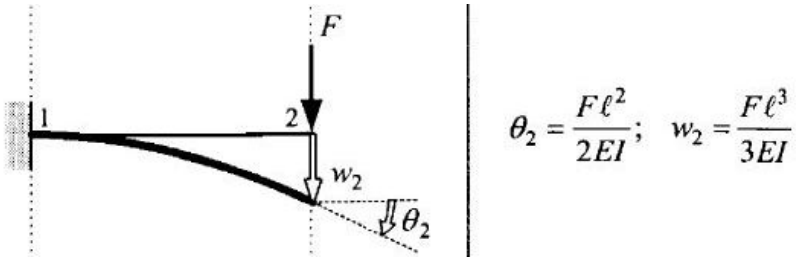

Figure 6.14: 'Forget-me-not' formula

Table 6.4: Results from the two ribbed elements models

Simple connection stiffness	Bending stiffness (N/mm^2)	Deflection (mm)
Ribbed elements		
without an incision	$6{,}312 \cdot 10^{13}$	3,38
with an incision	$5{,}845 \cdot 10^{13}$	3,65

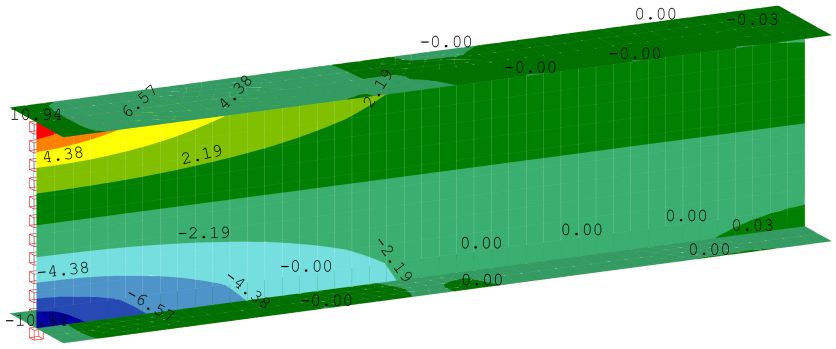

Figure 6.15: Bending stresses local x in N/mm^2 without incision

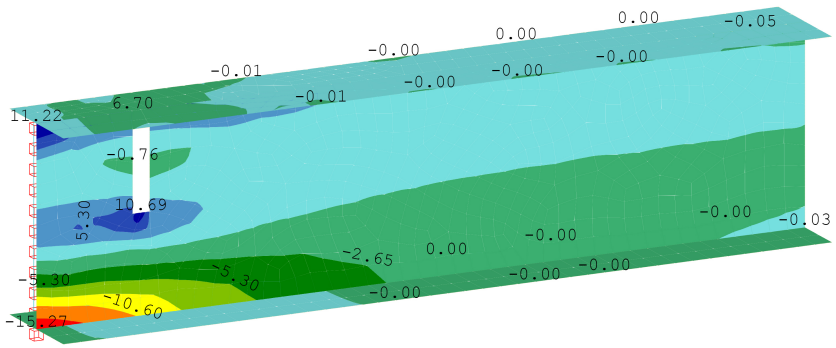

Figure 6.16: Bending stresses local x in N/mm^2 with incision

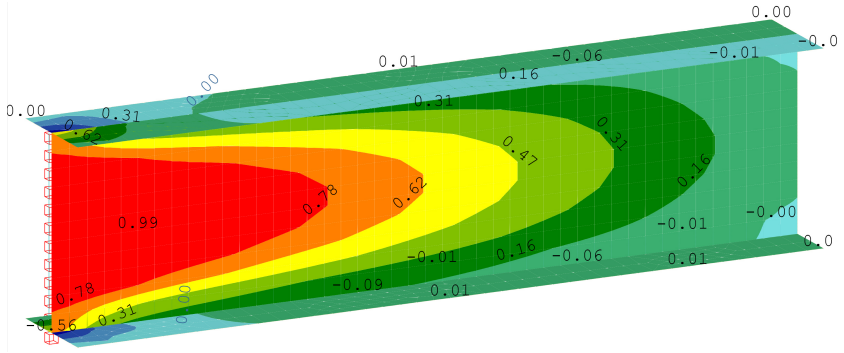

Figure 6.17: Shear stresses local x in N/mm^2 without incision

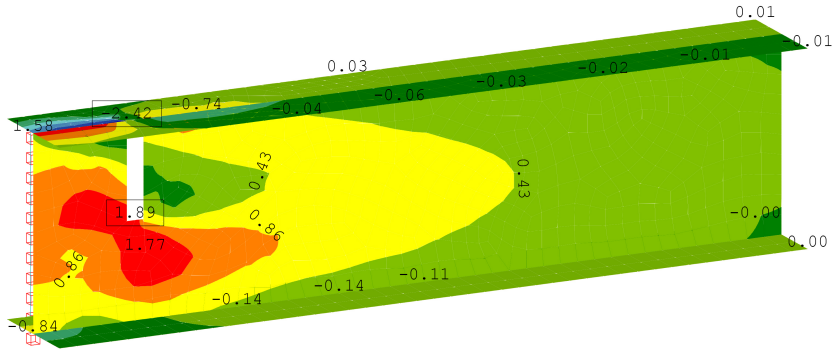

Figure 6.18: Shear stresses local x in N/mm^2 with incision

The two ribbed elements with an incision and without an incision are compared. The stresses are checked in the ultimate limit state. The maximum bending stress without incision is $10,94\ N/mm^2$. This occurs at the inclined support, which is stiffest part of the beam. The normal stresses are disturbed with an incision in the beam. However the forces can be distributed through the top plate. In figure 6.15 the bending stresses local x are shown. The difference for the bending stresses are shown in figure 6.16. At the position of the incision the bending stresses are increased from $6,57 N/mm^2$ to $10,60 N/mm^2$, this is a difference of $1,5$.

The shear stresses without incision are the highest at the inclined support. In figure 6.18 local shear stresses occur at the location where the incision is made. A clear difference can be seen with the shear stresses in figure 6.17. At the position of the incision the stresses are increased from $1,00\ N/mm^2$ to $1,90\ N/mm^2$, this is a difference of 1.9. Locally high shear stresses occur at the top plate of $2,42\ N/mm^2$.

Although the simple connection is easy for intersecting the ribbed elements. A side effect is that by taking away material for the incision that the stresses are increased. The bending stresses in local x should be reduced by a factor of $1,5$. The shear stresses should be reduced a factor of $2,0$. This will be included for the global model, see section 6.2.3.

6.2.2. Assumptions

The stiffness of connection has been calculated and it is approximately 50 percent. The incision of the ribbed elements gives a reduction of 7 percent stiffness. The reduction in stiffness of 40 percent will be taken into account for the calculation example and the global model, which can be achieved for the structure. Although the longer the length the stronger the stiffness will be in the imperial formula 6.19. First from this stiffness the assumption will be explained for the global model. The top and bottom plates will have a thickness of $2 \cdot 21\ mm$ plates. The plates will be orientated in two directions, which gives a difference in strength

and stiffness. The assumption for the plates will be discussed since this has an influence for the global model.

Assumption between plates and ribbed element

The stiffness of the screws will be assumed with a cooperation factor γ_u of $0,4$ for the connection between the plates and the ribbed element. The material properties of the plates and ribbed element are the same. In figure 6.19 the material properties are displayed by 100%. It is too complex and time consuming to make an exact approach for the global model. Therefore the connection will be fully stiff between plates and the ribbed element and a cooperation factor γ of $1,0$. The assumption of the connection is to reduce the material properties of the plates till 40%.

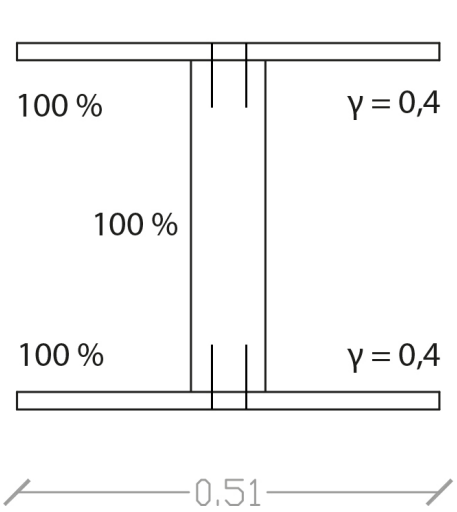

Figure 6.19: Stiffness connection

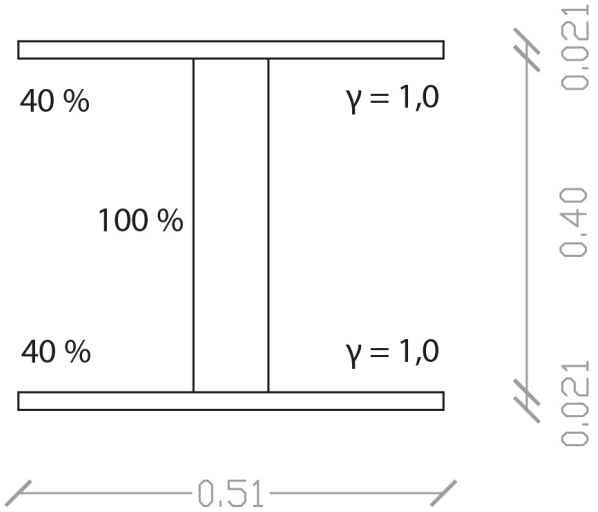

Figure 6.20: Approximation for SOFiSTiK model

A calculation example is made with SOFiSTiK. The model is made with quad elements according to the plate theory, see figure 6.21. In this model the grain direction of the plates and the ribbed element is among the longitudinal direction. The left support is pinned in all three directions and the right support is pinned in y- and z-direction. The span between the supports is $6\,m$. The plates have each four lateral supports, which provide them from moving in the y-direction.

The self weight of the cross section is $0,61\,kN/m$, with for plates $0,43\,kN/m$ and the ribbed element $0,18\,kN/m$. The dead load is $2,0\,kN/m^2$ over an area width of $2,0\,m$, a line load is applied of $4,0\,kN/m$. The total distributed load q of the beam is $4,61\,kN/m$.

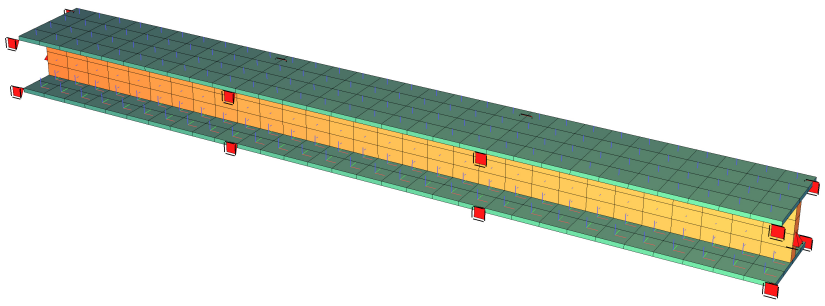

Figure 6.21: The SOFiSTiK model for the beam with a span of $6,0\,m$

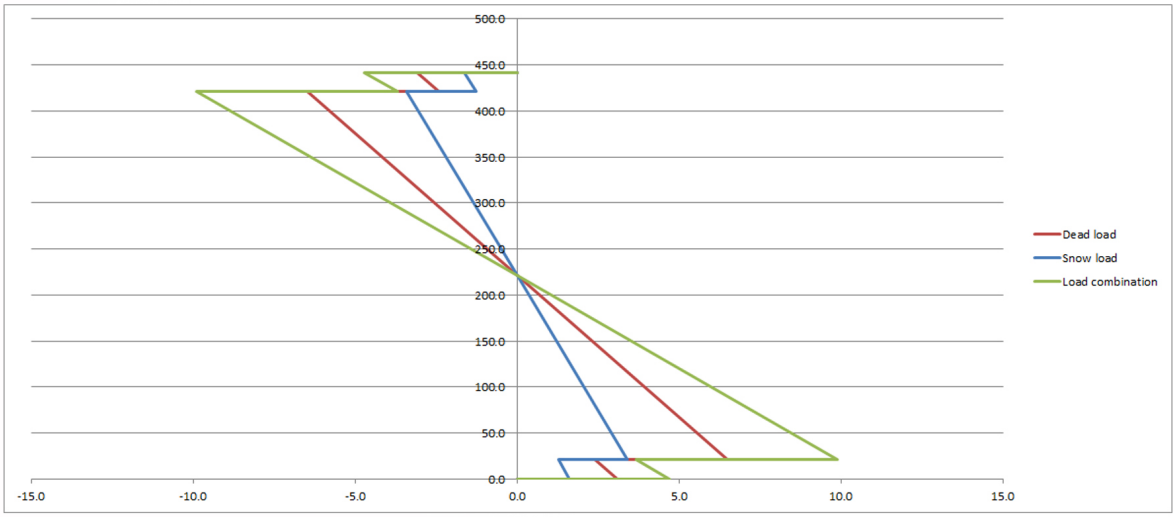

Figure 6.22: The stresses defined by hand calculation. Dead load: LC $1,35 \cdot G$, Snow load: LC $1,5 \cdot S$ and Load combination: LC $1,35 \cdot G + 1,5 \cdot S$

The design bending moment for this simple support beam has been calculated with equation 6.22.

$$M_{gd} = 1,35 \cdot \frac{1}{8} \cdot q \cdot l^2 = 1,35 \cdot \frac{1}{8} \cdot 4,61 \cdot 6^2 = 28,0kNm \tag{6.22}$$

The cooperation factor γ_u is $0,4$. The effective modulus of elasticity has been determined with equation 6.20. In this equation the top plate is number 2, the ribbed element is number 3 and the bottom plate is number 4. The modulus of elasticity is equal for all the different members. The moment of inertia of the cross section is $1,43 \cdot 10^9 mm^4$. From this the effective bending stiffness can be determined with equation 6.23 (EN 1995-1-1:2004 Annex B (B.1)).

$$(EI)_{eff_u} = (E_{eff,2} \cdot I_{eff_2} + \gamma \cdot E_{eff,2} \cdot A \cdot a^2) + (E_{eff,3} \cdot I_{eff_3}) + (E_{eff,4} \cdot I_{eff_4} + \gamma \cdot E_{eff,4} \cdot A \cdot a^2) = 5,04 \cdot 10^{12} Nmm^2 \tag{6.23}$$

The stresses for the different parts of the cross section has been calculated with equation 6.24 (EN 1995-1-1:2004 Annex B (B.7)) and equation 6.25 (EN 1995-1-1:2004 Annex B (B.8)). A dead load of $4,0\ kN/m$ and a snow load of $2,18\ kN/m$ is applied on the beam. The load combination is $1,35 \cdot G + 1,5 \cdot Q$. In figure 6.22 the stresses have been given for these different load cases.

$$\sigma_i = \frac{\gamma_u \cdot E_{eff} \cdot a \cdot M_{gd}}{(EI)_{eff_u}} \tag{6.24}$$

$$\sigma_{m,i} = \frac{0,5 \cdot E_{eff} \cdot h \cdot M_{gd}}{(EI)_{eff_u}} \tag{6.25}$$

In the ultimate limit state the stresses are checked under the load case of $1,35 \cdot G$, see red line in figure 6.22. From the hand calculation the top plate has normal stresses of $-3,09\ N/mm^2$. The ribbed element has normal stresses from $-6,49\ N/mm^2$ to $+6,49\ N/mm^2$. The bottom plate has normal stresses of $-3,09\ N/mm^2$.

In figure 6.23 the normal stresses in the local x-direction of the SOFiSTiK model are displayed. The stresses are $-2,73 N/mm^2$ for the top plate and $+2,73 N/mm^2$ for the bottom plate. The normal stresses for the ribbed element goes from $-6,49\ N/mm^2$ to $+6,49\ N/mm^2$.

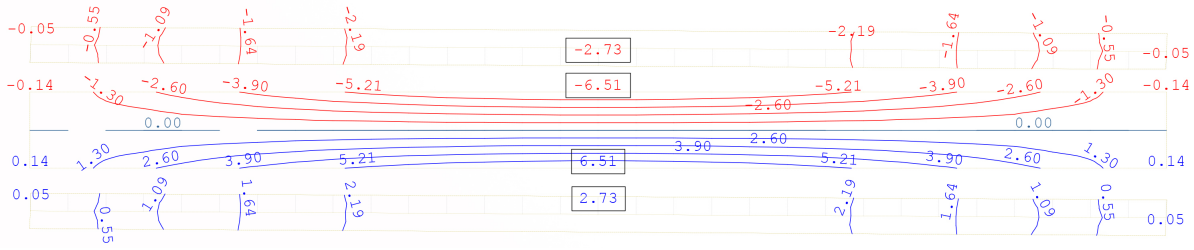

Figure 6.23: The stresses in local x-direction of the SOFiSTiK model. Dead load: LC $1,35 \cdot G$

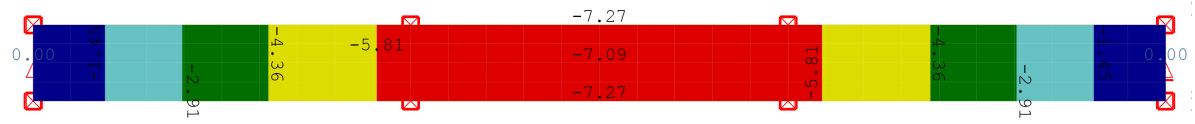

Figure 6.24: The deflection of the SOFiSTiK model

The deflection will be calculated for comparing the results as well. Using equation 6.18, the cooperation factor γ_{ser} can be determined with equation 6.26 for the serviceability limit state by taken into account E_{mean} and K_{ser}. In this case the K_{ser} and distance s will be different, since the cooperation factor γ_u has been reduced till $0,4$.

$$p_{ser} = \frac{\pi^2 \cdot E_{mean} \cdot A \cdot s}{K_{ser} \cdot l^2} = \frac{\pi^2 \cdot 10.500 \cdot (21 \cdot 510) \cdot 365}{16463,3 \cdot (6000)^2} = 0,49 \tag{6.26}$$

The cooperation factor γ is $0,59$. This gives an indication of 60 percent stiffness. The effective bending stiffness should be taken as EN 1995-1-1, B.2 (B.1) with equation 6.27.

$$(EI)_{eff,ser} = (E_1 \cdot I_{eff_2} + \gamma \cdot E_2 \cdot A \cdot a^2) + (E_3 \cdot I_{eff_3}) + (E_4 \cdot I_{eff_4} + \gamma \cdot E_4 \cdot A \cdot a^2) = 1,10 \cdot 10^{13} Nmm^2 \tag{6.27}$$

The deflection is $7,1\,mm$, which is determined with equation 6.28.

$$w = \frac{5}{384} \cdot \frac{q \cdot l^4}{(EI)_{eff,ser}} = \frac{5}{384} \cdot \frac{4,61 \cdot 6000^4}{1,10 \cdot 10^{13}} = 7,1\,mm \tag{6.28}$$

The results of the hand calculations for the deflection and the stresses have been determined. In the serviceability limit state the deflection is checked under the load case of $1,0 \cdot G$. The material properties of the plates have been increased till 60 %, while the γ_{ser} is $0,6$. From the hand calculation the deflection is $7,1mm$. SOFiSTiK has calculated a maximum deflection of $7,27\,mm$. The deflection along the beam is depicted in figure 6.24. The difference between the calculations is $2,5$ %.

The plate stresses are lower from SOFiSTiK than the hand calculation but the ribbed element stresses are higher. The average top stresses from SOFiSTiK are $4,62\,N/mm^2$ and from hand calculation $4,79\,N/mm^2$. A difference of 4 % between the average of both calculations. This difference comes from the fact that the SOFiSTiK model has been calculated with the plate theory, while the hand calculation has been made with the beam theory. However the results are quite similar and it has been proven that the approach works.

Plates assumption

In section 6.1 the different direction of the plates have been discussed. The plates with a total thickness of $42\,mm$, which will consist out of two layers each $21\,mm$. The layers will give stiffness in each another direction. However the plates are only connected through screws to the ribbed elements.

$$(EI)_{eff_{u1}} = (E_{eff,1} \cdot I_{eff_1} + \gamma \cdot E_{eff,1} \cdot A \cdot a_1^2) + (E_{eff,3} \cdot I_{eff_3}) + (E_{eff,5} \cdot I_{eff_5} + \gamma \cdot E_{eff,5} \cdot A \cdot a_1^2) \tag{6.29}$$

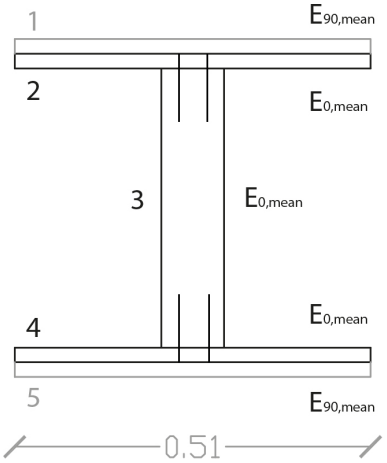

Figure 6.25: Build-up beam 1

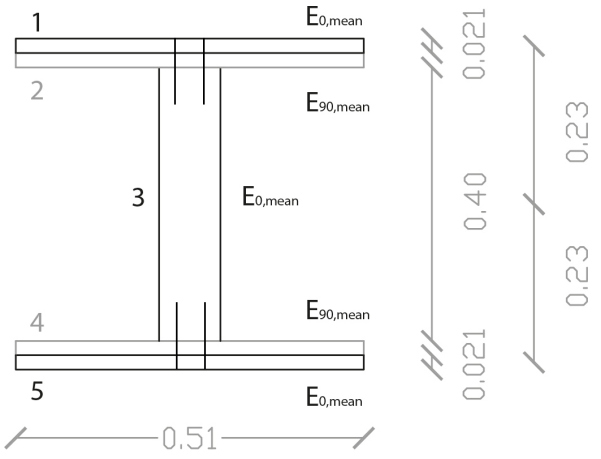

Figure 6.26: Build-up beam 2

In one direction the plates are directly attached to the ribbed elements, see figure 6.25. In this equation the top plate is number 2, the ribbed element is number 3 and the bottom plate is number 4. The effective bending stiffness can be determined with equation 6.29. The plate distance a_1 from the neutral axis of the build-up beam is $210,5\,mm$. In figure 6.27 the stresses are shown for the different load cases.

$$(EI)_{eff_{u2}} = (E_{eff,1} \cdot I_{eff_1} + \gamma \cdot E_{eff,1} \cdot A \cdot a_2^2) + (E_{eff,3} \cdot I_{eff_3}) + (E_{eff,5} \cdot I_{eff_5} + \gamma \cdot E_{eff,5} \cdot A \cdot a_2^2) \quad (6.30)$$

In the other direction the plates will be connected by screws, which go through the other plates. In figure 6.26 the grain direction of the top plate 2 and the bottom plate 4 lay in the other direction. These plates with $E_{90,mean}$ will contribute less than the other plates. Therefore it is assumed that there will be a gap in the built-up of the beam cross section. The plate distance a_2 from the neutral axis of the build-up beam is $231,5\,mm$.

$$K = \frac{K_1 \cdot K_2}{K_1 + K_2} = \frac{K}{2 \cdot K} = 0,5 \cdot K \quad (6.31)$$

This built-up will give two shear planes and the connection of the plates will be less stiff. The top plate 1 has a slip modulus K_1 and the top plate 2 has a slip modulus K_2. Although the modulus of elasticity are different, the density of both plates is equal. The slip modulus can be calculated with equation 6.31. In equation 6.19 the K_u will be reduced by half and this will give a cooperation factor γ_{u2} of 0,32. Since the reduction of simple connection needs be taken into account, γ_{u2} will be reduced till $0,20$. In figure 6.28 the stresses are shown for the different load cases.

In the global model one of the two layers will be modelled as one layer of $21\,mm$. This plate will have two different elasticity modulus. The material properties will be changed, for $E_{0,mean}$ is $0,4 \cdot 10.500\,N/mm^2$ and for $E_{90,mean}$ is $0,2 \cdot 10.500\,N/mm^2$, in $E_{0,mean}$ is $4.200\,N/mm^2$ and $E_{90,mean}$ is $2100\,N/mm^2$. The shear modulus from the plate material will be reduced by 30 percent, G_{mean} is $300\,N/mm^2$. These assumptions have been taken into account for the global model.

Table 6.5: Plates $2 \cdot 21\ mm$ with two different directions

	Slip Modulus K $-$	Distance a (mm)	Bending Stiffness EI_{eff_u} $\cdot 10^{12}\ (Nmm^2)$	Factor γ_u $-$
1	6163,2	210,5	5,46	0,48
2	3081,6	231,5	4,92	0,32

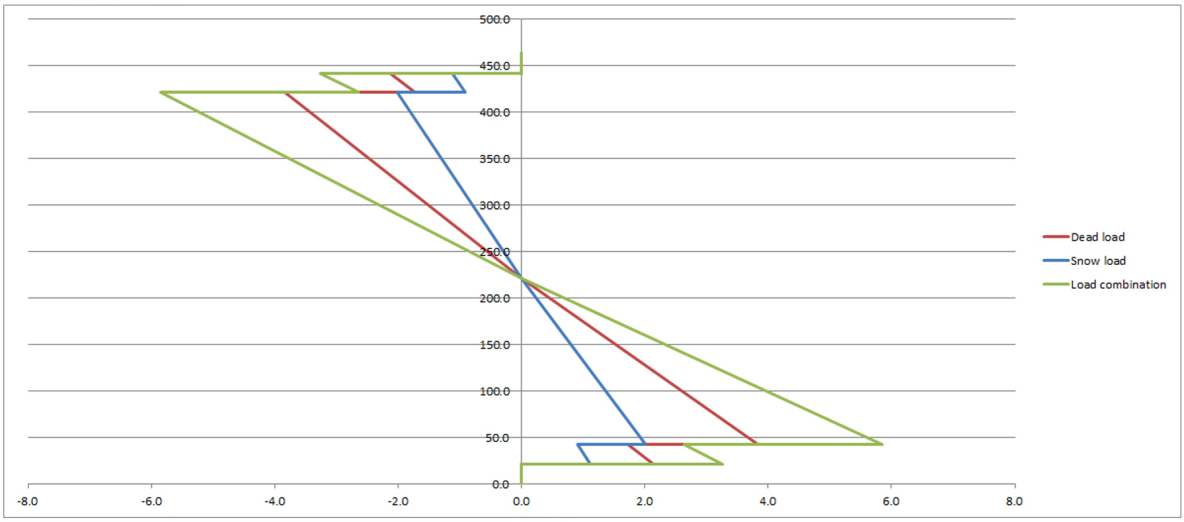

Figure 6.27: The stresses of build-up beam 1 in N/mm^2. Dead load: LC 201, snow load: LC 209 and load combination: LC 202

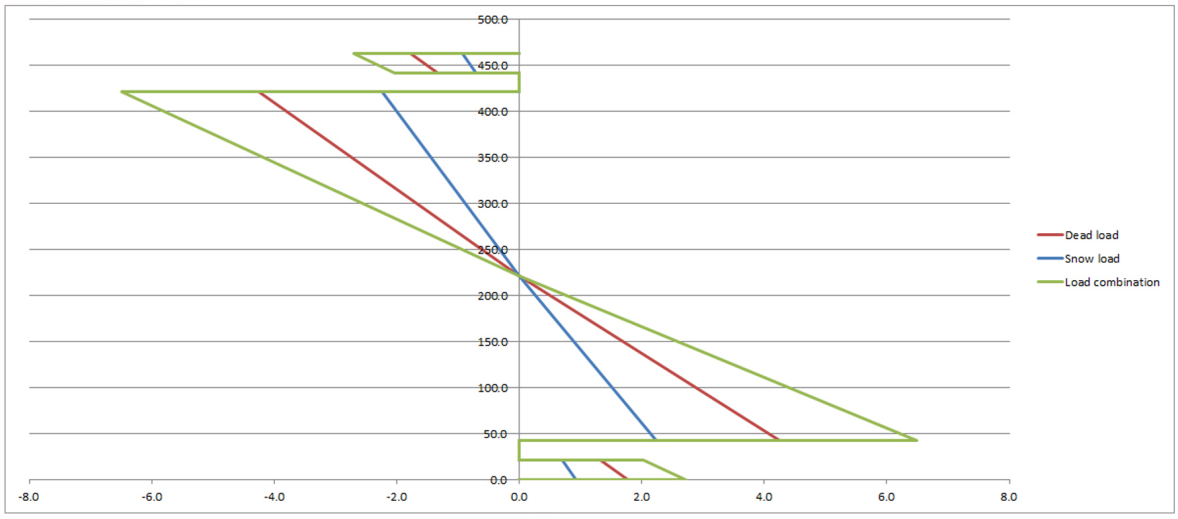

Figure 6.28: The stresses of build-up beam 2 in N/mm^2. Dead load: LC 201, snow load: LC 209 and load combination: LC 202

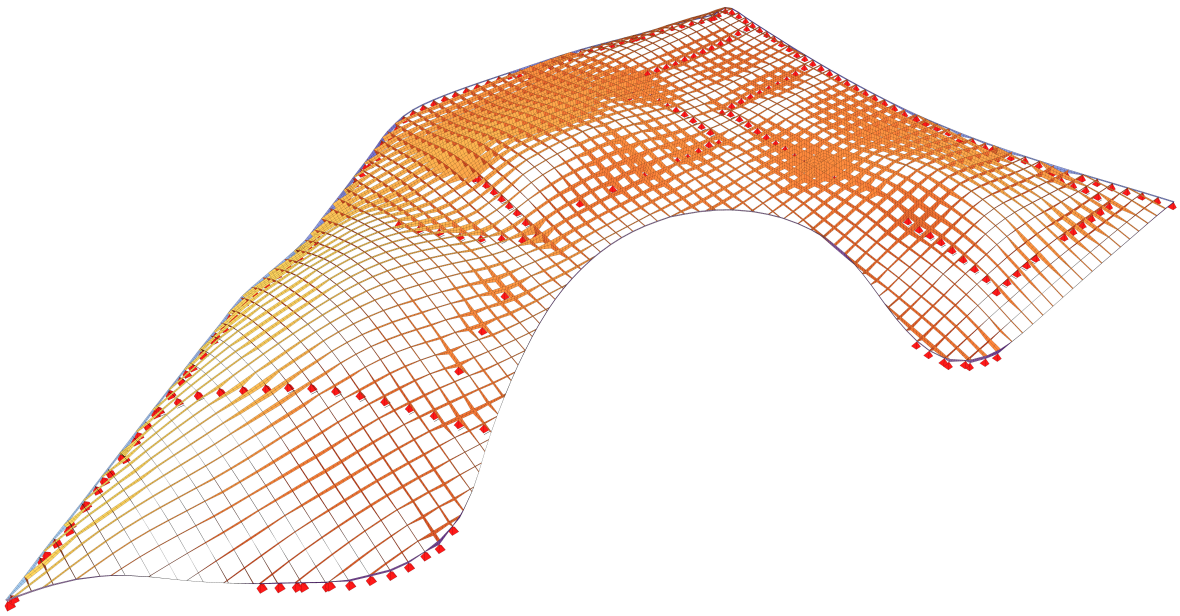

Figure 6.29: The smooth height variation of the free-form structure without plates for a better display

6.2.3. Final Analysis

The principle of smooth height variation has been explained in section 5.2 in the previous chapter. One of the major points of discussion is the height of the elements in the roof structure, as this is the key contributor for this structure to get the optimal height. The height has been calculated for the global model and the final results will be shown. In section 6.2.2 the assumptions have been explained for the complex free-form structure.

The roof surface has been divided by a grid of 2m by 2m. The roof surface consists out of ribbed elements and plates at the top and bottom. The ribbed elements will be modelled as surfaces with plates attached. The surfaces of the top plates and the bottom plates have been modelled as a continuous surface. The material properties of the plates will only be 40 percent of the original properties, which is more realistic as the connection between the plates and ribbed elements will not be fully stiff. One of the two layers will be modelled as one layer of 21 mm for the top plates and bottom plates. These plates will have two different elasticity modulus for the two different layer directions.

The ribbed elements will have a initial cross section of a width 90 mm and height 200 mm. The minimum height for the global model will be 200 mm. Otherwise the ribbed elements are too small to attach both plates with screws. The maximum height for the ribbed elements will be 2.500 mm, since this is the limited height which is available. The ribbed elements of the model will be assumed to be fully stiff connections. Although these connections will be made with less stiffness.

Global model with fine mesh

After multiple iterations and improvements the global model has met the requirements for the stresses and the deflections. The global model has been made of quad elements with fine mesh. It has been made with a mesh density between 0.1 m 0.4 m. The calculation has been made from the generated node values, where at the support positions higher stresses occurred. The dimensions of the ribbed elements are determined in the ultimate limit state. In figure 6.29 the optimal height for the free-form structure is depicted. The cross section heights have been checked in more detail according to the checking strategy, see section 5.3.

Table 6.6: Overview stresses criteria with all the factors

Allowable stresses (N/mm^2)	$f_{m,k}$	$f_{v,k}$	$f_{m,90,k}$
	$32,00$	$4,50$	$8,00$
Plates	$f_{m,d}$	$f_{v,d}$	$f_{m,90,d}$
Permanent	$16,00$	$2,25$	$4,00$
Variable	$24,00$	$3,38$	$6,00$
Ribbed elements	$f_{m,d}$	$f_{v,d}$	$f_{m,90,d}$
Permanent	$5,90$	$1,13$	$4,00$
Variable	$8,80$	$1,70$	$6,00$

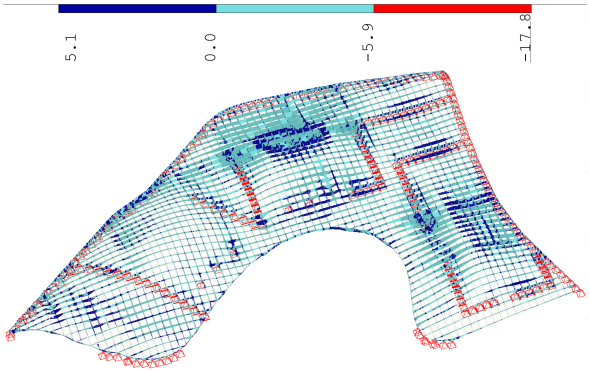

Figure 6.30: The local x stresses of the ribbed elements under permanent load

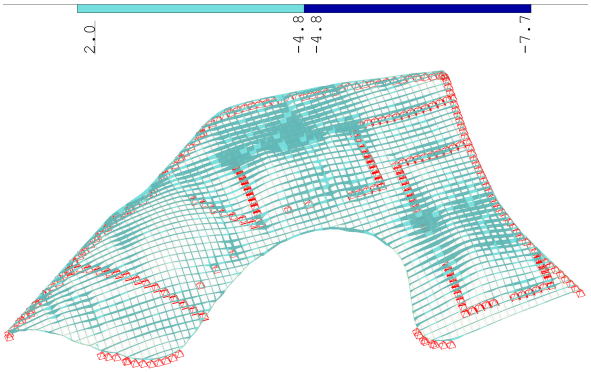

Figure 6.31: The local x stresses of the ribbed elements under variable load

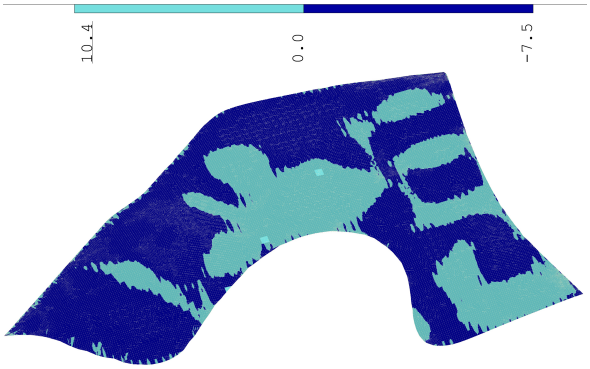

Figure 6.32: The local x stresses of the top plates under permanent load

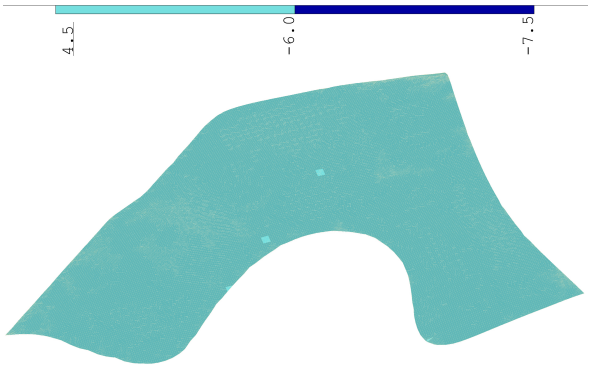

Figure 6.33: The local x stresses of the top plates under variable load

Stresses

The stresses have been checked for the permanent load case and the variable load case, see section for these combinations 4.1. In table 6.6 the allowable bending and shear stresses are displayed. In this table the stresses for $f_{m,d}$, $f_{m,90,d}$ and $f_{v,d}$ are depicted. The ribbed elements will be cut-out at average angle of 10° to the grain direction and the cross section reduction of $1,5$ due to the incision for the simple connection. The allowable bending stresses

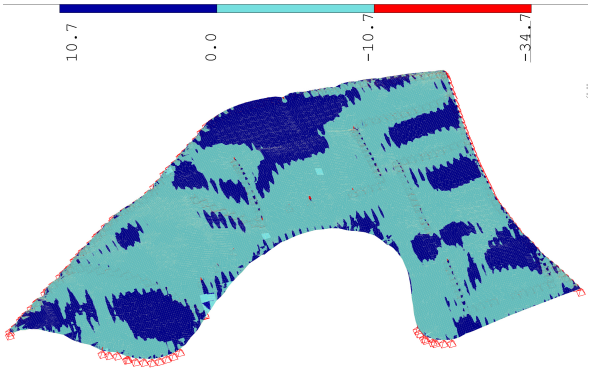

Figure 6.34: The local x stresses of the bottom plates under permanent load

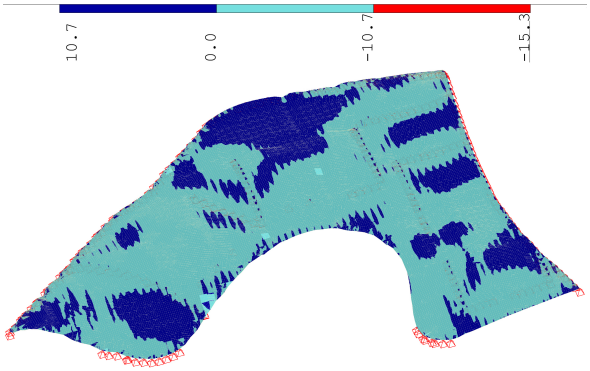

Figure 6.35: The local x stresses of the bottom plates under variable load

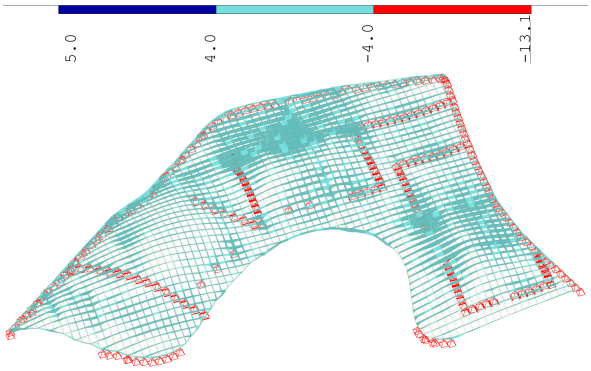

Figure 6.36: The local y stresses of the ribbed elements under permanent load

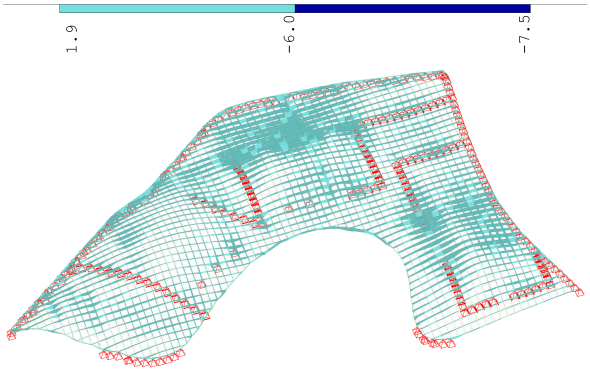

Figure 6.37: The local y stresses of the ribbed elements under variable load

of these elements are reduced by a total of approximately two.

The local x stresses are shown for the ribbed elements in figure 6.30 with a maximum compression stress of $-17,8\ N/mm^2$ and a maximum tension stress of $5,1\ N/mm^2$. The allowable stresses are $5,90\ N/mm^2$ under permanent load, which only exceed locally. The local x stresses are shown for the ribbed elements in figure 6.31 with a maximum compression stress of $-7,7\ N/mm^2$ and a maximum tension stress of $2,0\ N/mm^2$. The allowable stresses of $8,80\ N/mm^2$ are met under variable load.

The local x stresses are shown for the top plates in figure 6.32 with a maximum compression stress of $-7,5\ N/mm^2$ and a maximum tension stress of $10,4\ N/mm^2$. The allowable stresses are $16,00\ N/mm^2$ are met under permanent load. The local x stresses are shown for the top plates in figure 6.33 with a maximum compression stress of $-7,5\ N/mm^2$ and a maximum tension stress of $4,5\ N/mm^2$. The allowable stresses of $24,00\ N/mm^2$ are met under variable load.

The local x stresses are shown for the bottom plates in figure 6.34 with a maximum compression stress of $-34,7\ N/mm^2$ and a maximum tension stress of $10,7\ N/mm^2$. The allowable stresses are $16,00\ N/mm^2$ under permanent load, which exceed at the supports. The local x stresses are shown for the bottom plates in figure 6.35 with a maximum compression stress of $-15,3\ N/mm^2$ and a maximum tension stress of $10,7\ N/mm^2$. The allowable stresses of $24,00\ N/mm^2$ are met under variable load.

The local y stresses are shown for the ribbed elements in figure 6.36 with a maximum compression stress of $-13,1\ N/mm^2$ and a maximum tension stress of $5,0\ N/mm^2$. The allowable stresses are $4,00\ N/mm^2$ under permanent load, which only exceed locally. The local

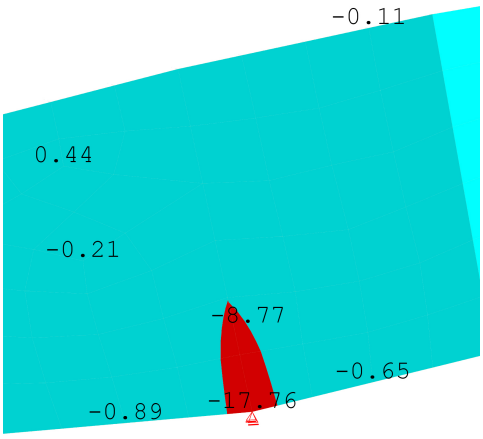

Figure 6.38: The high stresses, which occurs locally at the support conditions

y stresses are shown for the ribbed elements in figure 6.37 with a maximum compression stress of $-7,5\ N/mm^2$ and a maximum tension stress of $1,9\ N/mm^2$. The allowable stresses are $6,00\ N/mm^2$ under variable load, which only exceed locally.

The calculation has been shown from the generated node values, where at the support positions higher stresses occurred. However local stresses occur while the mesh density is fine for the global model. In figure 6.38 the local stresses are depicted for the local x stresses of the ribbed elements. These local stresses are not considered due to singularity effects with the checking strategy. However these high stresses needs to be solved with the detailing of the connections, see section 6.1.2. The high stresses can be taken by the steel plates in the support connections.

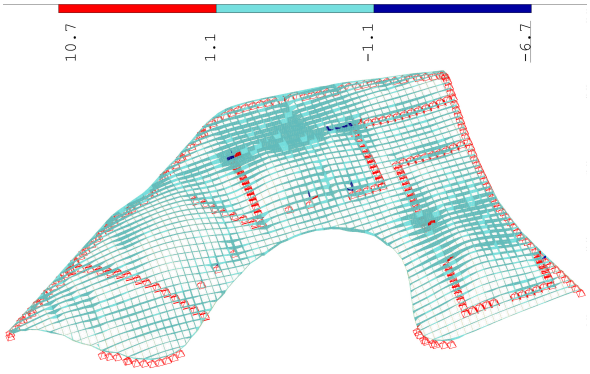

Figure 6.39: The shear stresses of the ribbed elements under permanent load

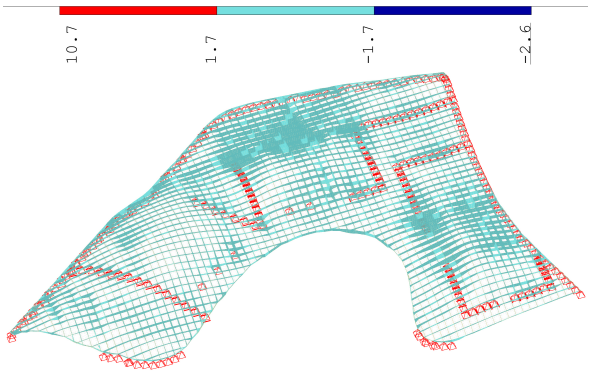

Figure 6.40: The shear stresses of the ribbed elements under variable load

The shear stresses have been checked for the permanent load case and the variable load case. The cross section reduction of $2,0$ due to the incision for the simple connection has been taken into account. The allowable shear stresses of the ribbed elements are reduced by a total of approximately two.

The shear stresses are shown for the ribbed elements in figure 6.39 with a minimum stress of $-6,7\ N/mm^2$ and a maximum stress of $10,7\ N/mm^2$. The allowable stresses are $1,13\ N/mm^2$ not met under permanent load. At a few locations the shear stresses are too high. Here, reinforcements will have to be made by adding timber strips (EN 1995-1-1:2004 6.1.7). The shear stresses are shown for the ribbed elements in figure 6.40 with a minimum stress of $-2,6\ N/mm^2$ and a maximum stress of $10,7\ N/mm^2$. The allowable stresses are $1,70\ N/mm^2$

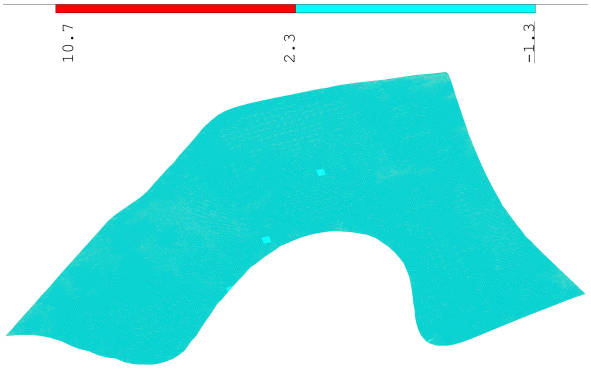

Figure 6.41: The shear stresses of the top plates under permanent load

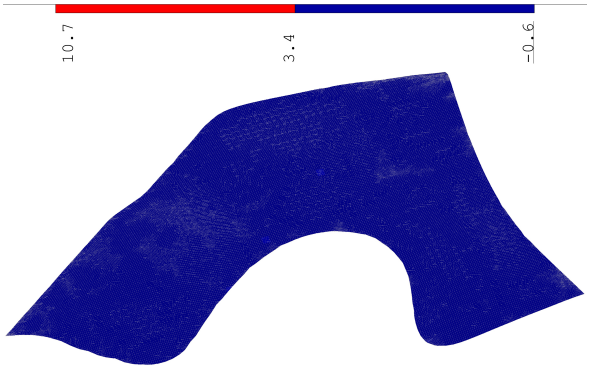

Figure 6.42: The shear stresses of the top plates under variable load

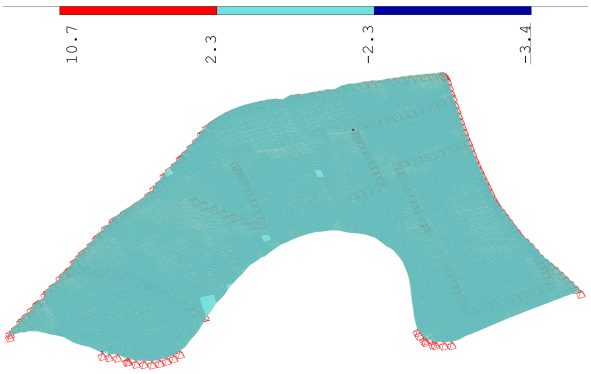

Figure 6.43: The shear stresses of the bottom plates under permanent load

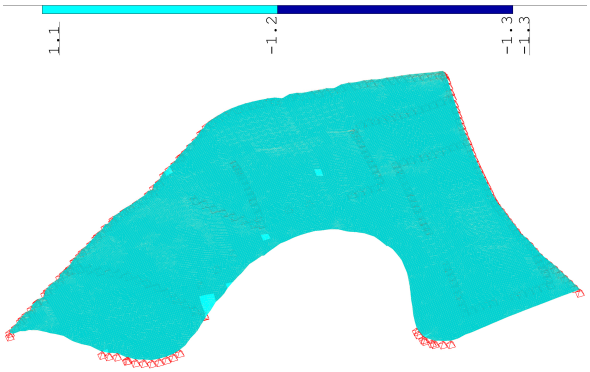

Figure 6.44: The bottom stresses of the bottom plates under variable load

under variable load, which only exceed locally.

The shear stresses are shown for the top plates in figure 6.41 with a minimum stress of $-1,3\ N/mm^2$ and a maximum stress of $10,7\ N/mm^2$. The allowable stresses are $2,25\ N/mm^2$ under permanent load, which only exceed locally. The shear stresses are shown for the top plates in figure 6.42 with a minimum stress of $-2,6\ N/mm^2$ and a maximum stress of $10,7\ N/mm^2$. The allowable stresses are $3,38\ N/mm^2$ under variable load, which only exceed locally.

The shear stresses are shown for the bottom plates in figure 6.43 with a minimum stress of $-3,4\ N/mm^2$ and a maximum stress of $10,7\ N/mm^2$. The allowable stresses are $2,25\ N/mm^2$ under permanent load, which only exceed locally. The shear stresses are shown for the bottom plates in figure 6.44 with a minimum stress of $-1,3\ N/mm^2$ and a maximum stress of $1,1\ N/mm^2$. The allowable stresses of $3,38\ N/mm^2$ are met under variable load.

Deflection

The deflections of the structure has been checked upon the design criteria in the serviceability limit state. The more detailed check will be made for the global model with the fine mesh. The maximum deflection is $142\,mm$ under the dead load in load combination 101, see figure 6.45. For the variable load in load combination 107, the maximum deflection is $56\,mm$ in figure 6.46. In figure 6.47 the load combination 102 with permanent and variable loads are depicted as well.

For the service class 2 the k_{def} is $0,8$ for permanent action and the k_{def} is $0,25$ for medium term action are used. The default factor ψ_2 is $0,0$ for the variable loads. The deflections are

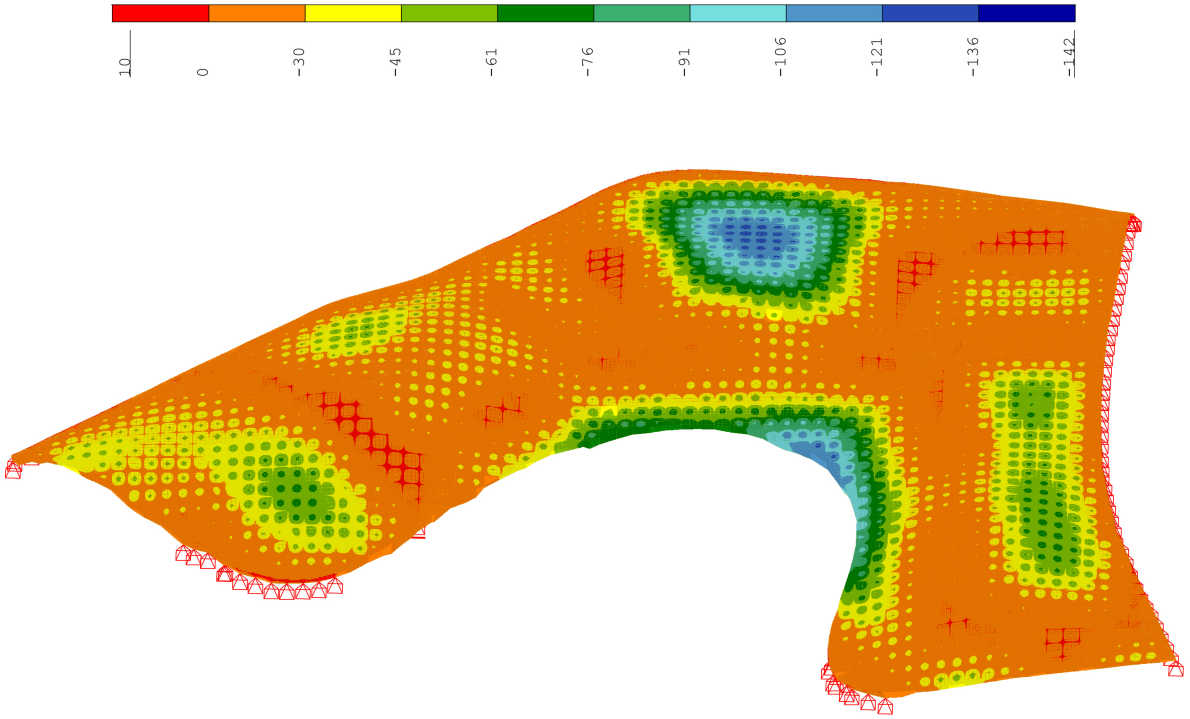

Figure 6.45: The deflection of the structure under dead load; LC 101

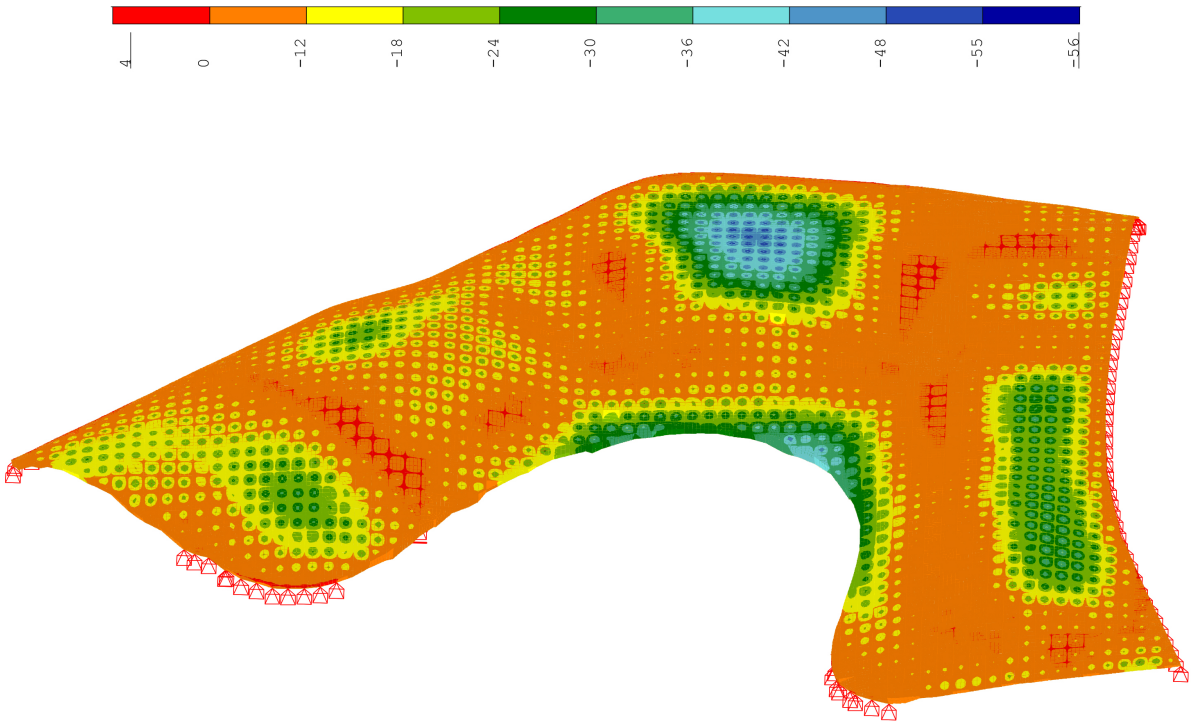

Figure 6.46: The deflection of the structure under variable load; LC 107

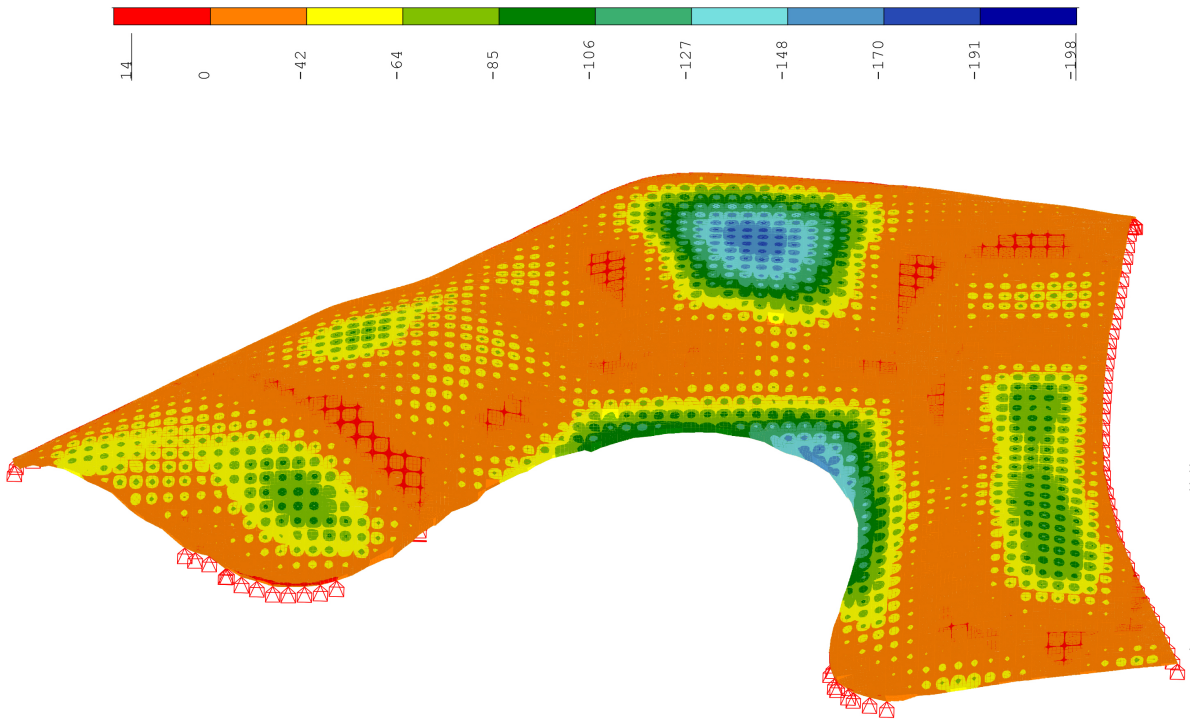

Figure 6.47: The deflection of the structure in LC 102

checked in the different states using the equation 4.12 and equation 4.13. The equation 4.13 is used in combinations with equations 4.15 and 4.14.

In table 6.7 the instantaneous deflection have been checked and in table 6.8 the final deflection have been checked at the critical areas as well. For the middle part all the values are above the criteria. For the cantilever part all the values are below and therefore improvement needs to be made. The solution will be that the cantilever part will be precambered. The deflection for the permanent loads will be checked and due to this deflection the elements will be curved the other way. This means that after loading the sagging of the beam will be relative to the straight line with the supports. The deflection has been checked with precambering the deflection of the dead load. The deflection under the self weight has been taken into account. For the cantilever part all the values are above the criteria, as can be seen in both tables 6.9 and 6.10.

Bending Moments

The model have been divided into two groups, the beams in global x-direction and the beams in global y-direction. The bending moments will be shown in these different groups to show a better behaviour along the surface.

First the bending moments of the beams in the global x-direction will be discussed. The distribution of the bending moments m_{xx} has a maximum of $3,3\,kNm/m$. The negative bending moments m_{xx} concentrate on top of the columns and walls with a minimum amount of $17,7\,kNm/m$, see figure 6.48. The moments should be zero at the edges but they are not exact zero due to average of an mesh element. The finer the mesh, the closer the moments should come to zero. The same behaviour like with the bending moments m_{xx} in global x-direction will occur, only in the other global direction. The maximum bending moment m_{xx} is $11,44\,kNm/m$ and the minimum bending moment m_{xx} is $12,0\,kNm/m$, see figure 6.49.

The bending moments of the beams in global x-direction are lower because the span di-

Table 6.7: Instantaneous deflection W_{inst}

Mid span						
$W_{inst} \leq \frac{L}{300}$	Length (L)	$W_{G,inst}$	$W_{Q,inst}$	W_{inst}	$\frac{L}{W_{inst}}$	
	$39,95\,m$	$81\,mm$	$32\,mm$	$113\,mm$	$355\,mm$	≥ 300
	$23,30\,m$	$52\,mm$	$22\,mm$	$74\,mm$	$314\,mm$	≥ 300
	$16,00\,m$	$35\,mm$	$15\,mm$	$51\,mm$	$316\,mm$	≥ 300
	$24,09\,m$	$28\,mm$	$12\,mm$	$40\,mm$	$536\,mm$	≥ 300
	$32,90\,m$	$43\,mm$	$20\,mm$	$61\,mm$	$537\,mm$	≥ 300
Cantilever						
$W_{inst} \leq \frac{L}{150}$	Length (L)	$W_{G,inst}$	$W_{Q,inst}$	W_{inst}	$\frac{L}{W_{inst}}$	
	$17,71\,m$	$118\,mm$	$53\,mm$	$170\,mm$	$104\,mm$	≤ 150
	$9,23\,m$	$67\,mm$	$31\,mm$	$98\,mm$	$94\,mm$	≤ 150
	$13,06\,m$	$82\,mm$	$35\,mm$	$117\,mm$	$112\,mm$	≤ 150

Table 6.8: Final deflection W_{fin}

Mid span						
$W_{fin} \leq \frac{L}{200}$	Length (L)	$W_{G,fin}$	$W_{Q,fin}$	W_{fin}	$\frac{L}{W_{fin}}$	
	$39,95\,m$	$146\,mm$	$32\,mm$	$178\,mm$	$224\,mm$	≥ 200
	$23,30\,m$	$94\,mm$	$22\,mm$	$116\,mm$	$201\,mm$	≥ 200
	$16,00\,m$	$63\,mm$	$15\,mm$	$79\,mm$	$203\,mm$	≥ 200
	$24,09\,m$	$51\,mm$	$12\,mm$	$62\,mm$	$389\,mm$	≥ 200
	$32,90\,m$	$75\,mm$	$20\,mm$	$95\,mm$	$346\,mm$	≥ 200
Cantilever						
$W_{fin} \leq \frac{L}{100}$	Length (L)	$W_{G,fin}$	$W_{Q,fin}$	W_{fin}	$\frac{L}{W_{fin}}$	
	$17,71\,m$	$212\,mm$	$53\,mm$	$264\,mm$	$67\,mm$	≤ 100
	$9,23\,m$	$120\,mm$	$31\,mm$	$151\,mm$	$61\,mm$	≤ 100
	$13,06\,m$	$147\,mm$	$35\,mm$	$183\,mm$	$72\,mm$	≤ 100

Table 6.9: Instantaneous deflection with precambering W_{inst}

Cantilever						
$W_{inst} \leq \frac{L}{150}$	Length (L)	$W_{self,inst}$	$W_{Q,inst}$	W_{inst}	$\frac{L}{W_{inst}}$	
	$17,71\,m$	$24\,mm$	$53\,mm$	$77\,mm$	$230\,mm$	≥ 150
	$9,23\,m$	$12\,mm$	$31\,mm$	$43\,mm$	$215\,mm$	≥ 150
	$13,06\,m$	$18\,mm$	$35\,mm$	$53\,mm$	$247\,mm$	≥ 150

Table 6.10: Final deflection with precambering W_{fin}

Cantilever						
$W_{fin} \leq \frac{L}{100}$	Length (L)	$W_{self,fin}$	$W_{Q,fin}$	W_{fin}	$\frac{L}{W_{fin}}$	
	$17,71\,m$	$44\,mm$	$53\,mm$	$96\,mm$	$184\,mm$	≥ 100
	$9,23\,m$	$22\,mm$	$31\,mm$	$53\,mm$	$174\,mm$	≥ 100
	$13,06\,m$	$33\,mm$	$35\,mm$	$68\,mm$	$192\,mm$	≥ 100

rection is more favourable. The distribution of the bending moments m_{yy} has a maximum of $8,1\ kNm/m$. The negative bending moments m_{yy} concentrate on top of the columns and walls with a minimum amount of $4,8\ kNm/m$, see figure 6.50. The same behaviour like with the bending moments m_{yy} will occur, only in the other direction. The maximum bending moment m_{yy} is $9,1 kNm/m$ and the minimum bending moment m_{yy} is $8,1 kNm/m$, see figure 6.51.

The twisting moments m_{xy} of the beams are low since this is prevented by the top and bottom plates. The maximum twisting moment m_{xy} is $1,9\ kNm/m$ and the minimum twisting moment m_{xy} is $1,8\ kNm/m$, see figure 6.52 in global x direction. The maximum twisting moment m_{xy} is $2,5\ kNm/m$ and the minimum twisting moment m_{xy} is $1,6\ kNm/m$, see figure 6.53 in global y direction.

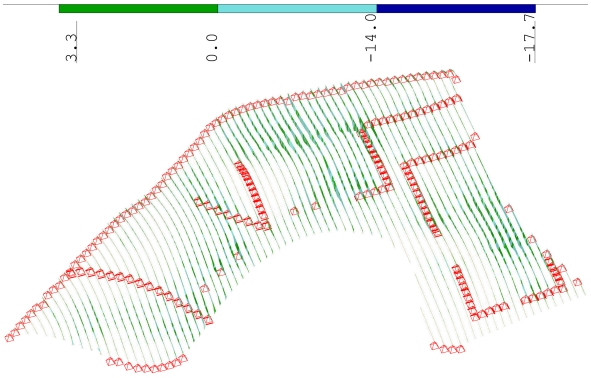

Figure 6.48: The bending moments m_{xx} of x-direction in LC 202

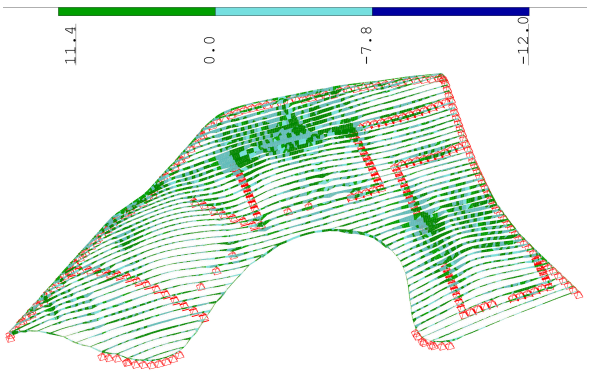

Figure 6.49: The bending moments m_{xx} of y-direction in LC 202

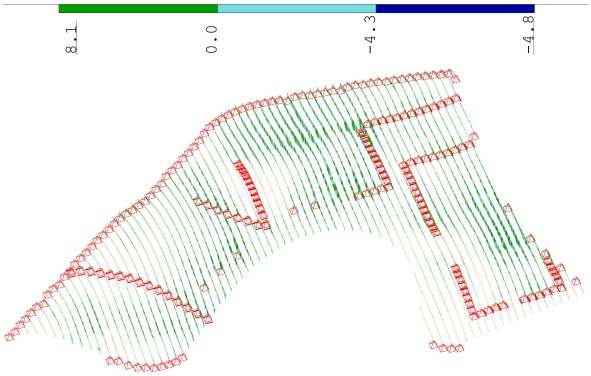

Figure 6.50: The bending moments m_{yy} of x-direction in LC 202

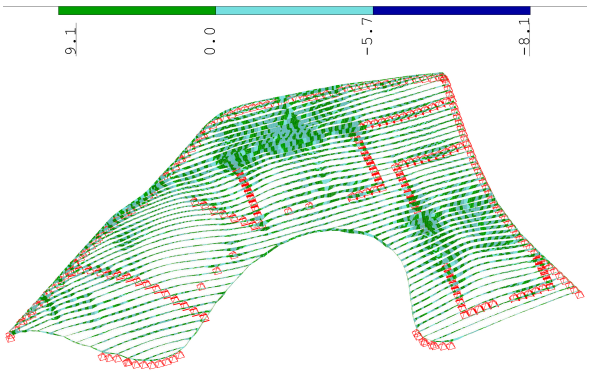

Figure 6.51: The bending moments m_{yy} of y-direction in LC 202

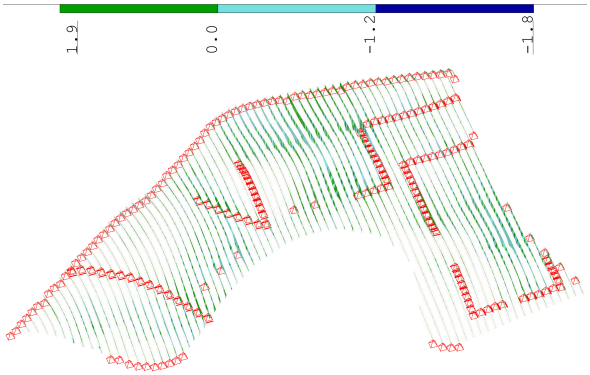

Figure 6.52: The bending moments m_{xy} of x-direction in LC 202

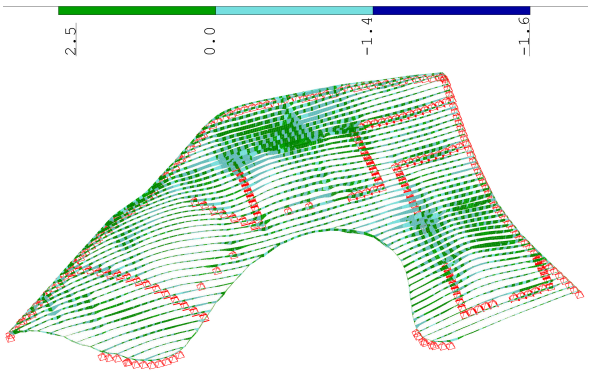

Figure 6.53: The bending moments m_{xy} of y-direction in LC 202

Ponding

The roof structure should be designed with a slight pitch to shed water off the sides. It should be take account of that no ponding occurs, which is the unwanted pooling of water. The curvature of the deflected roof structure has been checked. The building regulations encourage a minimum fall of $1:40$ [33]. However the critical area where the structure needs to span for $35m$ will deform excessively, where the water is not able to get away. The following options could be considered to solve this problem:

- The roof structure deflection of the dead load and imposed loads could be pre cambered such that a slight pitch will remain to shed water off the sides
- Water could drain from the roof into a scupper system
- An internal drainage system could be made into the roof structure

Waterproofing structures may be required to test for water tightness after completion of work. The test is to apply static pressure by means of ponding, which could happen in a later stage on the surface. Testing period may vary from 24 hours to 3 days [10]. Site supervisor should record any leaks or damp patches and submit to the engineer for assessment. Green roofs should have a fall of not less than $1:60$ and be built in accordance with manufacturer's details [33].

The structure will be precambered, which means that only after loading the required architectural shape of the roof structure is reached. Therefore in the critical area, the precamber will be adjusted to avoid ponding under long term loading conditions.

6.3. Conclusion

The idea behind the structural concept is that the material is present where it should be and in the right quantities. The ribbed elements will vary in height and on both sides will be attached by plates. The concept will primarily resists bending but shear and torsion as well. The construction method for the free-form structure has been discussed of what can be achieved in practice. The main reason behind this construction method is the reduction of steel and the benefit of large units, that make a significant amount of simple connections possible between the ribbed elements. The consequences and possibilities of the chosen structural concept with regard to manufacturing, detailing, and assembly have been assessed. The design of the details have been given for the integrated structural concept. It is important that the connections between the large units are made such that it transfer the forces equally since their is a lack of continuity. The design of the support connections also contribute to the overall structural system. Therefore the design of the column and wall

connections have been shown, which need to transfer the forces of the structure into the foundation.

The approximations for the simulation of the global model have been given. The global model is complex and large, which makes it difficult to approach exact each different connection. The computational modelling is time consuming, which has to be considered when this will be done in reality. Therefore it has been chosen to have a more general approach which is applicable for the whole structure. The material properties of the top and the bottom plates will have only 40 percent stiffness. At least this stiffness of connection is achievable for the timber roof structure. One of the two layers are modelled as one layer of $21\,mm$ for the top plates and bottom plates. These plates have two different elasticity modulus for the two different layer directions. Reduction factors have been taken into account since the ribbed elements will be cut-out at angle to the grain and the cross section is reduced due to the incision for the simple connection.

One of the major points of discussion is the height of the ribbed elements in the free-form structure, as this is a key contributor to the design of the final roof structure. The optimal height for this structure has been displayed. The results of the global model have shown that the requirements for the stresses and the deflections are met. It has been chosen to pre camber the whole structure. This means that after loading the sagging of the structure will be relative to the straight line with the supports. Therefore it has been possible to meet the desired shape from the architectural design's point-of-view.

7

Conclusions and Recommendations

In this chapter the results presented in the previous chapters of this thesis are critically reviewed and the conclusions are presented. On this basis, the main research question will be answered. After the conclusions, this chapter finishes with recommendations for future research.

7.1. Conclusions

The main research question is:

"How can timber be used to design an integrated structural concept for free-form structures that exhibits both shell and bending behaviour in a smooth, continuous and seamless fashion?"

An integrated structural concept was developed for free-form timber structures, which is light and yet strong while trying to keep difficult node connections to a minimum. The structural concept consists of ribbed elements that are covered with plates on the top and the bottom. The ribbed elements are cut from laminated veneer lumber to allow a smooth transition in depth according to the structural demands. The ease of fabrication is achieved by designing simple connections such as an incision in the ribbed elements and the plates are connected by screws. The maximum length subject to fabrication and transportation constraints has been considered. This has been achieved by determining the efficient height and the allowable stresses have been reduced.

For structural design, an automated procedure was developed to yield a smooth height variation of the roof structure and place the material where structurally required and thus achieving a significant weight reduction. Deep sections are used where bending govern the design and shallow section where shell action is dominant. Furthermore, the smooth height variation meets the desired shape from architectural design's point-of-view.

In general, it can be concluded that the developed structural concept is suitable for the design of a free-form timber structure that exhibits both bending and shell behaviour. In order to achieve an integrated structural concept, the inhomogeneous material properties of timber were incorporated in the structural concept. Precaution has been taken in the computational modelling by also taking into account the different directions for the anisotropic material properties.

More specifically the following is concluded:

- Due to the curved nature of the structure and the fabrication of the curved elements as cut-outs from plates. A reduction factor for the material capacity needs to be taken into account since the ribbed elements will be sawn at an angle to the grain direction. The global model has been set-up with a reduction factor for an angle of 5°. After multiple iterations, the tapered elements had an average angle of 10° and the allowable stresses are met.
- Because of cutting the ribbed elements at an angle to the grain direction and the cross section reduction due to the incision for the ribbed connection, the allowable bending stresses of these elements are reduced by a total factor of approximately two. Yet, it has been shown that despite this strength reduction, the structural integrity is met. At a few locations, particularly above supports, stresses are exceeded. Nonetheless, this can be addressed in practice by the solutions from the following points.
- For the largest part of the structure, the maximum allowed bending and shear stresses are met. Only in a few places the stresses are too high. These local supports need to be further addressed. However a solution has been given by applying steel plates for the support connections.
- The simple connection of making an incision in the ribbed elements works for almost the entire structure. Only for a few locations the shear stresses are still too high. Here, reinforcements will have to be made by adding timber strips.
- The straightforward connection between the plates to rib works mainly for the entire structure. However the shear forces were too high at the location for the span of 35 m and there the amount of screws needs to be increased.
- The global model is complex and large, which makes it difficult to approach exact each different connection. It has been chosen to have a more general approach since the computational modelling is time consuming. The plates to rib connection has been assumed by reducing the material properties of the plates. The two layers of plates have been assumed by taken into account one plate with different elasticity modulus.
- The calculation method of the smooth height optimization can be applied on any free-form or complex timber structure to get an efficient height with a constant width, when there are no limitations regarding the depth of these structures.
- The structure will be precambered, which means that only after loading the required architectural shape of the roof structure is reached. In the flat areas with a large span the structure does still deform excessively. In this area, the precamber is adjusted to avoid ponding under long term loading conditions.
- The ease of fabrication is achieved by designing simple connections. It is preferred to make mainly timber to timber connections, it was unavoidable to use steel plates for the connections between the large units since these connections need to be stiff and strong. These connections should be made in areas where bending is low but due to fabrication and transportation limits this is not always possible.
- The computer program Karamba was recommended for calculating a smooth cross section height from bending moments. This program does not take into account anisotropic material properties and it could not handle the required complexity of the structure. Therefore it has been decided not to use the program Karamba for the height calculation of the timber structure.
- Although the architectural shape of the roof has been set as a criterion, this does not change the fact that support conditions can be changed to achieve a more efficient structure within the fabrication constrains. It is not preferred from out of architectural point-of-view to change the placement of supports but this can be discussed. However optimising the support conditions by adding some extra or different supports could make the structure way more efficient.

7.2. Recommendations

It is recommended to:

- Perform research for a grid structure that spans in the main direction of forces from a free-form structure. For a free-form structure with different shapes of curvature, it is hard to clarify what the main span direction will be. It is interesting to study how to optimize a single span timber roof without removing its flexibility of a free form structure. It could be more effective to make independent grid structure on the direction which is required but this could occur in difficult connections. Therefore in this research a rectangular grid has been chosen.
- Investigate a more efficient grid to find a reasonable balance between the weight of the structure and the structural behaviour. In this research, a large height was needed for the large spans in the structure, which is not efficient. Therefore at different locations, the density of the grid could be optimised to reduce the height.
- Research more on the possibilities to generate double curvature of timber plates. Plates could be cold bent into the desired curvature but there are restrictions on the allowable curvature. For manufacturing purposes it is necessary to know how this will be done in detail. For analysis a stress reduction needs to be taken into account due to the fact that the plates have already residual stresses from bending.
- Investigate the ratio between the width and the height of the elements. Since the smooth height variation has been applied to get an efficient height but the width of the elements has remained the same.
- Verify numerical results with lab experiments to provide insight and validation of the assumed stress distribution between the curved beam and the plate interaction. A possibility could be to further reduce the required material weight of the structure.
- Have a closer look at the complex digital work flow from concept to fabrication. With some improvements, this could lead to a new software application that can speed up the design process. The parametrisation of the geometry and the automated design steps for the construction process should be further developed.
- Further investigate in more detail of how this kind of structure could be erected as it is difficult to assemble the bottom plates in a later stage during the erection process.

Bibliography

[1] Kerto-VTT-C-184-03-Certificate.

[2] Simon Aicher and C. Stritzke. Novel Lightweight Timber Composite Element: Web Design in Shear and Compression. *RILEM Bookseries*, 2014. ISSN 22110844. doi: 10.1007/978-94-007-7811-5{_}13.

[3] Andrew Lawrence Arup. RILEM Bookseries 9 - Recommendations for the Design of Complex Indeterminate Timber Structures. doi: 10.1007/978-94-007-7811-5{_}12.

[4] Hubert Berberich. Multihalle, 2012. URL `https://commons.wikimedia.org/wiki/File:Multihalle07.jpg`.

[5] Hans Jorgen Blass. *Timber Engineering STEP 1*. Centrum Hout, Almere, 1995. ISBN 90-5645-001-8.

[6] Johan Blauwenraad and Jeroen H. Hoefakker. *Structural Shell Analysis. Understanding and Application.* Springer, 1709 edition, 2013. doi: B011W9RVP4.

[7] R. Brandner, G. Flatscher, A. Ringhofer, G. Schickhofer, and A. Thiel. Cross laminated timber (CLT): overview and development. *European Journal of Wood and Wood Products*, 2016. ISSN 1436736X. doi: 10.1007/s00107-015-0999-5.

[8] Reinhard Brandner and | Area Manager. Production and Technology of Cross Laminated Timber (CLT): A state-of-the-art Report.

[9] Daniel Carrero. El Reciclaje de los Sueños. Shigeru Ban., 2014. URL `http://global-objective.com/ingenieria/el-reciclaje-de-los-suenos-shigeru-ban/`.

[10] Construction DB. Ponding test, 2017. URL `http://www.constructiondb.com/wiki/ponding_test`.

[11] Michael Dickson and Dave Parker. *Sustainable Timber Design*. New York, first edition edition, 2015. ISBN 978-0-415-46807-7.

[12] C Douthe, O Baverel, and J.-F Caron. FORM-FINDING OF A GRID SHELL IN COMPOSITE MATERIALS.

[13] David Garlan and Dewayne Perry. Introduction to the Special Issue on Software Architecture.

[14] Daniel Hambleton, Crispin Howes, Jonathan Hendricks, John Kooymans, and Halcrow Yolles Keywords. Study of Panelization Techniques to Inform Freeform Architecture.

[15] Richard Harris and Jonathan ROYNON Associate Buro Happold Bath. The Savill Garden Gridshell Design and Construction. 2008. URL `http://opus.bath.ac.uk/`.

[16] Richard Harris, Michael Dickson, Oliver Kelly, and Jonathan Roynon. The Use Of Timber Gridshells For Long Span Structures. .

[17] Richard Harris, Oliver Kelly, and Michael Dickson. Proceedings of ICE. .

[18] Henkel AG & Co. KGaA. Adhesive-Bonded Roof for an Elephant House, 2014. URL `http://www.henkel-adhesives.com/engineered-wood/news-41211-adhesive-bonded-roof-for-an-elephant-house-47573.htm`.

[19] HESS TIMBER GmbH & Co. KG. Hess Timber Free Form. URL http://www.hess-timber.com/en/products/hess-free-form/.

[20] ICD/ITKE/IIGS University Stuttgart. Landesgartenschau Exhibition Hall, 2014. URL http://icd.uni-stuttgart.de/?p=11173.

[21] Simone Jeska and Khaled Saleh Pascha. *Emergent Timber Technologies*. Birkhauser Verlag Ag, first edtion edition, 2014. ISBN 978-3-038-21502-8.

[22] Johns Building Supplies. Gluelam Beams, 2017. URL http://www.johnsbuildingsupplies.com.au/products/smartlam-gluelam-beams/.

[23] Marc Wilhelm Lennartz and Susanne Jacob-Freitag. *Neues Bauen mit Holz: Typen und Kostruktionen*. Birkhäuser, 2015. ISBN 978-3-035-60455-9.

[24] Ben Lewis. Centre Pompidou - Metz: Engineering the roof. *The Structural Engineer*, 89 (18):20–25, 2011.

[25] Jian-Min Li and Jan Knippers. Pattern and Form - Their Influence on Segmental Plate Shells. 2015.

[26] Jian-Min Li and Jan Knippers. Segmental Timber Plate Shell for the Landesgartenschau Exhibition Hall in Schwäbisch Gmünd—the Application of Finger Joints in Plate Structures. *International Journal of Space Structures*, 30(2), 2015.

[27] Felix Mara. The decade in detail, 2009. URL https://www.architectsjournal.co.uk/news/the-decade-in-detail/5212323.article.

[28] Optigreen. Optigreen System Type: 'Nature Roof', 2017. URL http://www.optigreen.co.uk/system-solutions/nature-roof/solution-1/.

[29] P Poinet, P Nicholas, M Tamke, M R Thomsen, Paul Poinet, Paul Nicholas, Martin Tamke, and Mette Ramsgaard Thomsen. Multi-Scalar Modelling for Free-form Timber Structures. 2016.

[30] Pollmeier. Pollmeier BauBuche - Section 02 - Product overview. URL https://www.pollmeier.com/en/service/downloads/brochures.html.

[31] Princeton University. Mannheim Multihalle, 2013. URL http://shells.princeton.edu/Mann1.html.

[32] Steico. Construction panel. URL http://www.archiexpo.com/prod/steico/product-59793-538953.html.

[33] Syspec Ltd. Flat roof - Drainage, 2017. URL https://www.buildingregs4plans.co.uk/guidance_flat_roof_drainage.php.

[34] Timber+ Design. Structural Robotic Fabrication, 2014. URL http://www.timberdesignmag.com/projects/robotic-fabrication/.

[35] Yves Weinand. Innovative timber constructions. *Journal of the International Association for Shell and Spatial Structures*, 2009. ISSN 1028365X.

[36] Jan Willmann, Michael Knauss, Tobias Bonwetsch, Anna Aleksandra Apolinarska, Fabio Gramazio, and Matthias Kohler. Robotic timber construction - Expanding additive fabrication to new dimensions. *Automation in Construction*, 2016. ISSN 09265805. doi: 10.1016/j.autcon.2015.09.011.

[37] X. W. Xu and S. T. Newman. Making CNC machine tools more open, interoperable and intelligent - A review of the technologies. *Computers in Industry*, 2006. ISSN 01663615. doi: 10.1016/j.compind.2005.06.002.

List of Figures

List of Tables